CHALMERS
UNIVERSITY OF TECHNOLOGY

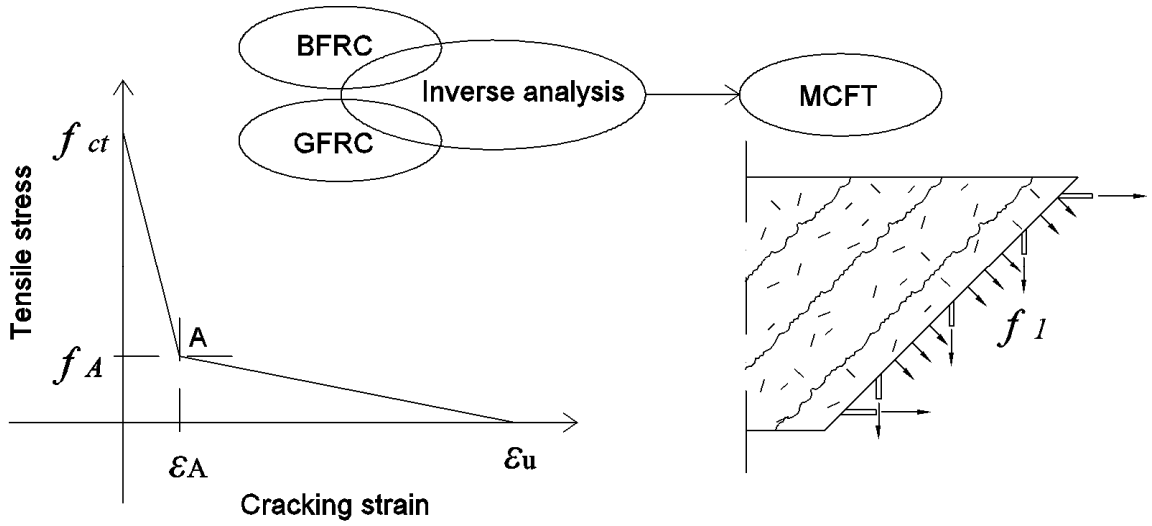

Application of Modified Compression Field Theory on glass and basalt fibre reinforced concrete

Master's Thesis in the Master's Programme Structural Engineering and Building Technology

ERIKA ABRAHAMSSON
JOSEFIN PETERSSON

Department of Civil and Environmental Engineering
Division of Structural Engineering
Concrete Structures
CHALMERS UNIVERSITY OF TECHNOLOGY
Gothenburg, Sweden 2015
Master's Thesis 2015:117

MASTER'S THESIS 2015:117

Application of Modified Compression Field Theory on glass and basalt fibre reinforced concrete

Master's Thesis in the Master's Programme Structural Engineering and Building Technology

ERIKA ABRAHAMSSON

JOSEFIN PETERSSON

Department of Civil and Environmental Engineering
Division of Structural Engineering
Concrete Structures
CHALMERS UNIVERSITY OF TECHNOLOGY
Göteborg, Sweden 2015

Application of Modified Compression Field Theory on glass and basalt fibre reinforced concrete
Master's Thesis in the Master's Programme Structural Engineering and Building Technology

ERIKA ABRAHAMSSON

JOSEFIN PETERSSON

Examensarbete 2015:117/ Institutionen för bygg- och miljöteknik,
Chalmers tekniska högskola 2015

Department of Civil and Environmental Engineering
Division of Structural Engineering
Concrete Structures
Chalmers University of Technology
SE-412 96 Göteborg
Sweden
Telephone: + 46 (0)31-772 1000

Cover:
Overview of the method in this thesis work.
Department of Civil and Environmental Engineering, Göteborg, Sweden, 2015

Application of Modified Compression Field Theory on glass and basalt fibre reinforced concrete

Master of Science Thesis in the Master's Programme Structural Engineering and Building Technology

ERIKA ABRAHAMSSON
JOSEFIN PETERSSON
Department of Civil and Environmental Engineering
Division of Structural Engineering
Concrete Structures
Chalmers University of Technology

ABSTRACT

To meet today's challenges of designing slimmer, more cost efficient and more architecturally appealing concrete structures, new alternatives to the conventionally used reinforcement materials need to be developed. One promising alternative is fibre reinforced concrete (FRC). There are many fibre reinforcement materials available for the building industry, where the steel fibre is the most common one. Glass and basalt fibre reinforcement are not as widely investigated as steel fibres when it comes to for example shear capacity in beams.

The purpose of this Master's thesis work was to analyse the possibilities to utilize the Modified Compression Field Theory (MCFT) on glass and basalt FRC by using the tensile strength curves received from inverse analysis.

The inverse analysis was based on results from three point bending tests (3PBT) of two sets of beams with 0.3% fibre volume and different concrete classes of C25/30 and C50/60. In the analysis, both a bi-linear and a tri-linear curve was evaluated as input tensile strength. Therefore the analysis resulted in four curves, one bi- and tri-linear curve for each of the concrete classes C25/30 and C50/60.

The tensile curves indicated on large increases in maximum tensile strength. This could not be verified against experimental testing or by conclusions drawn in the literature. Although, good correlation was shown in the comparison between the residual flexural strength curves from experimental testing and the curves received from inverse analysis.

Shear capacity calculations according to the Simplified FRC-MCFT were done using the tensile strength curves as input. The calculations resulted in convergence for all four curves. Although, the calculations with the bi-linear curves only converged for unreasonable reinforcement amounts. Therefore, the Simplified FRC-MCFT could be concluded not applicable on the tensile strength curves received with the bi-linear input curves. On the other hand, the Simplified FRC-MCFT could be concluded to be applicable on the tensile strength curves received with the tri-linear input curves.

Key words: Inverse analysis, Simplified FRC-MCFT, Modified Compression Field Theory, fibre reinforced concrete, glass fibre reinforced concrete, basalt fibre reinforced concrete, tensile strength, shear capacity.

Tillämpning av den Modifierade Tryckfältsteorin på glas- och basaltfiberarmerad betong

Examensarbete inom Structural Engineering and Building Technology

ERIKA ABRAHAMSSON, JOSEFIN PETERSSON
Institutionen för bygg- och miljöteknik
Avdelningen för konstruktionsteknik
Betongbyggnad
Chalmers tekniska högskola

SAMMANFATTNING

Att konstruera mer kostnadseffektiva, slanka och arkitektoniskt tilltalande betongkonstruktioner är några av de utmaningar byggindustrin står inför idag. Därför är det viktigt att utveckla alternativ till traditionell armering. Ett lovande alternativ är fiberarmering, vilken kan produceras av olika material där stål är det vanligaste. Glas- och basalt fibrer är inte studerade i lika stor utsträckning som stålfibrer, till exempel vad gäller tvärkraftskapacitet.

Syftet med detta exjobb var att analysera möjligheten att applicera den Modifierade Tryckfältsteorin på dragkurvor för glas- och basaltfiberarmerad betong, framtagna från inversanalys.

Inversanalysen var baserad på resultat från trepunkts böjtester på två uppsättningar av balkar. Balkarna hade fibervolym 0.3% och två olika betonghållfasthetsklasser, C25/30 respektive C50/60. I analysen var både indata i form av bi-linjära kurvor och tri-linjära kurvor utvärderade. Därför resulterade inversanalysen i fyra dragkurvor, två kurvor för betonghållfasthet C25/30 och två för C50/60.

Dragkurvorna visade på en hög ökning av maximal draghållfasthet, vilket inte kunde verifieras med utförda experimentella tester eller mot slutsatser från litteraturen. Även om dessa kurvor inte kunde verifieras, visade sig inversanalysen stämma bra överens med de tidigare utförda böjtesterna.

Dragkurvorna användes som indata till en tvärkraftsberäkningsteori för fiberarmerad betong som baseras på den modifierade tryckfältsteorin. Beräkningarna resulterade i konvergens för samtliga dragkurvor, men för de bi-linjära kurvorna konvergerade bara beräkningar med orimliga armeringsinnehåll. Därför kunde inte den förenklade modifierade tryckfältsteorin appliceras på de bi-linjära kurvorna. Däremot kunde den appliceras på de tri-linjära.

Nyckelord: Inversanalys, förenklad modifierad tryckfältsteori, modifierad tryckfältsteori, fiberarmerad betong, glasfiberarmerad betong, basaltfiberarmerad betong, draghållfasthet, tvärkraftskapacitet.

Contents

ABSTRACT I
SAMMANFATTNING II
CONTENTS III
PREFACE V
NOTATIONS VI
ABBREVIATIONS VIII

1 INTRODUCTION 1
1.1 Background 1
1.2 Purpose 2
1.3 Aim and objective 2
1.4 Outline 2
1.5 Method 3
1.6 Scope and limitations 5

2 LITERATURE STUDY 7
2.1 Fibre reinforced concrete (FRC) 7
2.1.1 Development of design rules for fibre concrete 9
2.1.2 Structural response of FRC in bending and tension 9
2.1.3 Fracture energy 11
2.1.4 Residual strength 11
2.1.5 Mechanisms related to mechanical behaviour of FRC 13
2.2 Different kinds of fibre reinforced concretes (FRCs) 15
2.2.1 Steel fibre reinforced concrete (SFRC) 16
2.2.2 Glass fibre reinforced concrete (GFRC) 18
2.2.3 Basalt fibre reinforced concrete (BFRC) 21
2.2.4 MiniBar reinforced concrete (MRC) 22
2.3 Shear behaviour of concrete structures 25
2.3.1 Principal stress 25
2.3.2 Mechanisms of shear 26
2.3.3 Compression Field Theory (CFT) 28
2.3.4 Modified Compression Field Theory (MCFT) 29
2.3.5 Modified Compression Field Theory (MCFT) extended to SFRC 34
2.3.6 Simplified FRC-MCFT (FRC-MCFT) 35
2.4 Bending tests of GFRC and BFRC beams 39
2.4.1 Testing procedure 39
2.4.2 Gathering of test results 40
2.5 Conclusions of literature study 51

3 INVERSE ANALYSIS OF BENDING TESTS 52
3.1 Methodology of inverse analysis 52
3.2 Inverse analysis of MRC 53
3.2.1 Modelling technique 54
3.2.2 Assumptions and simplifications 59
3.3 Results from inverse analysis 59
3.3.1 Bi-linear tensile curve 60
3.3.2 Tri-linear tensile curve 64
3.3.3 Comparison of bi-linear and tri-linear tensile strength curves 69
3.4 Conclusions of inverse analysis 71

4 ANALYSIS OF FRC-MCFT 72
4.1 Application of tensile strength curves 72
4.2 Shear capacity calculation of MRC 77
4.2.1 Input data 77
4.2.2 Results from shear capacity calculations 78
4.3 Sensitivity analysis of FRC-MCFT 81
4.4 Conclusions of analysis of FRC-MCFT 84

5 RESULTS 85

6 DISCUSSION 87

7 CONCLUSIONS AND FURTHER STUDIES 91
7.1 Conclusion 91
7.2 Further studies 92

8 REFERENCES 93

LIST OF APPENDICES 98

Preface

This thesis work has been carried out during the spring of 2015 at the Division of Structural Engineering, Concrete Structures, Chalmers University of Technology, Sweden. The work was done in co-operation with Skanska Teknik and ÅF Infrastructure.

In this study, test results from three point bending tests were received from ReforceTech, which we are very thankful for. The bending test results were used in an inverse analysis and the results from the inverse analysis were further used in a shear calculation analysis based on the Modified Compression Field Theory.

We would like to thank our supervisors Thomas Blanksvärd (Skanska) and Ludwig Lundberg (ÅF) for their guidance and support during our thesis work. Many thanks also to Rasmus Rempling, our supervisor and examiner at Chalmers University of Technology.

We would also like to thank Len Miller at ReforceTech, who arranged a visit at the production plant of the MiniBars, which was very interesting.

Finally, we would like to thank our opponents Birgit Amblie Solerød and Elin Alexandersson who gave us many good advices.

Göteborg June 2015

Erika Abrahamsson

Josefin Petersson

Notations

Roman upper case letters

A_v	Area of stirrups
A_{sz}	Area of stirrups
E_c	Modulus of elasticity for concrete
$E_{C25/30}$	Modulus of elasticity for concrete class C25/30
$E_{C50/60}$	Modulus of elasticity for concrete class C50/60
G_f	Fracture energy
M	Moment
M_u	Ultimate moment
N_v	Tensile force in longitudinal reinforcement
R_j	Residual flexural strength class, j= 1, 2, 3 and 4
V	Shear force
V_f	Fibre volume percentage
$V_{u,\exp}$	Experimental ultimate shear capacity
$V_{u,pre}$	Predicted ultimate shear capacity

Roman lower case letters

a	Maximum aggregate size
a/d	Span to depth ratio
b	Width
b_v	Effective web width, according to Modified Compression Field Theory
b_w	Effective web width, according to Simplified FRC-MCFT
d	Effective depth
d_v	Effective shear depth
f	Tensile longitudinal stress
f_A	Stress in point A
f_B	Stress in point B
f_1	Tensile principal stress
f_2	Compressive principal stress
f_c'	Maximum compressive stress observed in a cylinder test
f_{ck}	Characteristic concrete cylinder strength
f_{cr}	Stress at crack initiations
f_{ct}	Maximum concrete tensile strength
f_{ctm}	Average concrete tensile strength
f_{Ftu}	Ultimate residual tensile strength
f_p	Stress in the longitudinal prestressing tendons

$f_{R,j}$	Residual flexural strength, j= 1, 2, 3 and 4
f_{sz}	Tensile stress in the stirrups
f_{szcr}	Tensile stress in the stirrup at a cracked interface
f_v	Stress in the stirrups
f_{vy}	Yield stress in the stirrups
f_x	Stress in the longitudinal bars
f_z	Clamping stresses
h_{sp}	Distance between the notch tip and the top of the specimen
i_{corr}	Corrosion potentials
l_{cs}	Characteristic length
s	Stirrup spacing
s_{mv}	Average crack spacing in the vertical direction
s_{mx}	Average crack spacing in the longitudinal direction
$s_{m\theta}$	Average spacing of the diagonal cracks
s_x	Crack spacing in the longitudinal direction
$s_{x,FRC}$	Crack spacing in the longitudinal direction for fibre reinforced concrete
s_z	Crack spacing in the vertical direction, distance between stirrups
$s_{z,FRC}$	Crack spacing in the vertical direction for fibre reinforced concrete
s_θ	Crack spacing in the direction of the diagonal cracks
v	Shear stress
v_{ci}	Shear stress on crack surface
v_s	Shear stress contribution from transverse reinforcement
w	Crack mouth opening, crack width

Greek lower case letters

α_1	Factor considering the bond characteristics of the reinforcement
α_2	Factor considering the type of loading
ε	Strain
ε_1	Principal tensile strain
ε_2	Principal compressive strain
ε_A	Strain in point A
ε_B	Strain in point B
ε_{cr}	Strain at crack initiation
ε_{Fu}	Ultimate tensile strain
ε_u	Ultimate strain
ε_x	Strain in the longitudinal direction
ϕ	Reinforcement diameter
η_f	Fibre orientation factor

ν	Poisson's ratio
θ	Inclination angle of diagonal cracks
ρ_x	Reinforcement ratio of longitudinal reinforcement
ρ_z	Reinforcement ratio of stirrups
σ	Stress

Abbreviations

AR	Alkali Resistant
BFRC	Basalt Fibre Reinforced Concrete
BFRP	Basalt Fibre Reinforced Polymer
CFT	Compression Field Theory
CMOD	Crack Mouth Opening Displacement
CSA	Canadian Standard Association
DSFM	Disturbed Stress Field Model
E	Elasticity
FE	Finite Element
FIB	International Federation for Structural Concrete
FRC	Fibre Reinforced Concrete
GFRC	Glass Fibre Reinforced Concrete
HFRC	Hybrid Fibre Reinforced Concrete
HPFRCC	High Performance Reinforced Cementitious Composites
HS	High Strength
MCFT	Modified Compression Field Theory
MRC	MiniBar Reinforced Concrete
OPC	Ordinary Portland Cement
RC	Reinforced Concrete
SFRC	Steel Fibre Reinforced Concrete
SLS	Serviceability Limit State
SMCFT	Simplified Modified Compression Field Theory
ULS	Ultimate Limit State
2*D*	Two Dimensional
3*D*	Three Dimensional
3*PBT*	Three Point Bending Test

1 Introduction

In the following sections the introduction to this Master's thesis work is presented. First, the background is explained, followed by the purpose, the aim and objective, the outline, the method and finally the scope and limitations.

1.1 Background

Due to the concrete's low tensile strength, cracking occurs in almost all concrete structures. Cracking enables the structure to redistribute stresses to other areas which can contribute to an enhanced load carrying ability. However, the cracks become a problem when they are growing too large. Although, the cracking can be controlled with an appropriate amount of reinforcement and when controlled it can be seen as a minor problem (Engström 2014).

Since the reinforced concrete was invented in the 19th century, it has become one of the most used building materials (Elfgren 2015). The development today is heading towards more slender designs and it is therefore of importance to develop and study reinforced concrete to find slimmer, stronger and also less maintenance demanding solutions and alternatives.

One way to control cracking is to use fibre reinforced concrete (FRC). When fibres are added to concrete they bridge the cracks and contribute to an enhanced post-cracking behaviour. The fibres can be made out of different materials such as steel, polymer, carbon, glass or basalt. How much the different fibres affect the structural response is more or less investigated with experimental studies for different fibre materials. According to (Chugh et al. 2013) and (Kabay 2013), glass and basalt fibres are not as widely investigated as the steel fibre, which is the most investigated and applied fibre.

One favourable aspect of using FRC is the reduction of workmanship on the construction site if used instead of reinforcement bars. The workmanship stands for approximately 40% of the total cost of a concrete structure. The reinforcement arrangement on site is one of the largest contributions to this cost together with formwork costs (Löfgren 2005). Another favourable aspect is the concrete thickness which can be decreased due to the reduced need of concrete cover, thus leading to slimmer and lighter structures with reduced material use.

There is a lack of standards and norms for design of FRC in Sweden today, which leads to more responsibility on the designer. The development of new standards is an ongoing work in the world. In Sweden, a complement to SS-EN 1992-1-1 is available for FRC in SS 812310. This guideline concerns steel and polymer fibres, but does not specifically deal with glass or basalt fibres (SIS/TK556/AG1 2014).

Mechanical properties that are important to take into account in the design of FRC in ultimate limit state (ULS) are, according to (SIS/TK556/AG1 2014); punching shear, torsion, partially loaded areas, fatigue, shear and bending, with or without axial force.

Shear failure of glass and basalt FRC is not widely examined in the literature, neither by experimental studies nor by assessment of sectional models (Chugh et al. 2013; Wang et al. 2014). To be able to use glass and basalt fibres as reinforcement in load-bearing structural members in a reliable and safe way, it is necessary to investigate both the shear behaviour during loading as well as the shear capacity.

When fibres are added to concrete they contribute with an additional isotropic tensile strength to the concrete matrix. Although, the tensile strength of conventionally reinforced concrete is not commonly taken into consideration in design rules and theories. One theory, that does take the tensile strength of the concrete into consideration, is the Modified Compression Field Theory (MCFT), which is used for shear capacity calculations (Collins & Mitchell 1987).

Many studies can be found in the literature regarding the MCFT applied on steel fibre reinforced concrete (SFRC). The possibilities of applying this theory on shear capacity calculations of less commonly used fibres, as glass and basalt, need to be further studied. This is important in order to investigate the possibilities of using these fibres as shear reinforcement. This may decrease the need of conventional shear reinforcement as well as labour costs of stirrup arrangement in production of concrete structures.

Before the glass and basalt FRCs can be used in load-bearing structures, they have to be known as safe and reliable choices in the construction industry. This can be reached by increasing the knowledge regarding their properties and how they affect the structural response.

1.2 Purpose

The purpose of this Master's thesis work was to analyse the possibilities to apply the Modified Compression Field Theory (MCFT) on tensile strength curves of glass and basalt fibre reinforced concrete (FRC) received from inverse analysis.

1.3 Aim and objective

The aim was to obtain tensile strength curves for glass and basalt FRC by an inverse analysis.

A further aim was to find a theory based on the MCFT that is applicable on FRC. If the MCFT was found applicable on the tensile strength curves received from inverse analysis, an additional aim was to investigate how the shear capacity is influenced by the addition of fibres. The objective was to compare the difference between the shear capacity of plain concrete and concrete with different strength and fibre volumes.

However, if the calculations according to the MCFT did not converge, the aim was to point out the observed difficulties and obstacles with the studied theory.

1.4 Outline

The outline of this report is based on the three sub-studies; (1) a literature study, (2) an inverse analysis and (3) a calculation according to the MCFT. The sub-studies can be found in Section 2, Section 3 and Section 4 where each sub-study is presented followed by its results and conclusions connected to its aims and objectives. The work in this Master's thesis is then discussed and results and conclusions regarding the purpose are presented and drawn, see Figure 1.

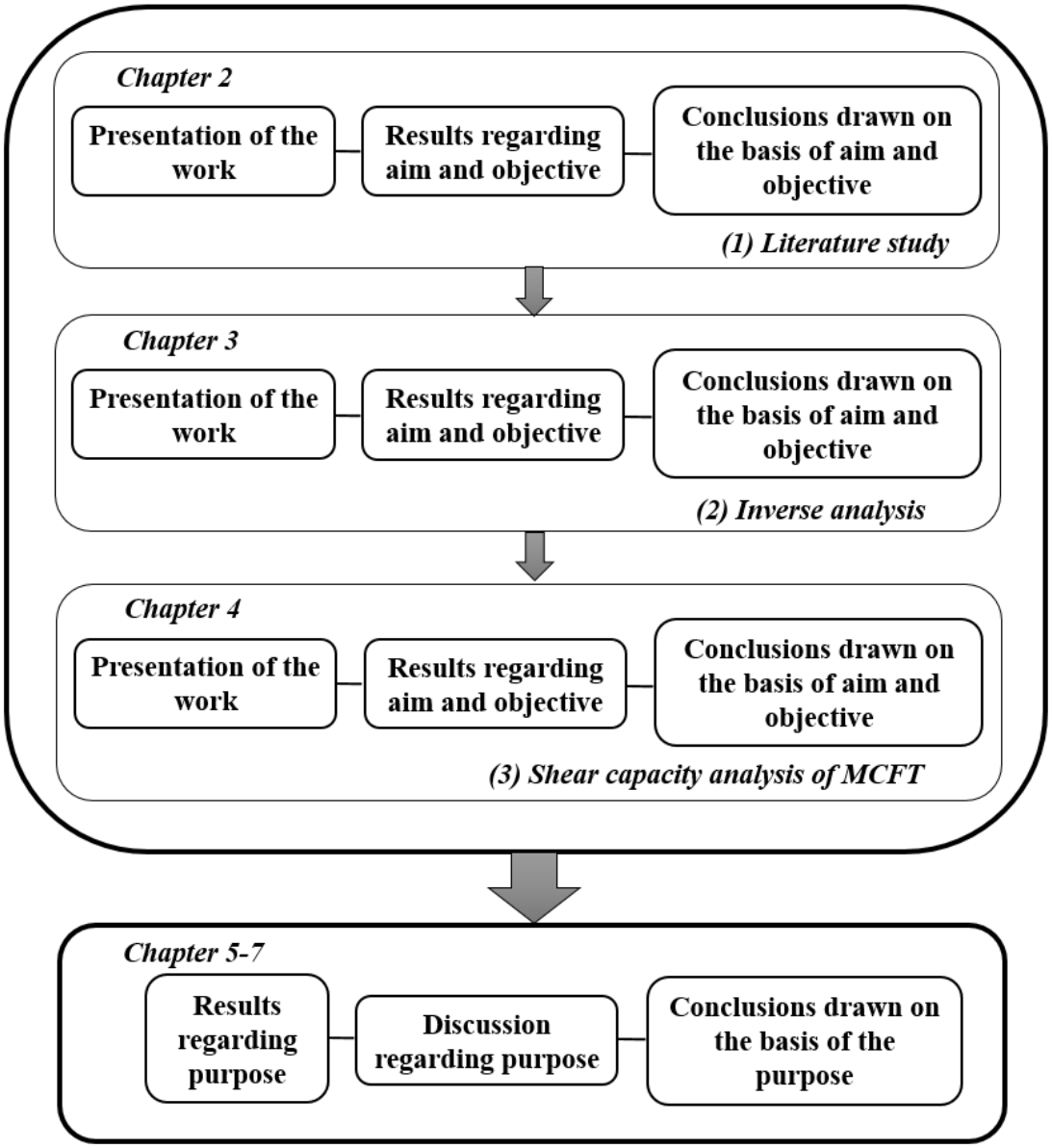

Figure 1 Outline of the report.

1.5 Method

This Master's thesis work was carried out in three partial studies: (1) a literature study, (2) an inverse analysis and (3) an analysis of the MCFT.

First, a literature study was carried out to receive knowledge within the field of theory in this Master's thesis work. The literature study included the following subjects:

- Structural behaviour of FRC
- Different kind of fibres used in the construction industry
- Material properties and structural response of glass and basalt FRC
- Shear behaviour of FRC
- Modified Compression Field Theory (MCFT)

- MCFT applied on FRC
- Gathering of bending test results

Glass and basalt fibre reinforcement can be produced in many different shapes. In this Master's thesis work only one fibre reinforcement product was chosen. The reason was that there is a large scatter in material properties and structural behaviour of different products. The chosen product was the MiniBar by ReforceTech, which can be produced both as Alkali Resistant glass (AR-glass) and basalt MiniBar. The AR-glass and basalt MiniBar have the same dimensions and structure, independent of material. Residual flexural strength curves of tests made on the AR-glass MRC were received from ReforceTech.

The second partial study was the inverse analysis where the tensile strength curves of MRC were obtained. This was made in order to be able to calculate the shear capacity, according to the MCFT, of MRC further on in the study. Due to difficulties in the operation of test methods of pure tensile strength of fibre concrete, data showing the tensile behaviour of MRC was not available in the literature. The tensile strength of MRC for different concrete classes was therefore obtained from inverse analysis in the Finite Element (FE)-software Abaqus.

The inverse analysis was carried out on the basis of the already made bending tests on MRC. The test setup used in the received bending tests was modelled in Abaqus. The input data to the model was a predicted stress-strain curve for the tensile strength of MRC. The real tensile strength curve was obtained when the results from the FE-model matched the residual flexural strength curve from the received experimental bending test results. To make the FE-model match the known curve, the predicted input tensile strength curve was changed manually in iterations. This was done both for a bi-linear and a tri-linear curve of the tensile strength. The final received tensile stress-strain curves were used further on as the real tensile curves of the different MRC's.

Finally, in the third and last partial study, an analysis of the possibility of applying the MCFT on MRC was made. The possibilities were investigated with a shear capacity calculation in Matlab. The calculations were made according to the MCFT on MRC beams with theoretical dimensions and reinforcement. The tensile strength curves received from the inverse analysis were used as an input in the calculations to take the contribution from the fibres into account. Moreover, the calculations were made on the basis of the MCFT extended to FRC. Several such theories are available in the literature, where one of these was chosen. When all partial studies were done, the applicability of the MCFT extended to FRC on tensile strength curves of glass and basalt FRC could be evaluated.

The method of this Master's thesis work is shown in Figure 2 with a flowchart.

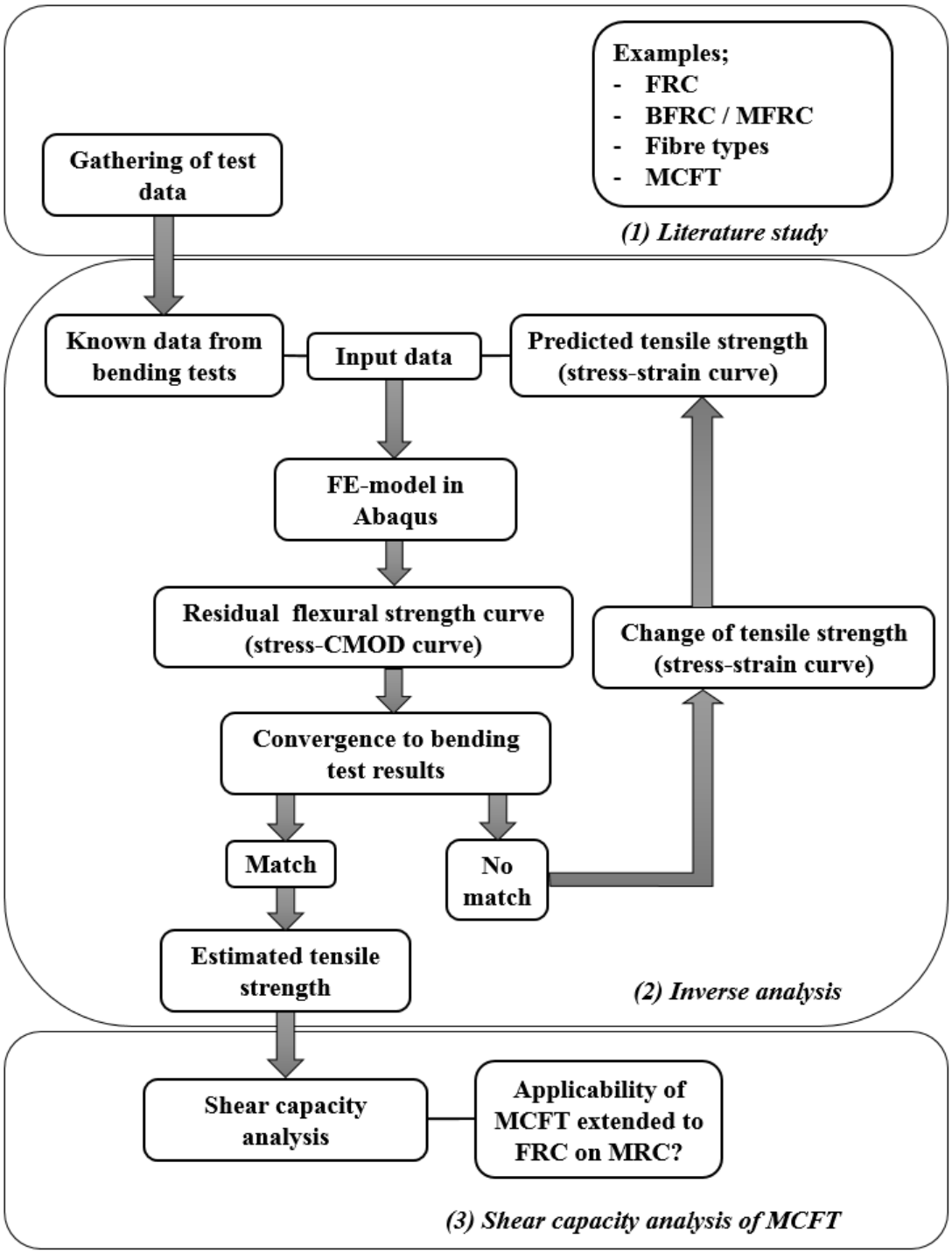

Figure 2 Method flowchart.

1.6 Scope and limitations

This Master's thesis work was limited to analyse the product MiniBar by the company ReforceTech, made from both AR-glass and basalt micro fibres. Other similar fibre reinforcement products are available on the market but the structural behaviour in combination with concrete varies and therefore only one product was chosen. Other fibre materials or other type of fibres were not analysed, only mentioned to enhance the

knowledge of the differences in properties of fibre reinforcement. Only SFRC was more explained to give knowledge to the MCFT extended to SFRC.

The inverse analysis and the shear capacity calculations were based on already executed flexural bending tests received from ReforceTech. Consequently, no flexural bending tests were to be executed in the scope of this thesis work. In addition, neither an experimental study on the tensile behaviour of MRC nor an experimental study on shear capacity of MRC beams was performed. These tests would be needed in order to validate the results from the inverse analysis and from the shear capacity calculations on MRC.

The focus in this thesis work was on the analysis of the shear capacity of MRC. Even though shear capacity was the main mechanical property studied, flexural bending strength, tensile strength and compressive strength were needed in order to eventually end up in shear strength. In the first partial study, flexural bending strength curves were gathered for later use in the inverse analysis. In the second partial study, tensile strength curves were the outcome of the inverse analysis in which also the compressive strength was used. In the third partial study, the tensile strength curves received were used together with compressive strength to calculate the shear capacity.

The MCFT extended to SFRC was applied on MRC. This theory made it possible to take the tensile strength of concrete into account in the calculations which was necessary to account for the added fibres. Other shear capacity theories with the same possibility were mentioned but not analysed further in the scope of this thesis work.

The intention of the work was not to develop design rules for MRC, in contrast the study used one theory which already existed in the literature for calculating shear capacity of FRC. To assess the most adequate method of all methods available in literature, a more comprehensive work needs to be carried out. This has not been done within this study. Such a work should include an extensive experimental work that could fit in the scope of a further Master's thesis.

Analyses were only done on normal strength and hardened concrete. Thus, neither high performance, self-compacting nor high rapid strength concrete were analysed. In addition, since the study excluded the behaviour of young concrete, a rheology study was not performed. Thus, the usage of fresh glass and basalt FRC on site was not discussed.

2 Literature study

The literature study was the first partial study within this thesis work. In this chapter, the properties of fibre reinforced concrete (FRC) will first be described followed by presentations of different kinds of FRC. Thereafter, the shear behaviour of concrete structures will be explained together with some existing methods of calculating shear capacity. Also, results of flexural bending tests of MiniBar reinforced concrete (MRC) are presented. In the end, conclusions of the first partial study are given.

2.1 Fibre reinforced concrete (FRC)

Plain concrete is characterized with a low tensile strength and a high compressive strength. Adding reinforcement, made of different materials and shapes, enhances the resistance of the possible different failure modes in ultimate limit state (ULS). In other words, it increases the strength parameters in different directions.

One way of increasing the post-cracking strength, the ductility and the toughness of plain concrete is to add freely dispersed fibres capable of adding a reinforcing effect to the concrete (Fib 2013). The main mechanisms contributing to the toughening in plain concrete are according to (Löfgren 2005);

- crack shielding
- crack deflection
- aggregate bridging
- crack surface roughness-induced closure
- crack tip blunted by voids and
- crack branching

In FRC, an additional mechanism working together with the other mechanisms to enhance the toughness is the fibre bridging effect (Löfgren 2005). The main toughening mechanisms in FRC are shown in Figure 3.

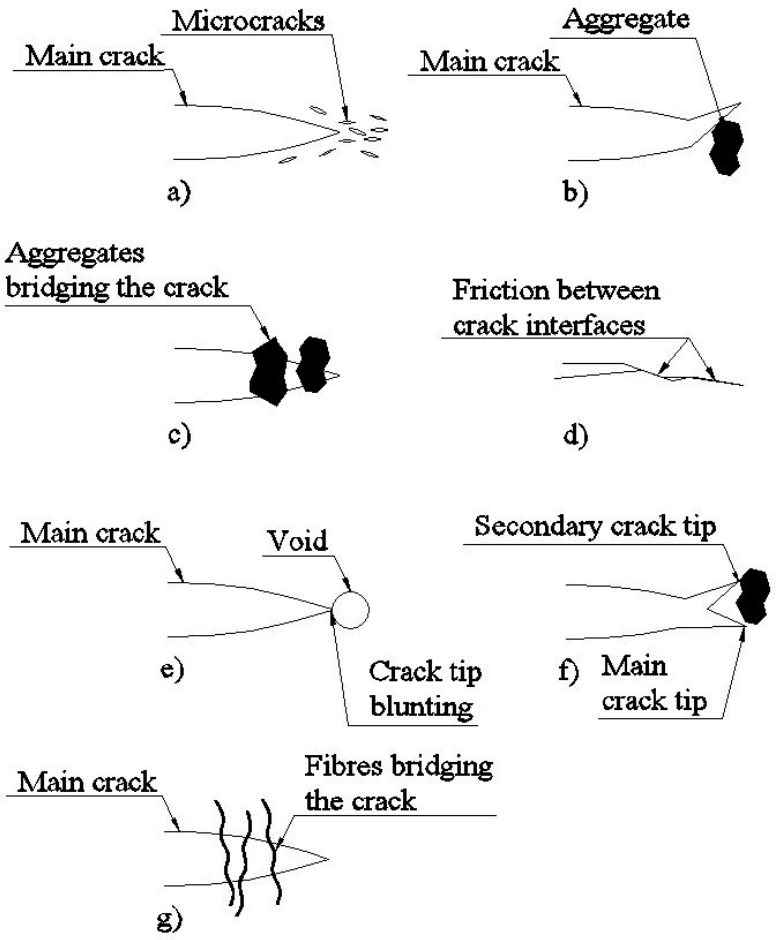

Figure 3 *The main toughening mechanisms in FRC; a) crack shielding, b) crack deflection, c) aggregate bridging, d) crack surface roughness-induced closure, e) crack tip blunted by voids, f) crack branching and g) fibre bridging, from* (Löfgren 2005).

In addition to the improved resistance of concrete in ULS, the serviceability limit state (SLS) behaviour including crack control and deflection can also be improved when adding fibres (Bernardi et al. 2015).

Also, by adding fibres, the amount of conventional reinforcement, i.e. steel rebars, can be reduced (Fib 2013; Prisco et al. 2009). The reduced amount varies depending on for example application and type of fibre reinforcement. One common application of FRC is in shotcrete structures as for example tunnel linings (Mondo 2011). Other applications are for example inner walls, floors, pavements, columns and slabs.

Different FRC composites differ in structural response, material properties etc., but can be characterized with some common mechanisms and responses. In this section the general response and basic mechanisms of FRC are described irrespectively of the fibre material. Although, it shall be noted that the general response in the literature is best applicable on steel fibre reinforced concrete (SFRC) which is the most common fibre material and hence the fibre that is studied the most.

2.1.1 Development of design rules for fibre concrete

Already in 1874, fibres were introduced as reinforcement in concrete. This was the starting point in the development of FRC in structural engineering applications (Löfgren 2005). Since then, fibres in many materials and shapes have been developed. However, the use is limited because of the lack of standardized design rules.

The development of design rules for FRC is an ongoing project in Europe. Some countries have developed their first recommendations and codes. In 2013, five design rules/recommendations were available according to (Blanco et al. 2013);

- the German code
- the RILEM scientific committee 162 recommendations
- the Italian guideline
- the Spanish code and
- the fib Model Code

In 2014, the Swedish standard "SS 812310:2014 - Fibre Concrete – Design of Fibre Concrete Structures" was released as a complement to Eurocode and as a national guideline (SS812310:2014 2014). The standard only treats steel and polymer fibres, but is a first step in the standardization of design rules for fibre concrete in Sweden.

According to Löfgren[1], it is not yet decided if the next revision of Eurocode 2 will include FRC. Although, if the next revision will include FRC, the design rules will be general for all kinds of FRC, though based on materials which researchers and designers have long experience of and where it exists many experimental test results. This applies for both mechanical properties as well as durability aspects. The revision will most likely not include basalt fibres for load bearing structures, if, only for special applications.

The revision of the Swedish Standard SS-14889-2, which includes definitions, specifications and conformity of polymer fibres, will include stricter requirements in terms of demonstrating alkali resistance of the fibres[1] as follows: "For fibres of unknown resistance to deterioration when in contact with the moisture and alkalis present in cement paste, the manufacturer shall demonstrate the long-term durability of the fibres in cement paste/concrete throughout the anticipated useful life of the structure".

2.1.2 Structural response of FRC in bending and tension

When loaded in bending or tension the FRC starts to deform. The response needs to be divided into two different stages: the uncracked and the post-cracking behaviour. In the first stage of the response, i.e. uncracked, the response is linear elastic which means that the deflection increases linearly with the increase of the load. In this stage the fibre reinforcement amount generally have no or low effect on the response i.e. the contribution from fibres is present first after cracking. This means that the response before cracking is not affected by the fibres and the response is the same of that of plain concrete (Skarendahl 1990).

The post-cracking response of FRC needs to be separated into a hardening and a softening behaviour according to (Skarendahl 1990), (SS812310:2014 2014) and

[1] Ingemar Löfgren (Adjunct Professor at Chalmers University of Technology, Civil and Environmental Engineering, Structural Engineering), email interview 2015-05-15.

(Prisco et al. 2009). Softening behaviour is characterized by cracking in a single crack while hardening is characterized with several cracks before the peak value is reached (Fischer & Li 2007; Fib 2013). Softening behaviour is when the strength after crack initiation is lower than the strength at crack initiation. Hardening behaviour is when the strength after crack initiation is higher than the strength at crack initiation. Whether the response of FRC follows the hardening or softening curve when loaded depends on several parameters. Such parameters are according to (Skarendahl 1990);

- fibre content
- bond between fibre and concrete matrix
- aspect ratio (relation between length of the fibre and the diameter of the fibre)
- performance of the concrete and
- shape of the fibre

Hardening is common for high performance fibre reinforced cementitious composites (HPFRCC) and also for concrete with high fibre volumes (Prisco et al. 2009). However, HPFRCC is excluded in this report and hence not treated further. In Figure 4, examples of the response for plain concrete loaded in tension and typical tension softening and tension hardening response for FRC (in this case SFRC) are shown. The stress-strain relation for FRC (both hardening and softening) loaded in bending has a similar shape as that of the response of FRC loaded in tension.

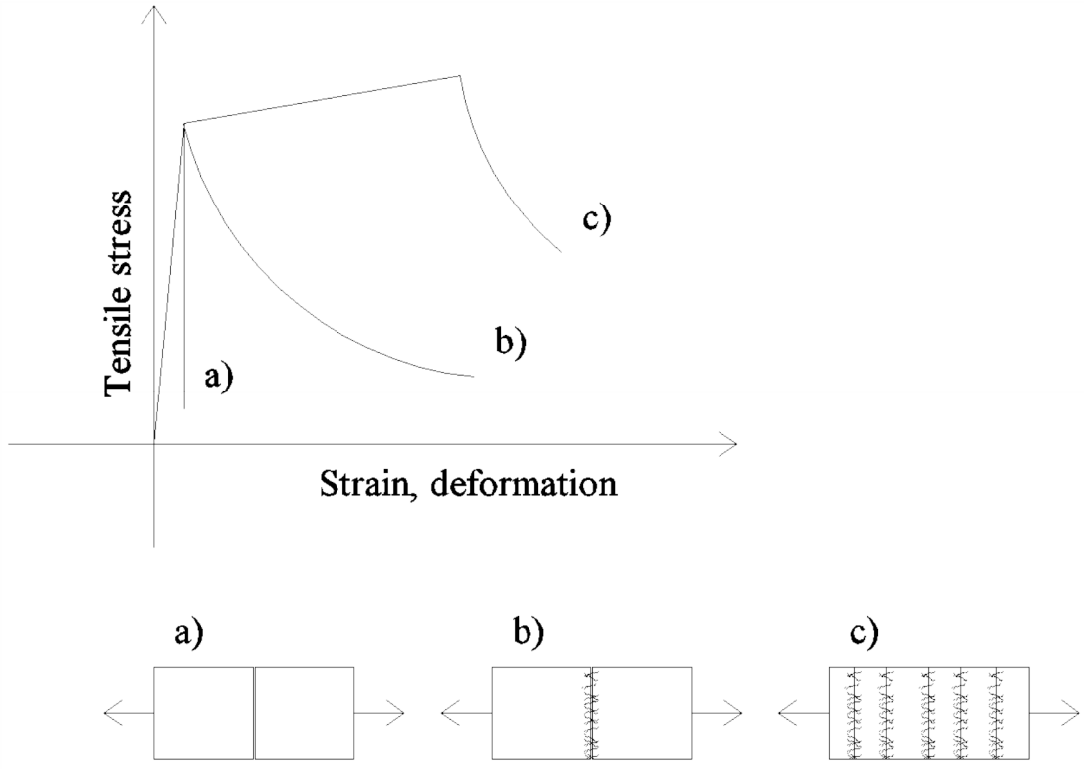

Figure 4 *Typical stress-strain behaviour of concrete; a) plain concrete, b) tension softening behaviour, and c) tension hardening behaviour.*

Although the tensile behaviour is similar to that of bending, the same concrete can have different behaviour regarding softening and hardening in bending and tension. If a FRC has a tension softening behaviour it can have either softening or hardening behaviour in bending. However, if it has a tension hardening behaviour it will also have a bending hardening behaviour (Löfgren 2005; Prisco et al. 2009), see Figure 5.

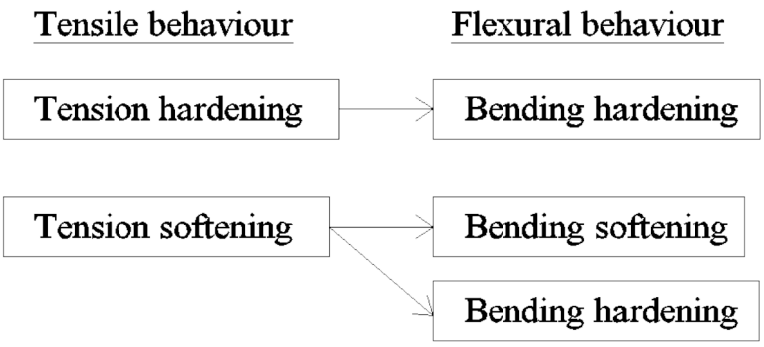

Figure 5 How the tensile behaviour is linked to the flexural behaviour of FRC.

2.1.3 Fracture energy

The so called fracture energy, G_f, represents the energy consumed when a crack develops (Peterson 1980; Plos 2000). The fracture energy is given by the area under the stress-crack opening relation (Plos 2000). Concrete without reinforcement is a brittle material, hence characterized by sudden failure. With added reinforcement the concrete matrix becomes more ductile and will therefore have higher fracture energy.

FRC has higher fracture energy than plain concrete, meaning that more energy is needed for a FRC to fail. Moreover, this property of having higher fracture energy is related to the enhanced toughness of FRC, i.e. higher fracture energy means better toughness properties (Löfgren 2005). In Figure 4 showed in Section 2.1.2, the increased fracture energy can be seen when comparing ordinary concrete (a) to FRC with tension softening behaviour (b) and tension hardening behaviour (c).

2.1.4 Residual strength

The residual strength can be characterized by the remaining load carrying capacity of a cracked concrete structure. A crack can significantly decrease the strength of a structure, therefore it is important to predict the remaining strength in a potentially cracked structure to be able to prevent failure throughout its service life (Lubliner et al. 1989; Miedlar et al. 2002). As mentioned before, fibres are added to concrete to positively affect the post cracking behaviour, including increasing the residual strength (Skarendahl 1990).

The residual strength, received from bending tests of FRC beams, is often used to classify FRC. The fact that it is based on bending tests and not pure tensile tests is due to the difficulties in operation of uniaxial tension tests for FRC (Prisco et al. 2009). Residual flexural tensile strengths in FRC structures are hence classified by residual flexural tensile strength classes, so called R-classes (SS812310:2014 2014), see Table 1.

Table 1 *Residual flexural tensile strength classes for fibre concrete according to* (SS812310:2014 2014).

Class R_1	$f_{R,1}$ [MPa]	Class R_3	$f_{R,3}$ [MPa]	Class R_4	$f_{R,4}$ [MPa]
$R_1$1	1.0	$R_3$1	1.0	$R_4$1	1.0
$R_1$2	2.0	$R_3$2	2.0	$R_4$2	2.0
$R_1$3	3.0	$R_3$3	3.0	$R_4$3	3.0
$R_1$4	4.0	$R_3$4	4.0	$R_4$4	4.0
$R_1$5	5.0	$R_3$5	5.0	$R_4$5	5.0
$R_1$6	6.0	$R_3$6	6.0	$R_4$6	6.0

The residual flexural tensile strength for $f_{R,1}$, $f_{R,2}$, $f_{R,3}$ and $f_{R,4}$ are the characteristic values obtained from beam testing in accordance to SS-EN 14651 at an age of 28 days. The strength values $f_{R,1}$, $f_{R,2}$, $f_{R,3}$ and $f_{R,4}$ are related to the crack mouth opening displacement (CMOD) of 0.5, 1.5, 2.5 and 3.5 mm respectively (SS812310:2014 2014). See the relationship in Figure 6.

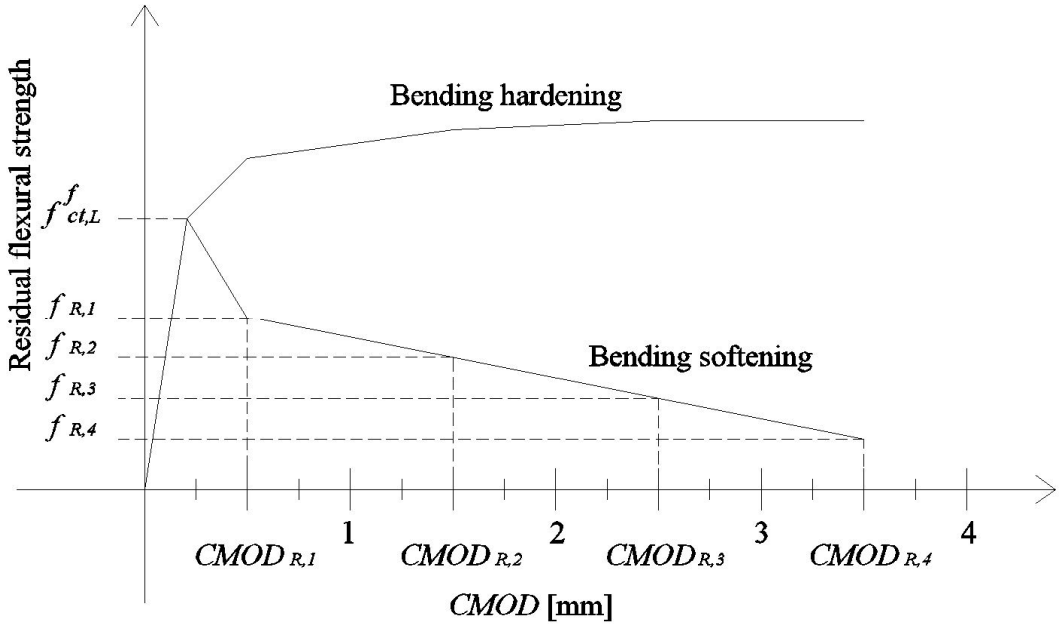

Figure 6 *Schematic behaviour of fibre reinforced concrete with flexural strength in relation to CMOD.*

The behaviour in SLS is related to the $f_{R,1}$ value while the ULS is related to a combination between $f_{R,1}$ and $f_{R,3}$. The classification of FRCs, according to (SS812310:2014 2014), is therefore including both class R_1 and R_3 as follows:

$$CAA / BB - R_1C / R_3D \tag{2-1}$$

Where:

AA Cylinder compressive strength

BB Cube compressive strength

C $f_{R,1}$

D $f_{R,3}$

According to (SS812310:2014 2014) the ultimate residual tensile strength, f_{Ftu}, is defined as the tensile strength at $CMOD_{R,3}$, i.e. at 2.5 mm. Thus the ultimate residual tensile strength, f_{Ftu}, can be received as shown in Figure 7.

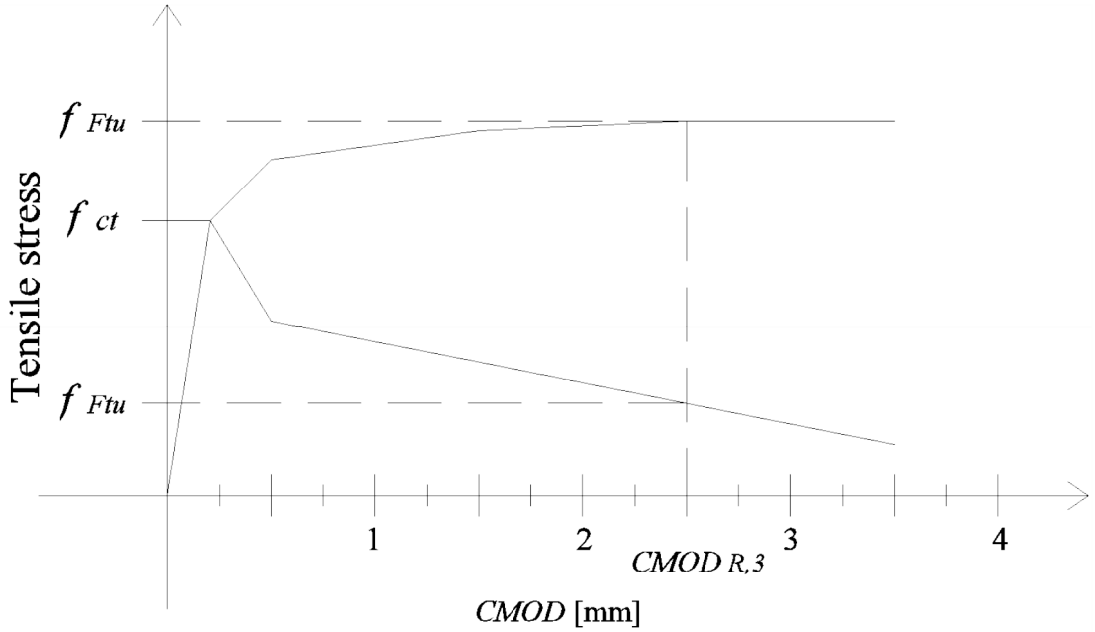

Figure 7 *Visualization of how to obtain the ultimate residual tensile strength f_{Ftu}, according to* (SS812310:2014 2014).

2.1.5 Mechanisms related to mechanical behaviour of FRC

The mechanical behaviour, i.e. the enhanced fracture energy and the residual flexural strength, of FRC is related to many different mechanisms. In this chapter some of these important mechanisms are presented; the crack bridging effect, the direction of the fibres and the bond between the fibre and the concrete matrix. Some specific mechanisms leading to the enhanced mechanical properties in FRC is the following according to (Löfgren 2005);

- matrix fracture and matrix spalling
- fibre-matrix interface debonding
- fibre pull-out
- fibre fracture

- fibre abrasion and plastic deformation of the fibre

These mechanisms are shown in Figure 8.

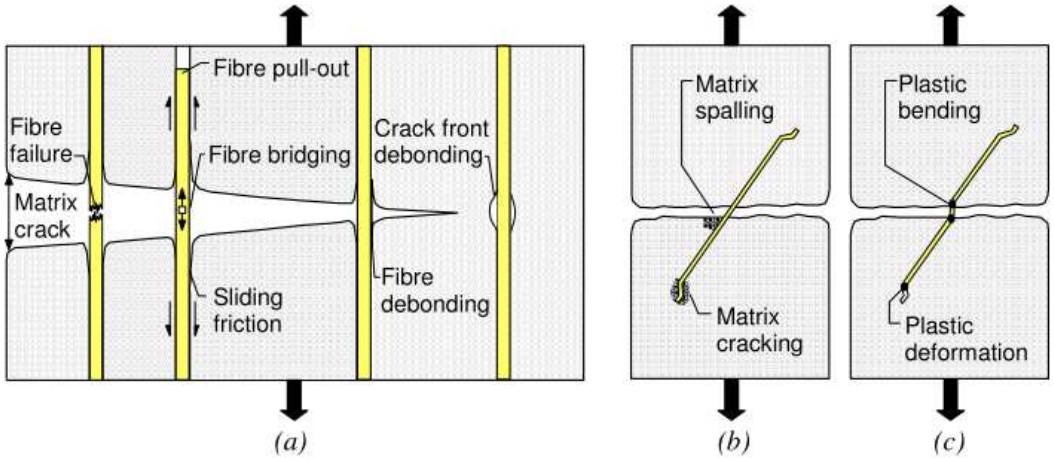

Figure 8 *Mechanisms leading to enhanced fracture energy in FRC; a) fibre failure, fibre bridging and fibre pull-out and debonding, b) matrix spalling and cracking, and c) plastic bending and deformation* (Löfgren 2005).

In plain concrete, the only crack bridging effect is the aggregates bridging the cracks. The increase in post-cracking residual strength of FRC in comparison to plain concrete is due to the additional crack bridging effect of the fibres (Löfgren 2005). The contribution to the post-cracking tensile strength in FRC is hence a combined effect from both fibres and aggregates bridging the crack (Li et al. 1993; Zhang & Li 2004).

In addition to the crack bridging effect, the mechanical properties of FRC members are also affected by the direction of the fibres dispersed in the concrete. This since the direction of the fibres affects how effectively the fibres bridge the cracks. Consequently, it also affects the residual tensile strength. To measure the bridging effect of the fibre due to the orientation of fibres, a fibre orientation factor (η_f) is used in the design of FRC according to the Swedish standard SS 812310:2014. The value of η_f depends on the casting method, fibre length and the dimensions of the structural member. The most favourable orientation of fibres in a structure loaded in bending is horizontally, i.e. in the direction of the load (SS812310:2014 2014).

Another important property of FRC is the bond characteristics between the fibre and the concrete matrix. When mixing concrete together with fibres and the hydration process begins, the bond starts to develop, thus changing its characteristics with time (Löfgren 2005). The resulting final bond is the load transferring mechanism between the fibre and the concrete. Moreover, the fracture energy is generally analogous with the pull-out energy of the fibres (Alwan et al. 1999). According to (Löfgren 2005), the pull-out behaviour of a fibre is dependent on the following factors;

- the type of fibre and its mechanical and geometrical properties
- the mechanical properties of the interface between the fibre and matrix
- the angle of inclination of the fibre with respect to the direction of loading
- the mechanical properties of the matrix

According to (Alwan et al. 1999), the components of bond can be characterized as follows;

- the physical and/or chemical adhesion between fibre and matrix
- the frictional resistance
- the mechanical component (coming from a particular geometry of the fibre, e.g. deformed, crimped or hooked fibres)
- the fibre-to-fibre interlock

Examples of ways to improve the bond characteristics of the fibre are by changing the geometry of the fibre (see Section 2.2 for different fibre geometries) and by adding different coatings to the fibre (Löfgren 2005).

2.2 Different kinds of fibre reinforced concretes (FRCs)

Fibres used as reinforcement in concrete are of relatively short length and diameter in comparison to reinforcement bars. The fibres are freely dispersed in the concrete matrix with short distance between them which results in an even distribution in the concrete section (Löfgren 2005).

Different types of fibres can be used for different aims depending on for example how they affect the uncracked and post-cracking response of the concrete member, how they affect the durability with regard to corrosion, spalling of the concrete or resistance to fire. As an example, steel fibres are used for both ULS and SLS control while the application most common for synthetic fibres is to control cracking in early stages (Löfgren 2005).

Depending on the application, fibres can be combined with other type of fibres, so called hybrid fibre reinforced concrete (HFRC), or rebars to attain a specific wanted behaviour.

In order for the fibres to have a reinforcing effect in the concrete, some properties are advantageous according to (Naaman 2003);

- the tensile strength of the fibre needs to be higher than that of the concrete matrix (2-4 times greater).
- the modulus of elasticity of the fibre needs to be greater than the one of the concrete (3 times greater).
- the bond between the fibres and the concrete needs to have the same or higher strength than the tensile strength of the concrete (the bond needed at least until first crack).
- ductile fibre material, i.e. to increase the fracture toughness of the concrete.

Moreover, for the FRC to be a safe and reliable choice in the construction industry, it needs to be durable. One important aspect of durability is the alkalinity. The reason is due to the chemical environment in the concrete which can lead to a relatively high alkalinity. This high alkalinity can lead to a degradation of the fibre if it has not been taken into account in design or in the choice of fibres (Löfgren 2005).

Today, there are many different fibres available on the market. Some of them are presented in this section classified with regard to their main material. Focus in this chapter are steel, glass and basalt fibres. Fibres can also be divided and described in terms of shape, size, production method and intended use.

The cross sectional area of a fibre can be shaped for example as a circle, a quadrant, a rectangle, a triangle, an ellipse, a hexagon, an octagon or be irregular in shape (Löfgren 2005), see Figure 9.

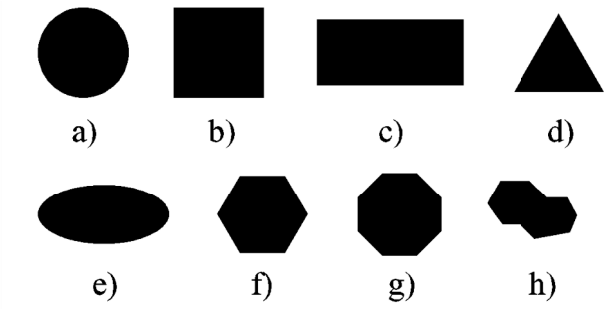

Figure 9 *Different cross sectional shapes of fibres, a) circular, b) quadratic, c) rectangular, d) triangular, e) elliptical, f) hexagonal, g) octagonal and h) irregular.*

The shape of the fibres can be for example coned, straight with or without end-hooks, end knobs or paddles, crimped, bow shaped, toothed, surface intended, irregular or twisted (Löfgren 2005), see Figure 10.

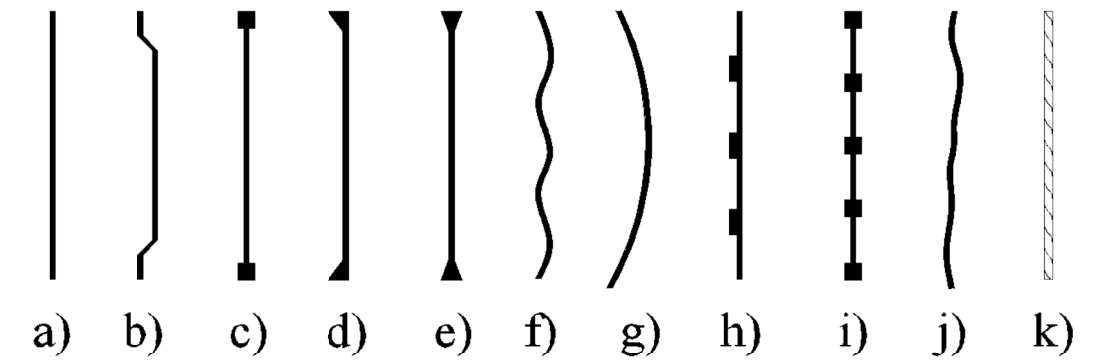

Figure 10 *Different geometries of fibres.*

When talking about FRC in this study, the fibre mentioned is a fibre freely dispersed in the concrete. This reinforcing fibre can either be made of a solid material or being built up by many micro fibres, which depends on the material and manufacturing process. In addition, there is also something called micro FRC. This concrete is reinforced by freely dispersed micro fibres, which in comparison to FRC, are not bundled together to create bigger fibres. According to (Löfgren 2005), these two kinds of concrete reinforcement give different behaviours on the fracture process. Obviously, if wanting the same amount of bigger and smaller fibres, measured in kg/m^3, there is a need of a higher number of the smaller fibres compared to the bigger ones.

2.2.1 Steel fibre reinforced concrete (SFRC)

Within all industries worldwide, the steel fibre is the most common fibre reinforcement since it stands for around 50% of the total fibre production. Fibres made out of metal are also the most common ones in the building material industry. The shape of the fibre has been developed and improved during the past years and can now be found more slender and with more complex shapes. The fibre can be produced with shaped ends to improve the bond strength with the concrete and it can also have different coatings such as brass, for improving bond characteristics, or zinc, to improve corrosion resistance (Mondo 2011).

(CEN 2006) defines steel fibres as “straight or deformed pieces of cold-drawn steel wire, straight or deformed cut sheet fibres, melt extracted fibres, shaved cold drawn wire fibres and fibres milled from steel blocks which are suitable to be homogeneously mixed into concrete or mortar”.

In year 1910 in California, the idea of reinforcing concrete with short wires was patented. A few years after, in 1918, a method of modifying concrete by adding long fibres of steel, wood or any other material was patented in France by H. Alfsen. He was also the one that paid extra attention to the interfacial bond between fibres and mortar. After these first patents, many other followed. These were generally modifications of the already patented fibres and applications of already made SFRC. In 1943, G. Constancinesco patented the steel fibres with some shape modifications from earlier patens. Also, he mentioned the increased amount of energy absorption of SFRC (Katzer 2006).

Since the 1960’s, there have been made extensive researches on the behaviour of SFRC. The researchers were driven by the enhanced durability, strength and toughness of the concrete when adding steel fibres (Musmar 2013).

SFRC has been commonly used in the building industry within structures where the fibre reinforcement is not essential for the safety of the structure, e.g. industrial floors and pavements (Brandt 2008). Nowadays, the research is heading towards using the fibres as a substitute of the shear reinforcement (Mondo 2011). Compared to other FRCs, more experiments and research have been performed on SFRC. Standards and codes are today being developed within the SFRC and the research is still an ongoing process. The first serious attempts of testing and modelling the behaviour of SFRC were made in the beginning of the 21th century when the RILEM Technical Committee 162 TDF published draft recommendations on how to perform tests (Kooiman 2000).

The Swedish standard (SS812310:2014 2014) has been developed to complement SS-EN 1992-1-1, which does not include the design of FRC. The standard is developed on the basis of steel fibre concrete, and just to a small extent of polymer fibre concrete. The intention is to develop a standard that can be applicable on any fibres, which explains the chosen name “fibre concrete”.

According to (Kooiman 2000), a small amount of added steel fibres does not enhance the tensile strength, but it do increase the deformation capacity in uniaxial tension. In addition to the tensile properties of SFRC with small fibre volumes, the compressive strength is neither increased, as reported by (Shan & Zhang 2012) for fibre volumes less than 0.4%. In bending, on the other hand, a small amount can increase the flexural load-bearing capacity (Kooiman 2000). However, for higher fibre volumes both the compressive strength as well as the tensile strength is enhanced (Kooiman 2000) and (Shan & Zhang 2012). According to (Kooiman 2000) the maximum tensile stress, f_{ct}, is increased from approximately 2.7 MPa for plain concrete to 3.5 MPa for concrete with a steel fibre volume of 3%.

When adding steel fibres to concrete it affects the post-cracking behaviour the most, whereas the pre-cracking behaviour is more affected by the concrete matrix (Olivito & Zuccarello 2010). In addition, (Minelli 2005) and (Kooiman 2000) report that the modulus of elasticity, i.e. the response before cracking, is not markedly affected by the addition of steel fibres.

In a study by (Jansson et al. 2012), experimental tests of SFRC showed that for the same crack width there was an increase in tensile stress with increasing fibre volume, see Figure 11.

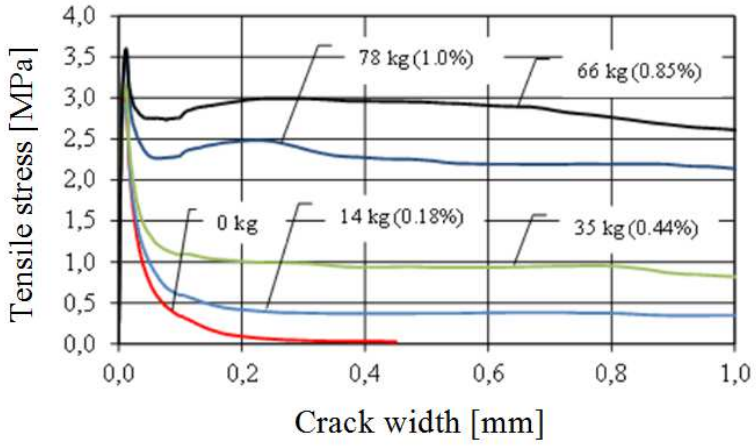

Figure 11 *Tensile stress curves of SFRC by* (Jansson et al. 2012).

It is common knowledge that steel without protection easily corrode. The corrosion resistance of SFRC is depending on if the concrete is cracked or not (Kooiman 2000). The steel in a cracked concrete is more exposed to corrosion than in an uncracked concrete where the protective concrete layer around the steel is reduced.

At the outer surface of an uncracked SFRC, in the carbonation zone, the fibres will corrode quickly. In this zone, the carbon dioxide from the air is penetrating the concrete and is reducing the alkaline environment for the steel fibres, i.e. lowering the pH-value, which makes it easier for the steel to corrode. The depth of this zone depends on the density of the matrix and can be reduced by adding fillers such as fly ash or silica fume (Kooiman 2000).

The fibres beyond the carbonation zone will not corrode since all fibres are embedded in the matrix and no electrical conductor is formed. Besides, the corrosion of fibres in the carbonation zone will not cause any concrete spalling since the increase of fibre cross area will not initiate such high peak stresses. It has been showed that initially the increase of fibre diameter is enhancing the bond between the fibre and mortar. On the contrary, over time the fibres will break due to decreased cross area instead of a slip failure (Kooiman 2000).

2.2.2 Glass fibre reinforced concrete (GFRC)

Glass fibre reinforced concrete (GFRC) is one type of FRC. The GFRC is in comparison to SFRC a new concept in the building industry. However, the development of new fibre types with different compositions is an ongoing process as well as the research of understanding their mechanical properties.

The development of producing glass fibres as reinforcement in concrete starts with the Phoenicians, Egyptians and Greeks, who knew how to stretch melted glass into thin micro fibres. Later on, between year 1933 and 1937, the main development within the glass fibre industry was made. It consisted of the possibility to produce continuous glass filaments with a diameter of 4 microns, by using discontinuous-fibre wool (Gardiner 2009).

The raw material when producing the glass fibre is silica (SiO_2) sand. SiO_2 can be found in the natural rock quartz, where it represents at least 99% of the material. To manufacture glass fibres, SiO_2 is heated up to a temperature of 1720°C and is then cooled quickly. This is the same production procedure as used in the 1930s. The main steps in this procedure of making glass micro fibres are; (1) Batching, (2) melting, (3) fiberization, (4) coating and (5) drying/packaging (Gardiner 2009). See the production process in Figure 12.

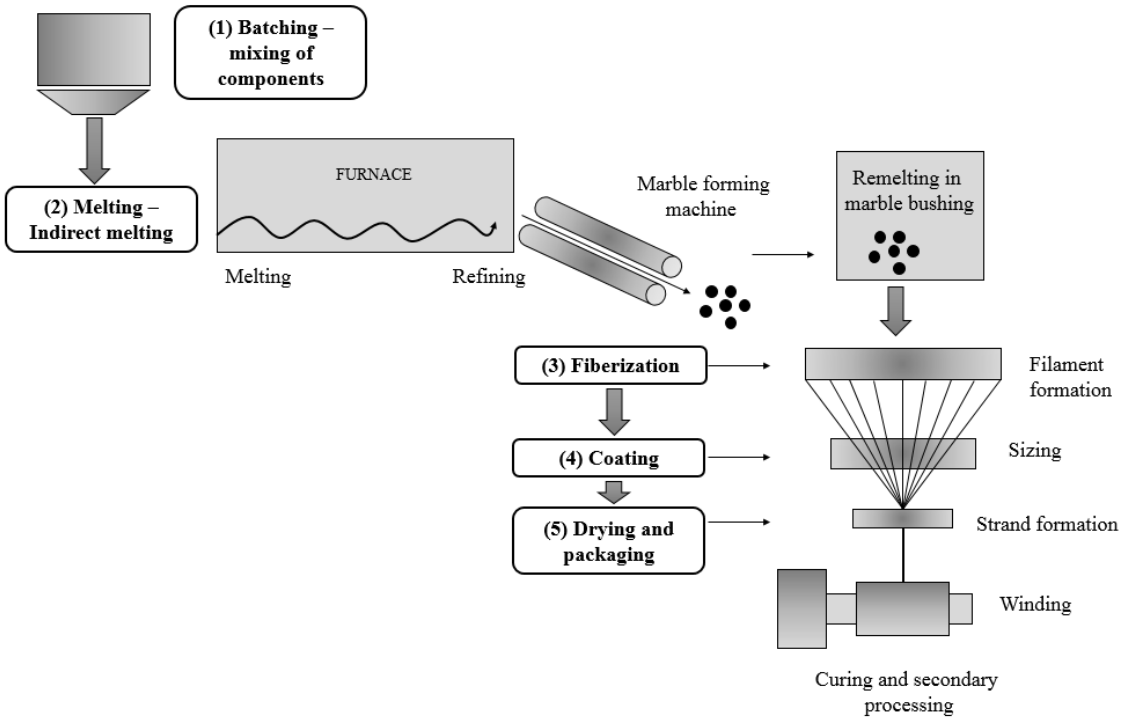

Figure 12 Manufacturing process of glass micro fibres.

Batching (1) is the first production process where all components of the glass micro fibre are mixed together. Glass micro fibres can be made from SiO_2 alone but other ingredients can be added to enhance properties for certain applications or to reduce the working temperature (Gardiner 2009). It is of high importance to carefully weigh the exact quantities of the different contents and that these are batched thoroughly.

The most widely used melting process (2) of making glass micro fibres is the indirect melting, also called marble remelt. In this process, the molten glass is divided and rolled into marbles of 15 to 16 mm in diameter which are cooled and sent to a fibre manufacturing facility where it is remolten. Using the marble shape enables visible inspection of the glass to reduce impurities which results in less quality defects in the final product (Gardiner 2009).

When sent to a fibre manufacturer, the fiberization process (3) can begin where the glass marbles are remolten and the molten glass is pushed through an erosion resistant bushing with 200 to 8000 very fine openings. When the continuous filament fibres exit the bushing of a temperature of around 1200°C, water jets are used to cool the material. Thereafter, a winder catches the molten streams of filaments and since it spins in a higher speed than the filaments exit the bushing, it stretches the fibres into even thinner diameters. The filaments have diameters of 4 up to 34 µm, which is around one-tenth of the diameter of human hair (Gardiner 2009).

In the coating process (4), a chemical coating called "size" is added to the filaments. This size can consist of lubricants, binders and/or coupling agents. Usually, size is added by weight in an amount of 0.5 to 2.0 percent. The lubricants help the fibres from abrading and breaking while the coupling agents for example are strengthening the adhesive bond at the fibre-matrix boundary (Gardiner 2009).

Finally, the drying and packaging process (5) is performed. Around 50 to 1600 filaments are collected into a bundle to form a glass strand. The strand is then wounded onto a drum and into a forming package which is being dried in an oven since it still can be wet from water cooling and sizing. The forming package is then ready to be processed into chopped fibres, roving or yarn. A roving is a collection of a number of strands, for instance 15 strands, which have little or no twist. Yarn, on the other hand, consists of one or more strands and can also be twisted to protect it from abrasion of following processes (Gardiner 2009). These products can be developed into fibres suitable as reinforcement in concrete.

There are many studies regarding the durability of glass fibres in concrete with focus on the degradation of the fibre due to the alkaline environment within the concrete. Three of these are (Karbhari et al. 2003), (Purnell & Beddows 2005) and (Lipatov et al. 2015).

(Karbhari et al. 2003) stated that within the glass fibre industry, it is well known that bare glass fibres are harshly deteriorated in alkali solutions. Concrete can be seen as one such alkali environment. Even though sizes around each filament can be expected to protect from alkali attacks, an alkali environment can accelerate the degradation of the resin and the bond mechanism between the fibre and the concrete matrix (Karbhari et al. 2003).

According to (Purnell & Beddows 2005), ordinary Portland cement (OPC) is very alkaline in damp conditions due to the soluble alkalis. It is the OH^- ions that attack the Si-O-Si structure of the glass. The so called, alkali resistant (AR-glass) fibre is not as vulnerable to alkali environment as other glass fibres due to the high content of zirconium oxide (ZrO_2). This is since the Zr-O bond is shown to be less reactive compared to the Si-O bond. With an AR-glass fibre, the rate of corrosion is being slowed down due to a rich zirconia layer being built up at the surface of the glass fibre. The alkalinity of the concrete matrix, i.e. the available OH^- ions, is likely determining the rate of corrosion of the glass fibre (Purnell & Beddows 2005).

The AR-glass fibre was developed in order to increase the durability of the glass fibre in cementitious materials, according to (Lipatov et al. 2015). This fibre is now commonly used in the construction industry. The study by (Lipatov et al. 2015) also presents three main approaches to increase the alkali resistance of fibres;

- improving glass composition
- applying new sizing and coating, and
- using cements and concrete additives

The alkali resistance of glass fibres increases with higher zirconia content and that is why the majority of all AR-glass fibres contain a high amount of zirconia

One study which did not evaluate the durability of only the fibre itself, but the durability of the GFRC, was (Criado et al. 2014). The durability was evaluated when partially replacing OPC with pyrolysis glass fibres in a steel bar reinforced concrete. The corrosion potentials, i_{corr}, were measured for the OPC with 5%, 10% and 15% of the recycled glass. The smaller amounts showed similar values as the reference material of

0% fibres, but the OPC with 15% of fibres showed a significant increase in i_{corr}. The high i_{corr} value, was a value typical for very high corrosion rates according to standards (Criado et al. 2014).

2.2.3 Basalt fibre reinforced concrete (BFRC)

Basalt fibre reinforced concrete (BFRC) is one type of FRC. The BFRC is, as the GFRC, not as widely investigated as the more commonly used SFRC. The manufacturing of basalt micro fibres is similar to the one of glass micro fibres (Fiore et al. 2014).

Basalt is a raw material originated from frozen lava (Fiore, V. et. al., 2014), which is the most common volcanic rock (Loberg, B., 2015). Its melting point is between 1500-1700°C (Fiore, V. et. al., 2014). The natural material basalt can in Sweden be found in central Skåne, where tens of smaller basalt volcanoes were active 65-200 years ago (Loberg 2015). Much larger areas of basalt plateaus can be found in Deccan in western India, in Paraná in Brazil and both the Columbia River plateau and Snake River plateau are examples of these plateaus that can be around hundreds of thousands square meters big. The primary composition of the basalt rock is generally comprised by various forms of oxides where silica-oxide is the most ample one (Adhikari 2013).

In 1953-1954 the basalt micro fibre was developed by Moscow Research Institute of Glass and Plastic (Fiore et al. 2014). Since all basalt rocks are not chemically identical, the basalt deposits needs to be carefully chosen to produce the basalt micro fibres (Zych & Krasodomski 2012). To make this fibre, basalt rock is first crushed and washed before it is melted in a furnace at 1450-1500°C. The melted material is thereafter forced through small nozzles to produce the continuous fibres and this method is called continuous spinning. Basalt rocks which contains at least 46 percent of silica-oxide is generally consisted good for producing fibres (Adhikari 2013). Figure 13 shows basalt material, from stones to micro fibres.

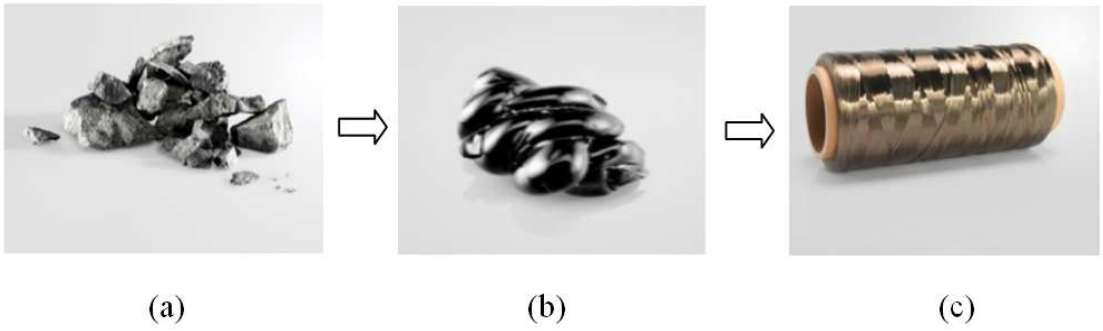

Figure 13 *Production procedure from basalt stone to fibre roving, (a) basalt stone, (b) melted basalt, and (c) basalt micro fibre* (ReforceTech 2015).

The production process of the basalt micro fibre is both easier and less energy consuming than for other fibres (Dhand et al. 2014). Moreover, the basalt fibre is not containing any additives which is an advantage in cost (Kabay 2013). The basalt micro fibre is also a fibre with high tensile strength and temperature resistance (Dhand et al. 2014).

Except from being developed into reinforcing fibres in concrete, the basalt micro fibre is being transformed into products within other industries. Such products can be textile

fibre, rock wool, friction materials such as brake pads and linings, high-temperature insulation, fire protection and floor tiles (Parnas et al. 2007).

Within the building industry, the basalt micro fibres can be developed into many reinforcement products for concrete structures such as bars, nets and also as dispersed fibres, which are built up by a high number of micro fibres. Currently, the basalt micro fibre has only been used in construction engineering to a certain extent since it is a fairly new material with not as much research, experiment and experience within the area compared to other reinforcement materials (Chen 2013).

Through crack bridging, see Section 2.1.5, the dispersed basalt fibres can improve the mortar's properties such as ductility, impact resistance, compressive strength and tensile strength of concrete matrices. It can also restrain cracking due to plastic shrinkage (Chen 2013). Since the basalt fibre is ceramic and has similar specific density as cement mortar it will not sink or float in the fresh casted concrete, instead it has the advantage of being uniformly distributed.

Concrete reinforced with dispersed basalt fibres has higher strength in bending, reduced shrinkage and increased crack resistance compared to plain concrete (Stupishin et al. 2014).

In comparison to steel, the basalt reinforcement is non-corrosive, non-conductive and also non-magnetic (Knudsen & Lie Skadal 2012).

Like the glass fibres, the basalt fibres can also be vulnerable for alkali environments. Some studies made within this area are (Scheffler et al. 2009), (Rybin et al. 2013) and (Lipatov et al. 2015).

In the study by (Scheffler et al. 2009), the ageing of AR-glass and basalt micro fibres were studied in NaOH and cement solutions. A strong dissolution of the outer layer of all fibres in the NaOH solution led to a decrease in filament diameter and strength. In comparison, when subjected to ageing in a cement solution, the fibres did not show any decrease in failure stresses but local attacks were revealed. According to this study, the alkaline resistance of basalt micro fibre was assumed to be much lower than the resistance of the AR-glass.

(Rybin et al. 2013) made a study of the alkali resistance of basalt micro fibres. The study compared the durability of bare basalt fibres with fibres which had been coated with either a porous or dense zirconia (ZrO_2) layer. The experimental tests in NaOH solutions gave the results that the presence of a zirconia layer is slowing down the corrosion of the basalt fibre in alkali solution. A denser coating gives a better resistance to corrosion of the fibre.

In (Lipatov et al. 2015), the lower alkali resistance of basalt fibres compared to glass fibres is again stated. When subjected to alkali solutions of NaOH, the basalt fibres got a corrosion layer at the surface. Other studies have described a similar layer for glass fibres in alkali solutions. Even though the tests were done in more severe condition than in ordinary concrete, the alkali resistance of zirconia doped basalt fibres had an equivalent performance with AR-glass fibres in concrete.

2.2.4 MiniBar reinforced concrete (MRC)

One specific fibre reinforcement product available on the market is the macro fibre MiniBar. The MiniBar is shaped as a helix with a rough surface to interlock with paste

and aggregate to receive better pull-out resistance, see Figure 14. It has a resin to lock in the helix geometry so the micro fibres, which the MiniBar consists of, cooperate. To produce the helix shape of the fibre, a large number of parallel micro fibres are twisted around the main collection of parallel micro fibres (Adhikari 2013).

Figure 14 *MiniBar structure.*

The production of MiniBars is done by using an automated Wet lay-up process where fibres are drawn into polymer filled baths of vinyl ester which when cured is yielding the reinforcing fibres together (Adhikari 2013). The MiniBars are mixed directly in fresh concrete with the main intention of increasing the tensile and residual strength of the hardened concrete. The MiniBar can be made both of AR-glass and basalt micro fibres, see Figure 15. In Figure 16, the steps from basalt micro fibre to MRC can be seen.

(a) (b)

Figure 15 *MiniBars in different materials; a) AR-glass MiniBars, and b) basalt MiniBars.*

(a) (b) (c)

Figure 16 *Steps from basalt microfiber to MRC; (a) shows basalt fibre roving before production of MiniBars, (b) is one type of MiniBar, and (c) shows a failure surface of basalt MRC* (ReforceTech 2015).

The fibres can be chosen with different lengths to achieve the appropriate embedment length, i.e. longer for lower strength concretes and shorter for higher strength concretes. When using the MiniBars, a bond failure is wanted and the length of the fibre is therefore designed for this (ReforceTech 2015).

In a study made by (Adhikari 2013), tests were done on both the MiniBar fibre and also on the MRC. The tests of the bare MiniBars were done with diameters of 0.66 mm. Uniaxial tests of both AR-glass and basalt MiniBars showed a similar modulus of elasticity (E-module) of the two fibres and higher tensile strength for the AR-glass MiniBar. See mean values of the tests in Table 2. The stress-strain curves obtained from the uniaxial tensile tests also showed a linear curve until a brittle failure for both fibre materials.

Table 2 Material properties of AR-glass and basalt MiniBar.

	AR-glass MiniBar	Basalt MiniBar
E-module [GPa]	46	44
Max load [kN]	0.82	0.94
Rapture strain [-]	0.019	0.023
Max stress [MPa]	955	1079

Direct tensile tests of the MRC were done by (Adhikari 2013), but since no standard test method was available, an own test method was used. The concrete used had a MiniBar volume of 0.5%. From the test results obtained in the study, there could not be seen any significant increase in split tensile strength compared to plain concrete. The test performed, exhibited strain hardening behaviour. Since there was a lack of historic test standards, there were many uncertainties regarding parameters that might affect the results. It was also stated in the study that standard test methods are needed for direct tensile tests which can include the effect of e.g. fibre dosage and specimen geometry. Also, it was stated that more tests with varying fibre volume of the MiniBar were needed.

The specific gravity of the MiniBar fibre is closer to the specific gravity of concrete than for the steel fibre (Adhikari 2013). This gives the property of a fibre that neither floats nor sinks when mixed in fresh concrete.

Another study made on the specific basalt MiniBar was done by (Knudsen & Lie Skadal 2012). They wanted to show the influence of MiniBars in hardened concrete. The study included tests of three different large beam types, where each type was casted in two equal beams. The first beam couple included three longitudinal bars, which were placed in the longitudinal direction of the beams, and no fibres. The second beam couple included the same amount of the longitudinal bars but also a fibre amount of 0.75%. The third beam couple had the same fibre amount as the second couple but an increased longitudinal reinforcement to a total amount of seven bars. The results of the tests showed shear failures in beam couple one and three, but not in the second beam couple. Since the only difference between beam couple one and two is the added fibres this showed that the basalt fibres had a clear effect on the shear capacity. The increase in

shear capacity was at least 10%, based on the results of these beams (Knudsen & Lie Skadal 2012).

2.3 Shear behaviour of concrete structures

The aim of shear design of reinforced concrete structures is to avoid failure due to shear. Flexural failure is preferable to shear failure because of, according to (Minelli 2005), the fairly brittle and unstable nature of failure due to diagonal cracking. A solution to this problem, i.e. premature failure due to shear, is to reinforce the concrete member with sufficient shear reinforcement.

There are many theories of how to take the shear capacity of concrete structures into account in design calculations. Some examples of such theories are: the $(V_s + V_c)$ approach, the variable angle truss model, the Compression Field Theory (CFT) and the Modified Compression Field Theory (MCFT) (Collins & Mitchell 1987).

Different design codes treat shear design differently, regarding which method that is used. Model code treats this problem by suggesting four different levels of shear design, each level according to different shear theories. These four levels are (Fib 2013);

- Level 1: Simplification of level 3
- Level 2: Variable angle truss model
- Level 3: Simplified MCFT
- Level 4: MCFT

The international federation for structural concrete (fib) shear workshop was held in Italy in 2010 to evaluate different shear approaches to be used in the Model code 2010 edition. At the workshop the level of accuracy was also evaluated, which resulted in showing that all four models are more or less conservative. The most conservative model was the level 1 approach following the least conservative model in level 4, the MCFT (Minelli & Plizzari 2011).

To understand the theories behind shear behaviour, the concept of principal stresses is described in Section 2.3.1. This is followed by a more thorough description of the main shear theories in this thesis work; the CFT, the MCFT, the MCFT extended to SFRC and the Simplified FRC-MCFT.

2.3.1 Principal stress

Concrete beams subjected to bending are exposed to both longitudinal and vertical stresses, i.e. both flexure and shear. A Mohr circle is used to visualize how the stress components in a small stressed element work together as principal stresses, in this case for principal stress inclination of 45 degrees (Minelli 2005), see Figure 17.

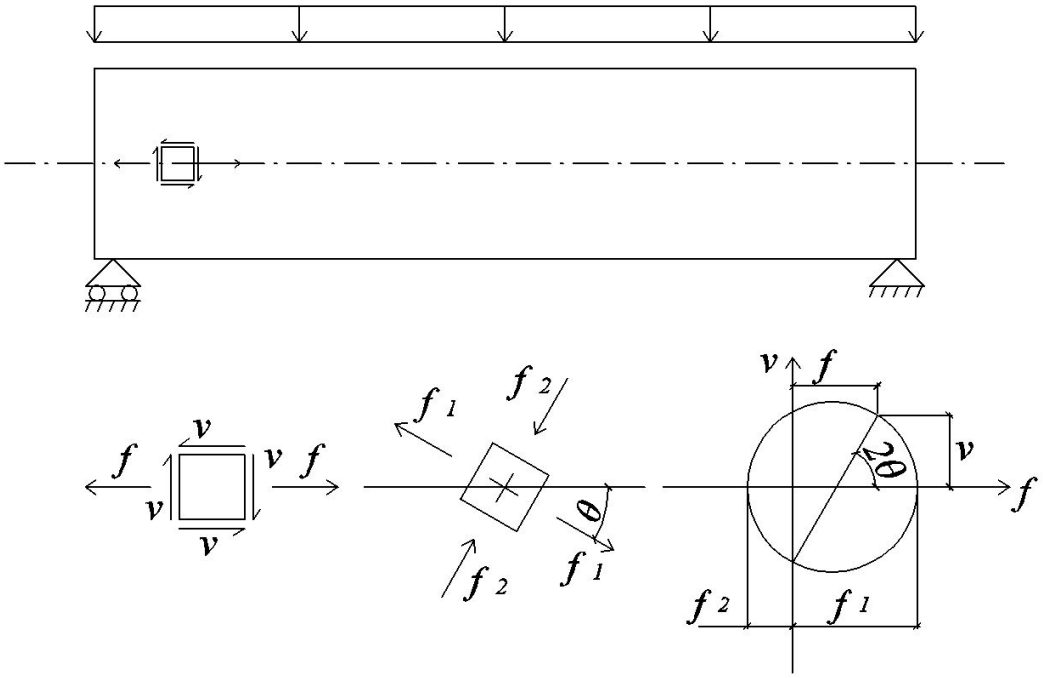

Figure 17 Visualization of principal stresses in a beam loaded in bending.

Further, the principal tensile stress and the principal compressive stress (when inclination of principal stresses is 45 degrees) are, according to (Minelli 2005), being obtained from transformation of the longitudinal and vertical components of a small stressed element:

$$f_1 = \frac{1}{2}\left(f + \sqrt{\left(f^2 + 4v^2\right)}\right) \tag{2-2}$$

$$f_2 = \frac{1}{2}\left(f - \sqrt{\left(f^2 + 4v^2\right)}\right) \tag{2-3}$$

where f_1 is the tensile principal stress, f_2 is the compressive principal stress, f is the tensile longitudinal stress and v is shear stress.

The inclination angle of the principal stresses can be obtained from:

$$\tan 2\theta = \frac{2v}{f} \tag{2-4}$$

$$\tan \theta = \frac{v}{f_1} \tag{2-5}$$

where θ is the inclination angle of the principal compressive stress.

2.3.2 Mechanisms of shear

When the principal tensile stresses exceed the cracking strength of concrete, diagonal cracks will occur in a direction of 90° in relation to the stress direction. The cracks can appear in different ways, as web-shear crack or flexure-shear cracks (Collins & Mitchell 1987), see Figure 18.

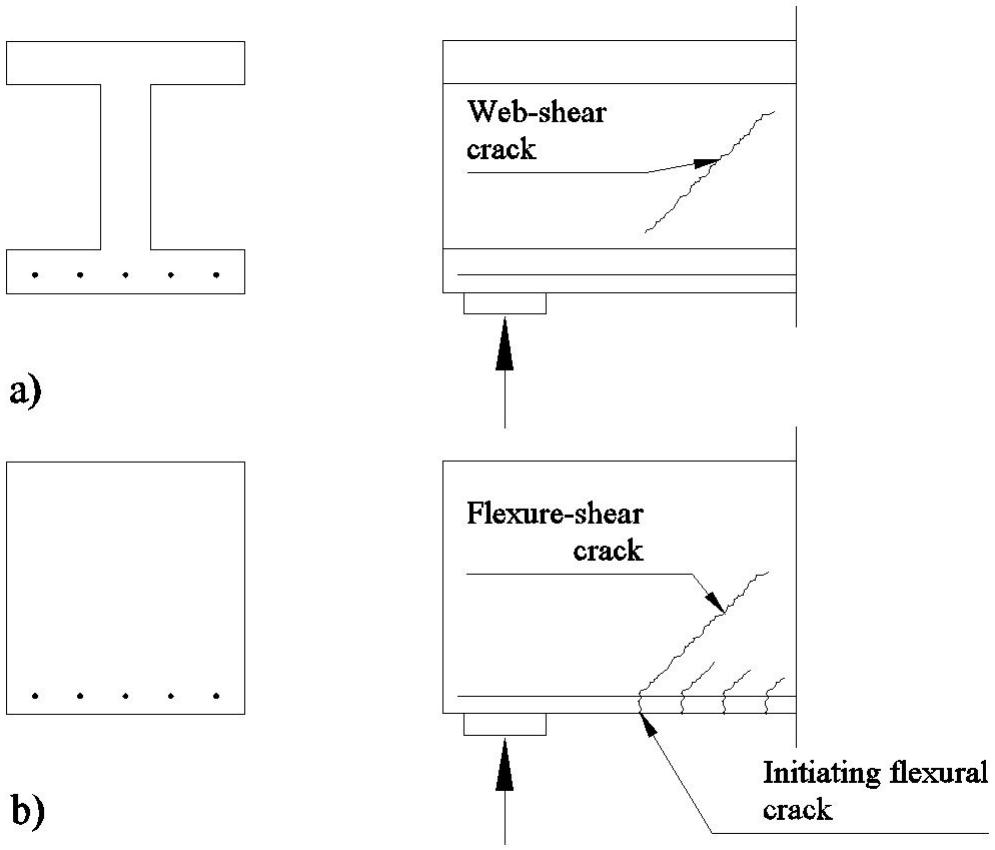

Figure 18 *Different kinds of diagonal cracking a) Web-shear crack, and b) Flexure-shear crack.*

Shear failure is characterized with brittle fracture behaviour, which is unfavourable in comparison to ductile failure due to its rapid failure process. There are several mechanisms which resist shear stresses, and hence prevent failure due to diagonal cracking. In concrete reinforced with conventional reinforcement these mechanisms are according to (Minelli 2005);

- the tensile stress in the stirrups
- the dowel action in longitudinal reinforcement
- the shear transfer in the uncracked compressive zone
- the residual tensile stresses
- the aggregate interlock or interface

The tensile stress in the stirrups contributes with a vertical force in the crossing of the diagonal cracks, which leads to enhanced shear strength. The contribution from the dowel action in longitudinal reinforcement is due to that the dowel (reinforcement bar) transfers the force between the concrete surfaces in the cracks. This effect comprises two failure modes, the splitting failure (Mode I) and the concrete crushing or bar yielding (Mode II) (Minelli 2005), see Figure 19. The shear transfer in the uncracked compressive zone is due to that there still exist both tensile and compressive principal stresses in all uncracked concrete. Residual tensile stresses can, to some extent, be transferred over cracks with small crack width due to that some concrete remains intact even after cracking and hence bridges the cracks. Finally, the aggregate interlock or interface contributes to the shear transfer mechanism by the friction between surfaces.

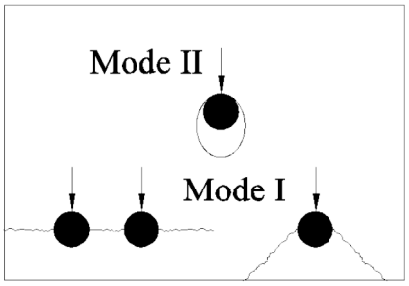

Figure 19 *Failure modes due to dowel action, Mode I: splitting and Mode II: crushing of concrete or yielding in bar.*

The increase in shear strength when adding fibres in concrete is due to the enhanced tensile behaviour after cracking. The mechanisms contributing to this are: the crack bridging effect of the fibres and the increased dowel effect. This leads to residual strength of the structure after cracking. The enhanced tensile strength in FRC due to the bridging effect contribute with a vertical component crossing the diagonal crack and hence increase the shear strength (Adhikari 2013).

FRC is characterized by the fact that when adding fibres in concrete the shear failure can change from brittle to ductile fracture behaviour. Moreover, the shear capacity can also be enhanced. The amount of conventional shear reinforcement can then be reduced for some reported applications, such as in joints where the space for the reinforcement is a problem (Adhikari 2013).

2.3.3 Compression Field Theory (CFT)

The Compression Field Theory (CFT) is adopted for calculation of shear in conventionally reinforced concrete members, i.e. not including fibre reinforcement. To explain the CFT, a beam subjected to a known level of shear force, V, which is symmetrically reinforced and longitudinally prestressed can be analysed. This beam has five unknown parameters: the stress in the longitudinal prestressing tendons, f_P, the stress in the longitudinal bars, f_x, the stress in the stirrups, f_v, the diagonal compressive stress in the concrete, f_2, and the inclination angle, θ, of the diagonal compressive stresses. There are two compatibility equations, three equilibrium equations and the constitutive relationships between the stresses and strains of the materials, which all are used to find the five unknowns. By using these equations and relationships, the load-deformation response of a member subjected to shear can be determined (Collins & Mitchell 1987).

It can be noticed that no tensile strength of the concrete is assumed in the CFT. Assuming that the tensile stresses in concrete will be zero when the strain exceeds the cracking strain, ε_{cr}, is the same as neglecting the concrete after cracking. By doing this, the load-deformation of the bar inside the concrete is assumed to have the same response as for the bar itself in tension. Even though this is not the case, which was experimentally shown in the late 1890s, it's a conservative assumption. It has been showed that the higher strength of the reinforced concrete compared to only a bare bar is due to an effect called tensioning stiffening. This effect is due to that tensile strength still exists in pieces between cracks and by friction between the reinforcement and the matrix (Collins & Mitchell 1987).

2.3.4 Modified Compression Field Theory (MCFT)

The Modified Compression Field Theory (MCFT) was presented by Vecchio and Collins in a paper in the American Concrete Institute Journal (ACI Journal) in 1986. As the name of the theory indicates, it is based on CFT, see Section 2.3.2. In Figure 20, the difference between CFT and MCFT can be seen when the concrete is cracked. MCFT takes the tensile strength of the concrete between cracks into account (c), which the CFT does not (b) (Collins & Mitchell 1987). The MCFT, as well as the CFT, do not account for fibre reinforcement, only conventional bars.

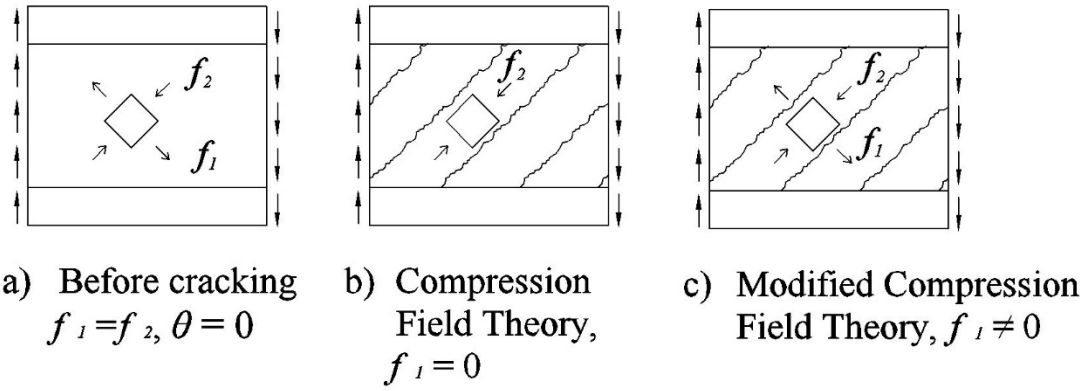

Figure 20 Stress fields in the web of a reinforced concrete I-beam.

The MCFT will in this report be presented based on the work made by (Collins & Mitchell 1987). Their work includes some smaller simplifications and adjustments from the originally developed MCFT by (Vecchio & Collins 1986).

The symmetrical cross-section shown in Figure 21 is by (Collins & Mitchell 1987) used to introduce the equilibrium conditions for MCFT, subjected to pure shear. The principal stresses which are the diagonal compressive stresses, f_2, and diagonal tensile stresses, f_1, will together resist the shear in the section.

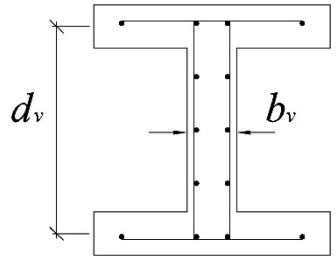

Figure 21 Cross section used in the MCFT to introduce the equilibrium conditions.

The diagonal tensile stresses vary in magnitude in the concrete between the cracks, from zero at the crack locations to highest stresses in the midsection between the cracks, see Figure 22. When hereon stating the equilibrium expressions the average value of f_1 is used, since the equilibrium expressions are obtained by integrating the stresses over the cross-sections (Collins & Mitchell 1987).

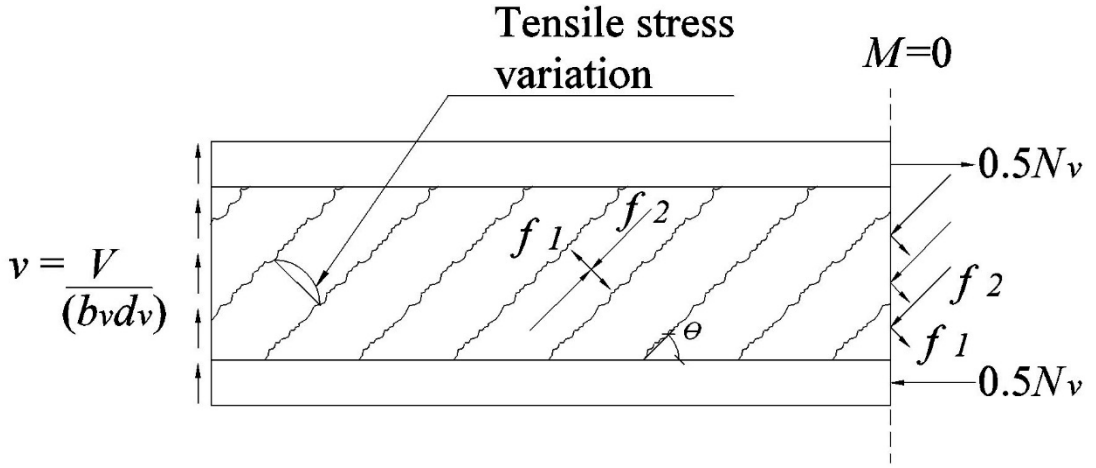

Figure 22 *Equilibrium conditions of a part of a beam according to MCFT and tensile stress variation between cracks.*

In Figure 23 below, the components of the equilibrium needed over one web-reinforcement bar can be seen. This is also shown in equation (2-6) where b_v is the effective web width according to MCFT, s is the stirrup spacing, A_v is the area of stirrups and f_v is the stress in the stirrups.

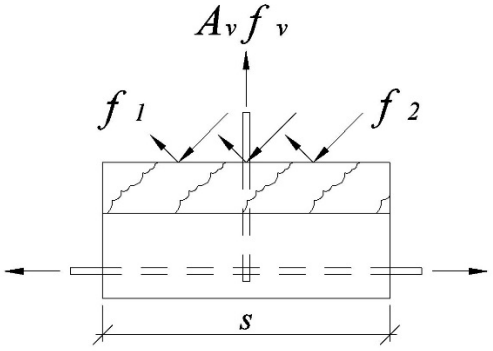

Figure 23 *Equilibrium condition, tension in web reinforcement, according to MCFT.*

$$(f_2 \sin^2\theta - f_1 \cos^2\theta) b_v s = A_v f_v \tag{2-6}$$

From Mohr's stress circle, which has been more deeply explained in Section 2.3.1, the following expression can be established for the principal compressive stress, f_2. V is the shear force and d_v is the effective shear depth.

$$f_2 = (\tan\theta + \frac{1}{\tan\theta})\frac{V}{b_v d_v} - f_1 \tag{2-7}$$

Substituting f_2 in equation (2-6) with f_2 from equation (2-7) gives the following expression:

$$V = \frac{A_v f_v}{s}\frac{d_v}{\tan\theta} + \frac{f_1 b_v d_v}{\tan\theta} \tag{2-8}$$

If there are no axial stresses, there is an unbalance between the compressive and tensile stresses also in the longitudinal direction of the beam. This is equilibrated by a tensile force, N_v, in the longitudinal reinforcement, which is given by the following expression:

$$N_v = (f_2 \cos^2\theta - f_1 \sin^2\theta) b_v d_v \tag{2-9}$$

Substituting f_2 in equation (2-9) with f_2 from equation (2-7), gives the following expression:

$$N_v = \frac{V}{\tan\theta} - f_1 b_v d_v \tag{2-10}$$

(Collins & Mitchell 1987) are recommending to use the relationships for cracked and uncracked concrete seen in equation (2-11) and (2-12), where the bond characteristics of the reinforcement and the type of loading are taken into account by α_1 and α_2 (Collins & Mitchell 1987). This relationship can be seen in Figure 24.

$$\text{if} \quad \varepsilon_1 \le \varepsilon_{cr} \text{ then } f_1 = E_c \varepsilon_1 \tag{2-11}$$

$$\varepsilon_1 > \varepsilon_{cr} \text{ then } f_1 = \frac{\alpha_1 \alpha_2 f_{cr}}{1 + \sqrt{500\varepsilon_1}} \tag{2-12}$$

where ε_1 is the principal tensile strain, ε_{cr} is the strain at crack initiation, E_c is the modulus of elasticity for concrete and f_{cr} is the stress at crack initiation.

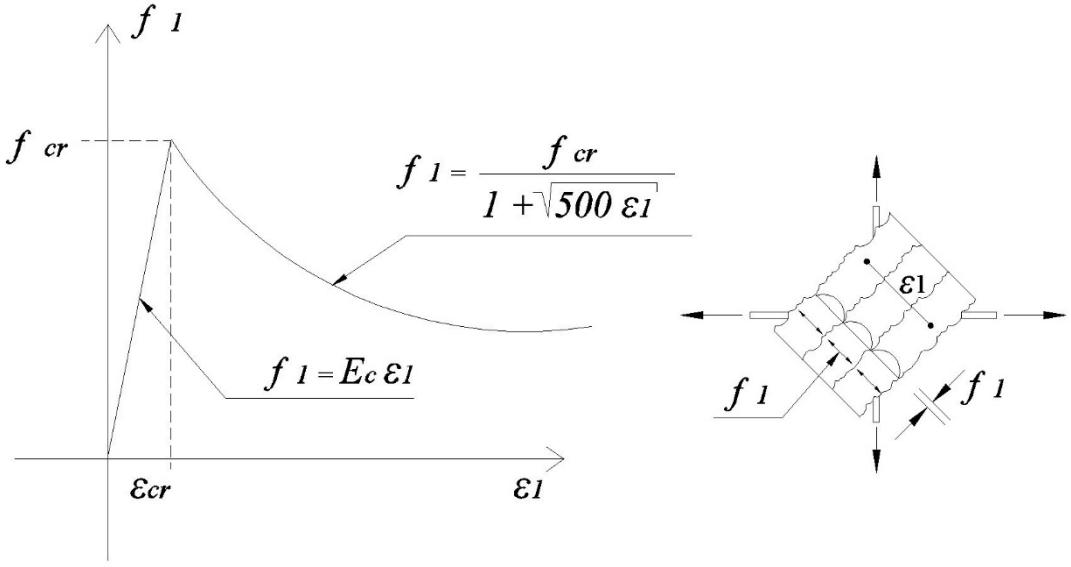

Figure 24 Tensile stress-strain relationship for diagonally cracked concrete.

As mentioned before, the above equations are based on average stresses and strains. Moreover, local variations are not taken into account, e.g. in reality there are no tensile stresses at the crack interface in the concrete and the tensile stresses in the reinforcement are greater than average. The capability of transmitting forces across the crack may limit the shear capacity of the structure (Collins & Mitchell 1987).

When shear forces are low, local increase in the reinforcement stresses are transmitting the tension. The reinforcement will yield at the crack location when the shear force is large enough. To transmit tension across a crack at higher shear forces, local shear stresses, v_{ci}, at the crack surface is required, see Figure 25.

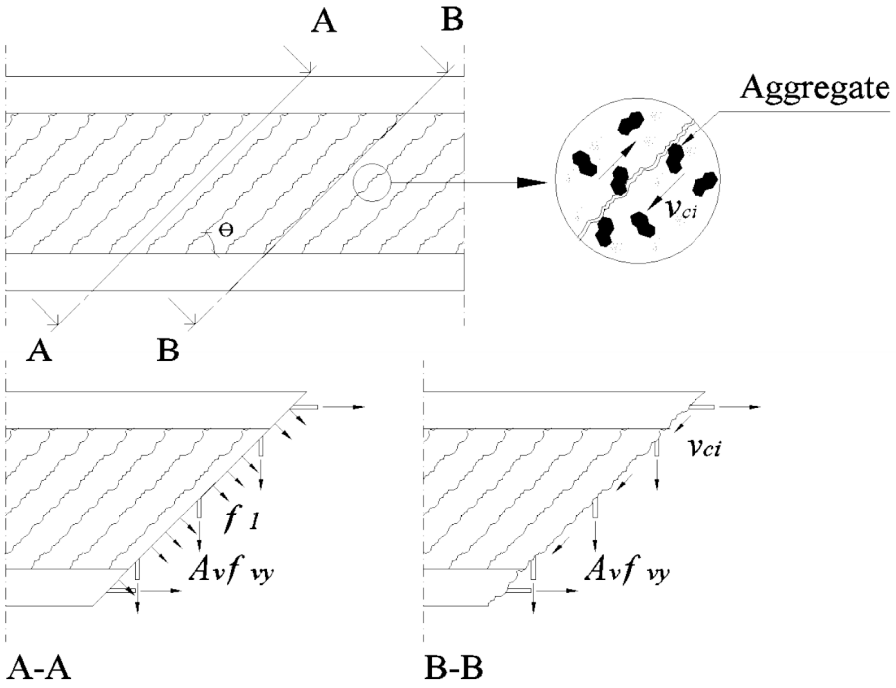

Figure 25 *Stress flow in between cracks: (A-A) average stresses, and (B-B) local stresses at crack.*

A larger crack makes it harder to transmit these shear stresses, i.e. the ability of transmitting shear stresses depends on the crack width. (Collins & Mitchell 1987) suggests such a relationship which is a simplification from an expression developed by (Vecchio & Collins 1986). The following expression is in comparison to the one by (Vecchio & Collins 1986) not taking into account the beneficial effects of local compressive stresses across the crack.

$$v_{ci} = \frac{0.17\sqrt{f_c'}}{0.3 + 0.6w} \quad \text{(MPa and mm units)} \tag{2-13}$$

where v_{ci} is the shear stress on the crack surface, f'_c is the maximum compressive stress and w is the crack width.

The average tensile stresses and the shear stresses transmitted by the crack, which can be seen in Figure 25 (A-A) and (B-B), need to be statically equivalent. The two sets of load shall give the same vertical force. This gives:

$$A_v f_v \left(\frac{d_v}{s \tan\theta} \right) + f_1 \frac{b_v d_v}{\sin\theta} \cos\theta = A_v f_{vy} \left(\frac{d_v}{s \tan\theta} \right) + v_{ci} b_v d_v \tag{2-14}$$

where f_{vy} is the yield stress in the stirrups. f_1 can be developed into:

$$f_1 = v_{ci} \tan\theta + \frac{A_v}{s b_v} (f_{vy} - f_v) \tag{2-15}$$

The crack width, w, which is used in equation (2-13), can be expressed as the product of the principal tensile strain and the average spacing of the diagonal cracks, $s_{m\theta}$:

$$w = \varepsilon_1 s_{m\theta} \tag{2-16}$$

Furthermore, the spacing of the inclined cracks depends on both the transversal and longitudinal reinforcement. (Collins & Mitchell 1987) suggests the following spacing equation:

$$s_{m\theta} = \frac{1}{\left(\frac{\sin\theta}{s_{mx}} + \frac{\cos\theta}{s_{mv}}\right)} \tag{2-17}$$

where s_{mx} is the average crack spacing in the longitudinal direction and s_{mv} is the average crack spacing in the vertical direction.

In Figure 26, the average crack spacing, s_{mx} and s_{mv}, are shown. In the longitudinal direction, (Collins & Mitchell 1987) are assuming that the spacing of the cracks is equal to the spacing of the stirrup. Also, the spacing between cracks aligned in the longitudinal direction is assumed to be equal to the spacing of the longitudinal bars.

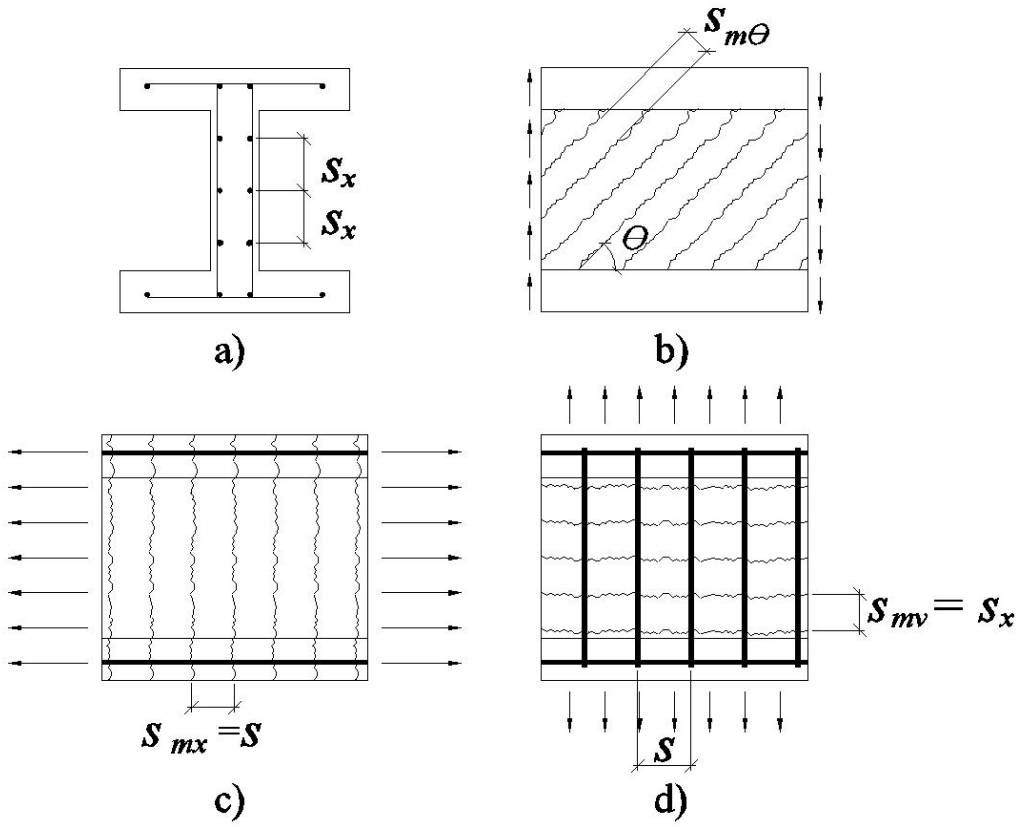

Figure 26 *Definitions of spacing; a) cross section and spacing between horizontal bars in the web, b) spacing between inclined cracks, c) spacing between vertical cracks (due to axial tension), and d) spacing between horizontal cracks (due to transverse tension) and stirrups.*

(Collins & Mitchell 1987) made the assumptions that s_{mx} and s_{mv} are equal to the spacing of the stirrups and of the longitudinal reinforcement in the web, though lowest value permitted is 100 mm.

The process above, with relationships and equilibriums, are enabling the prediction of the shear response of a beam. In (Collins & Mitchell 1987) a stepwise procedure of how to practically use the MCFT is given.

2.3.5 Modified Compression Field Theory (MCFT) extended to SFRC

Since the MCFT takes the tensile strength of the concrete into account, the increased tensile strength due to added fibres can be applied to enhance the shear capacity. Many studies and experiments have therefore been made on applying the MCFT on steel fibre reinforced concrete (SFRC) to predict the shear capacity. To include the advantageous toughness of FRC due to added fibres, the MCFT is in many cases being modified and extended to take this specific toughness parameter into account when predicting the shear capacity.

Since the steel fibres are the most common used fibres in the construction industry, the largest numbers of experiments and studies have been done on SFRC within this area. The same amount of studies has not yet been done for glass and basalt FRC.

Some studies made on shear calculations of SFRC based on the MCFT are (Minelli & Vecchio 2006), (Spinella et al. 2012) and (Ding et al. 2012) which are presented below.

(Minelli & Vecchio 2006) made several laboratory experiments of full-scale SFRC beams in order to show the possibility of substituting the minimum code-required shear reinforcement with fibre reinforcement, mainly in high-performance concrete. They also wanted to add knowledge within the numerical analyses of FRC in the MCFT, because then at the beginning of the 21st century, there mostly existed experimental results. A finite element code, based on the MCFT and also the Disturbed Stress Field Model (DSFM), was established which was adopted for the properties of a FRC. The experimental tests were then used to validate the developed numerical model. The DSFM is proposed to extend the MCFT to, in an accurate way, take the crack shear slip strains into account (Collins & Mitchell 1987). (Minelli & Vecchio 2006) could determine that the numerical model used adequately simulated the stiffness, crack pattern development, strength, ductility and failure modes of all specimens tested, even those elements reinforced with fibres only. Also, the experiments as well as the numerical analyses showed that conventional shear reinforcement could be partially or totally replaced by steel fibres. Finally, (Minelli & Vecchio 2006) stated in their study that the method of using an appropriate tension softening behaviour in the Finite Element (FE)-model is a quite precise, easy and effective procedure to model FRC.

In (Spinella et al. 2012), modifications of the MCFT were done to extend the theory to the case of FRC, in this case of high strength (HS) concrete. The study specified that a correct illustration of the tensioning-softening performance of SFRC is the most essential tool to prolong MCFT to accurately work for FRC. Several already existing numerical models for SFRC subjected to direct tension were compared in order to reproduce the shear behaviour of beam experiments. The most effective model was then the basis of a developed finite element code, which included both the MCFT and the DSFM. The code was then modified to the case of FRC, with the purpose of taking the advantageous effects of FRC into account by modelling the tensile crack and compressive post-peak softening behaviour of SFRC. By developing this model, which accurately predicted the shear response of SFRC beams subjected to shear, (Spinella et

al. 2012) again showed the accuracy of using the MCFT as the base for shear calculations of SFRC.

(Ding et al. 2012) examined the viability of using the MCFT for assessing the shear resistance of self-consolidating concrete beams with fibre and steel rebar reinforcement. Their study also proposed a theoretical method for FRC members, based on the MCFT, which was verified by a comparison with own experimental test results. The tests made in the study kept constant dimension, constant longitudinal reinforcement ratio and constant shear span-to-depth ratio (a/d). Three different hooked fibre volumes and three different stirrup ratios could then be examined. In order to extend the validity of the shear strength modified method, the prediction was also made for beams from previous studies. The proposed method equation which calculates the ultimate shear capacity of SFRC beams is based on the 2004 Canadian Standard Association (CSA) equation. It could be stated that the predicted method gave good correlation with the experimental results in concrete without stirrups, having a mean $V_{u,exp}$ / $V_{u,pre}$ (ratio between experimental and predicted ultimate shear capacity) of 1.07 and a coefficient of variation of 0.098. Therefore, it could be concluded that the modified method is capable of providing reasonable estimates for the shear capacity of SFRC beams (Ding et al. 2012).

2.3.6 Simplified FRC-MCFT (FRC-MCFT)

Furthermore, another study which also propose an extension of the MCFT to predict the shear response of FRC is the one made by (Minelli & Plizzari 2011). The method presented was rather promising, based on tests performed at the University of Brescia.

The study presented an extended version of the Simplified Modified Compression Field Theory (SMCFT) by (Bentz et al. 2006), since analytical procedures are accepted more easily if based on reliable physical models and strong mechanical backgrounds, according to (Minelli & Plizzari 2011). The presented theory, named Simplified FRC-MCFT (FRC-MCFT), is therefore based on equilibrium, compatibility and constitutive laws. The authors stated in their work that the fibre role should be incorporated into the concrete contribution since FRC is characterized by its toughness, which is generally neglected in plain concrete. Therefore, it is important to model the characteristic behaviour of FRC, which is enhanced residual tensile stresses at cracks and also enhanced aggregate interlocks, since the cracks are smaller due to fibre bridging (Minelli & Plizzari 2011). As the SMCFT, the FRC-MCFT includes the following assumptions:

- clamping stresses $f_z = 0$. This is a reasonable assumption for beams since these stresses are limited and therefore could be neglected.
- a tensile softening behaviour is assumed, i.e. the peak load is not exceeded. A simplified rigid-plastic behaviour is assumed which makes the ultimate residual tensile strength, f_{Ftu}, to the only parameter that needs to be taken into account. This parameter shall be lower than the tensile strength, f_{ct}, of the concrete. Other developed methods are needed for strain hardening behaviours.

The vertical equilibrium along a section between two cracks is the same in the FRC-MCFT by (Minelli & Plizzari 2011) as in the equilibrium for the MCFT for plain concrete by (Collins & Mitchell 1987), presented in Section 2.3.4. The difference between the two models can be seen in the conditions at a cracked interface, see Figure

27. In the extended model, the contribution by the fibres bridging the cracks is given by the ultimate residual tensile strength, f_{Ftu}.

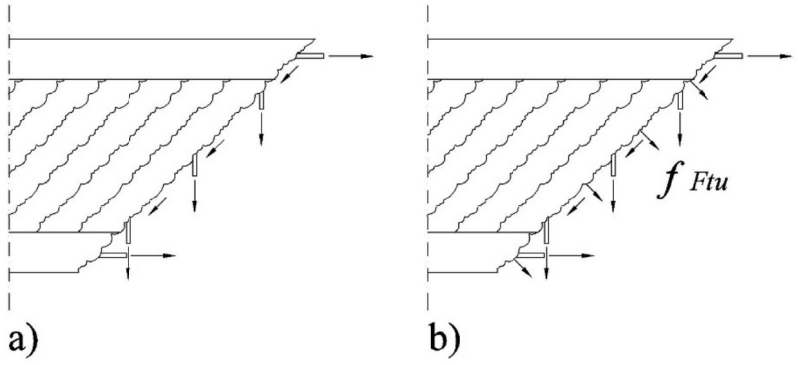

Figure 27 *Equilibrium at a cracked interface (a) according to MCFT and (b) according to FRC-MCFT (with addition of f_{Ftu}).*

The notations and equilibrium conditions between cracks and in the cracked interface according to FRC-MCFT is shown in Figure 28.

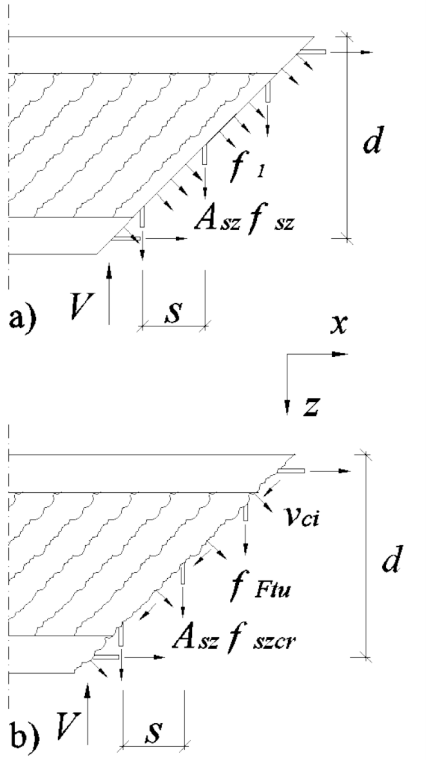

Figure 28 *Equilibrium conditions for FRC-MCFT: a) average stresses between cracks, and b) local stresses at cracked interface. From* (Minelli & Plizzari 2011).

Between two shear cracks, the vertical equilibrium is given as:

$$V = A_{sz} f_{sz} \frac{d \cot \theta}{s} + f_1 \cot \theta b_w d \tag{2-18}$$

where A_{sz} is the area of the stirrups, f_{sz} is the tensile stress in the stirrups, d is the effective depth and b_w is the effective web width.

At a cracked interface, the vertical equilibrium for the FRC-MCFT is given by:

$$V = A_{sz} f_{szcr} \frac{d \cot\theta}{s} + f_{Ftu} \cot\theta b_w d + v_{ci} b_w d \tag{2-19}$$

where f_{szcr} is the tensile stress in the stirrup at a cracked interface and v_{ci} is the shear stress at a cracked interface, which is a model developed by (Vecchio & Collins 1986) and is expressed as:

$$v_{ci} = \frac{0.18\sqrt{f_{ck}}}{0.31 + \frac{24w}{a+16}} \tag{2-20}$$

where a is the maximum aggregate size, w is the crack width and f_{ck} is the characteristic concrete cylinder strength.

The crack width in members with stirrups is in the study by (Minelli & Plizzari 2011) being calculated as the following relationship where s_θ is the crack spacing in the direction of the diagonal cracks:

$$w = s_\theta \varepsilon_1 = \frac{1}{\left(\frac{\sin\theta}{s_{x,FRC}}\right) + \left(\frac{\cos\theta}{s_{z,FRC}}\right)} \varepsilon_1 \tag{2-21}$$

where $s_{x,FRC}$ and $s_{z,FRC}$ are the crack spacing in the longitudinal respectively the vertical direction for fibre reinforced concrete:

$$s_{x,FRC} = s_x \left(1 - \frac{f_{Ftu}}{f_{ct}}\right) \tag{2-22}$$

$$s_{z,FRC} = s_z \left(1 - \frac{f_{Ftu}}{f_{ct}}\right) \tag{2-23}$$

where s_x and s_z are the crack spacing in the longitudinal respectively the vertical direction and f_{ct} is the maximum concrete tensile strength.

According to (Minelli & Plizzari 2011), the crack width is limited when using FRC which in the equation for the crack width is represented by the ultimate residual tensile strength, f_{Ftu}. A higher f_{Ftu} gives smaller cracks and a denser crack pattern.

For the average principal tensile stress in cracked concrete, a simple extension for FRC was made based on the one developed by (Vecchio & Collins 1986), see equation (2-24). The model developed for FRC-MCFT is presented in equation (2-26).

$$f_1 = \frac{f_{ct}}{1 + \sqrt{500\varepsilon_1}} \tag{2-24}$$

where $f_{ct} = 0.33\sqrt{f_{ck}}$ (2-25)

$$f_1 = f_{Ftu} + \frac{f_{ct} - f_{Ftu}}{1 + \sqrt{500\varepsilon_1}} \tag{2-26}$$

When f_{Ftu} is equal to zero, the principal tensile stress according to FRC-MCFT will give the same curve as the one by (Vecchio & Collins 1986). It shall be noted that the ultimate tensile strain, ε_{Fu}, is limited to 2% for the FRC if the strain distribution is varying over the cross section and to 1% for constant tensile-strain distribution. These relationships are experimentally developed and result in a maximum crack width of 2.5 mm (Minelli & Plizzari 2011).

Along a crack, the stresses in the FRC-MCFT are given as:

$$v \le f_{Ftu}\cot\theta + v_{ci} + v_s = f_{Ftu}\cot\theta + \frac{0.18\sqrt{f_{ck}}}{0.31 + \frac{24w}{a+16}} + v_s \tag{2-27}$$

where v_s is the shear stress contribution from transverse reinforcement.

The configuration with average stresses is given by:

$$v = f_1\cot\theta + v_s = \left(f_{Ftu} + \frac{0.33\sqrt{f_{ck}} - f_{Ftu}}{1+\sqrt{500\varepsilon_1}} \right)\cot\theta + v_s \tag{2-28}$$

The angel for the principal compressive stresses, θ, can in members without transverse reinforcement be expressed as:

$$\cot\theta = \frac{v_{ci}}{f_{ct} - f_{Ftu}}\left(1+\sqrt{500\varepsilon_1}\right) \tag{2-29}$$

The principal tensile strain can, by enforcing compatibility, be written as:

$$\varepsilon_1 = \varepsilon_x(1+\cot^2\theta) + \varepsilon_2\cot^2\theta \tag{2-30}$$

where ε_x is the strain in the longitudinal direction and ε_2 is the principal compressive strain.

In a member without stirrups, equilibrium can give:

$$f_2 = f_1\cot^2\theta \tag{2-31}$$

A linear stress-strain relationship can be assumed in compression if assuming small compressive stresses:

$$\varepsilon_2 = \frac{f_2}{E_c} \tag{2-32}$$

$$E_c = 4950\sqrt{f_{ck}} \tag{2-33}$$

By above compatibility and equilibrium laws, the principal tensile strain can now be given as:

$$\varepsilon_1 = \varepsilon_x(1+\cot^2\theta) + \frac{f_1\cot^4\theta}{4950\sqrt{f_{ck}}} \tag{2-34}$$

where ε_1 depends on itself, since the principal tensile stress f_1 depends on ε_1.

A structural member which includes fibres has different behaviour depending on the fibre content, fibre typology and concrete matrix. The authors of the FRC-MCFT

therefore stated that further studies are needed to develop analytical models for crack spacing and tension stiffening to cover the range of different FRCs.

It was concluded that FRC, even with a low toughness (f_{Ftu}<1 MPa) can significantly increase the shear capacity of members without stirrups. On the contrary, in members which have stirrups, a FRC with low toughness (0<f_{Ftu}<1.5 MPa) does not seem to make any significant increase of the shear capacity. The FRC-MCFT was developed by a research group at the University of Brescia where studies had been made of the shear behaviour of FRC members during ten years before the study was presented. The group had done about 60 tests to evaluate different parameters influencing the shear capacity (Minelli & Plizzari 2011).

2.4 Bending tests of GFRC and BFRC beams

Bending test results on AR-glass MRC specimens of a three point bending test (3PBT), executed in accordance with (EN 14651 2005), and test results from cube compression tests were received from ReforceTech. Corresponding test results from 3PBT in accordance to (EN 14651 2005) on basalt MRC beams were not to be found in the literature. Hence only the results from AR-glass MRC were used in the inverse analysis described in Section 3.

2.4.1 Testing procedure

The 3PBT results received from ReforceTech included beams with three different fibre volumes and with two different concrete classes. For each fibre volume and concrete class four beams were tested. The tests were executed in accordance with the European testing standard (EN 14651 2005). The same concrete mixes, with the same three fibre volumes and concrete classes were also tested with cube compression strength test.

The 3PBT was performed on beams with a length of 550 mm and a height of 150 mm. The beams were supported on two rolling line supports and loaded with a line load in the middle of the beam. To control where the initial cracking occurs, the beams were notched in the bottom and in the centre of the beam. Specimens with any initial cracking outside the notch were rejected in accordance with (EN 14651 2005). The notch was wet sawed up to a height of 25 mm. Because of the limitation of maximum 5 mm width of the notch, according to the testing standard, the width is in this thesis work assumed to be 5 mm. The test setup is shown in Figure 29. The load on the beam was applied displacement controlled until failure.

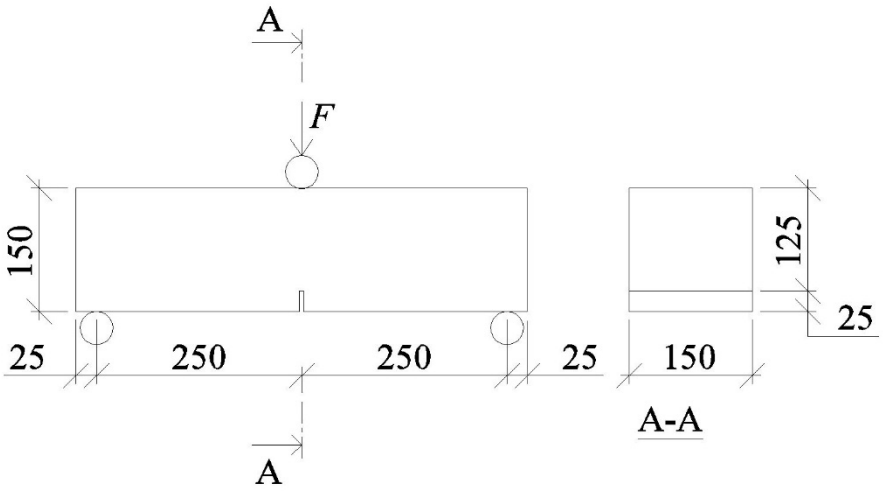

Figure 29 Test setup of 3PBT according to (EN 14651 2005).

2.4.2 Gathering of test results

The test results were received as residual flexural strength values. Six different concrete mixes were tested, namely two different concrete classes (C25/30 and C50/60) with three different fibre volumes (0.3%, 2.5% and 4%) respectively. The fibre volumes correspond to 6.3, 52.5 and 84 kg/m^3. First, the results from concrete class C25/30 are shown followed by the results for concrete class C50/60. The fibres used in all tested beams were the AR-glass MiniBars Gen3, which have a length of 43 mm and a diameter 0.65-0.7 mm.

The residual flexural strengths, received from the beams tested with 3PBT, for concrete class C25/30 and AR-glass MiniBar volumes 0.3%, 2.5% and 4% respectively are shown in Table 3, Table 4 and Table 5. The same results are visualized in Figure 30, Figure 32 and Figure 34. The mean value of the residual flexural strength curves are shown in Figure 31, Figure 33 and Figure 35. Moreover, the tested concrete had a density according to Table 6. Observe that the curves for the beams with fibre content 0.3% indicate a bending softening behaviour while the curves for the other fibre contents indicate bending hardening behaviour.

Table 3 *Residual flexural strengths from test result of 3PBT, according to (EN 14651 2005), on four beams with concrete class C25/30 and AR-glass MiniBar content 0.3%.*

Beam	$f_{ct,L}^{f}$	$f_{R,1}$	$f_{R,2}$	$f_{R,3}$	$f_{R,4}$
	[MPa]				
1	3.931	0.869	0.928	0.620	0.486
2	4.232	0.760	0.771	0.737	0.571
3	4.562	1.132	1.077	1.066	0.901
4	4.693	0.957	1.013	0.968	0.935
Mean	4.354	0.929	0.947	0.848	0.723

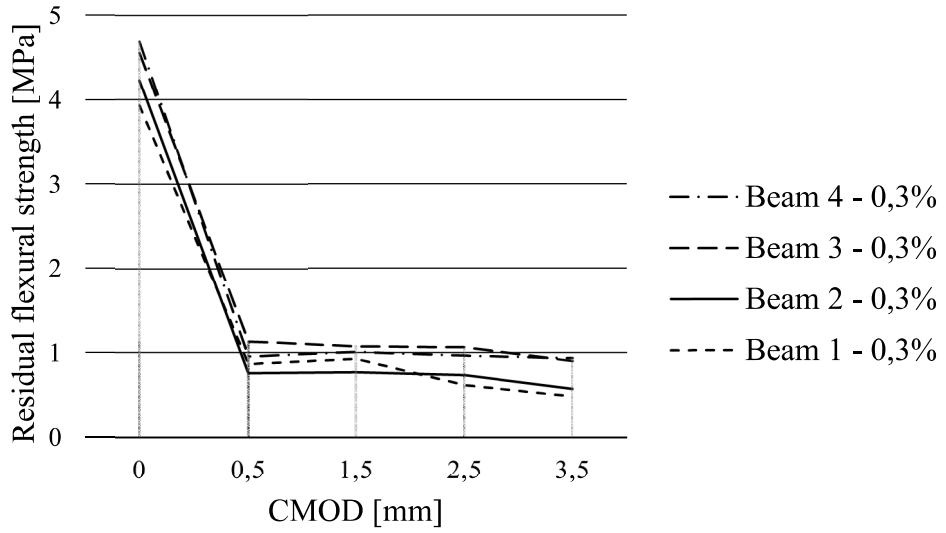

Figure 30 *Visualization of residual flexural strength from test result of 3PBT, according to (EN 14651 2005), on four beams with concrete class C25/30 and AR-glass MiniBar content 0.3%.*

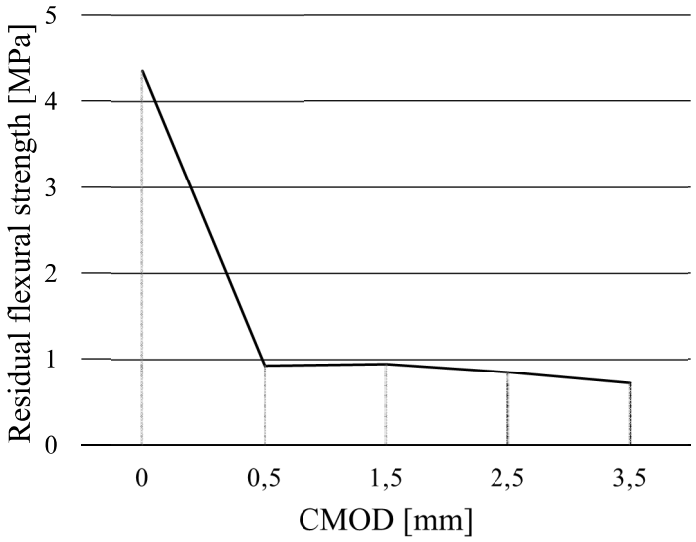

Figure 31 *Visualization of mean value of test results of 3PBT, according to (EN 14651 2005), on four beams with concrete class C25/30 and AR-glass MiniBar content 0.3%.*

Table 4 *Residual flexural strength from test result of 3PBT, according to (EN 14651 2005), on four beams with concrete class C25/30 and AR-glass MiniBar content 2.5%.*

Beam	$f_{ct,L}^{f}$	$f_{R,1}$	$f_{R,2}$	$f_{R,3}$	$f_{R,4}$
	[MPa]				
1	5.771	8.445	8.652	7.289	6.494
2	5.849	9.748	10.499	9.631	9.068
3	6.141	9.899	9.653	8.694	8.119
4	5.367	8.008	8.314	7.847	7.092
Mean	5.782	9.025	9.280	8.365	7.693

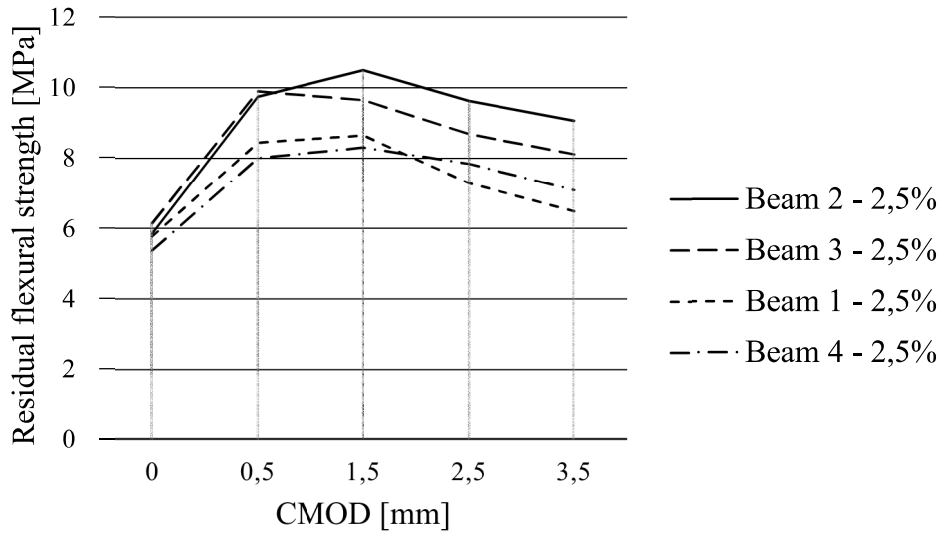

Figure 32 *Visualization of residual flexural strength from test result of 3PBT, according to (EN 14651 2005), on four beams with concrete class C25/30 and AR-glass MiniBar content 2.5%.*

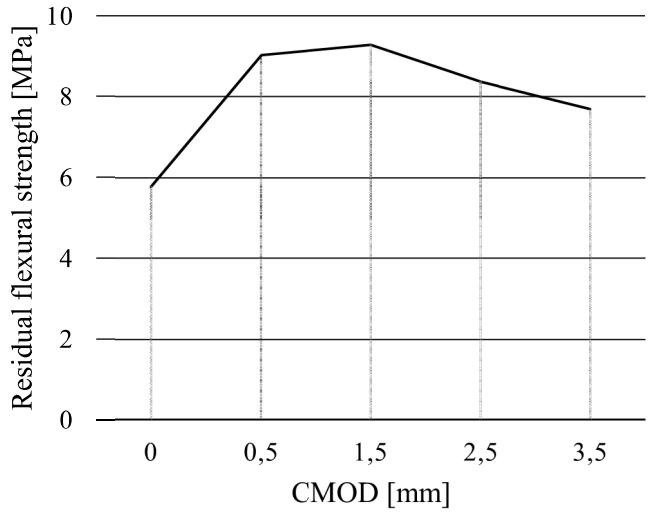

Figure 33 *Visualization of mean value of test results of 3PBT, according to (EN 14651 2005), on four beams with concrete class C25/30 and AR-glass MiniBar content 2.5%.*

Table 5 *Residual flexural strength from test result of 3PBT, according to (EN 14651 2005), on four beams with concrete class C25/30 and AR-glass MiniBar content 4%.*

Beam	$f_{ct,L}^{f}$	$f_{R,1}$	$f_{R,2}$	$f_{R,3}$	$f_{R,4}$
	[MPa]				
1	6.410	10.473	11.310	10.812	10.084
2	5.599	9.529	9.951	9.544	9.140
3	6.340	9.840	10.972	10.826	10.176
4	6.090	10.203	10.323	9.873	9.170
Mean	6.110	10.011	10.639	10.264	9.643

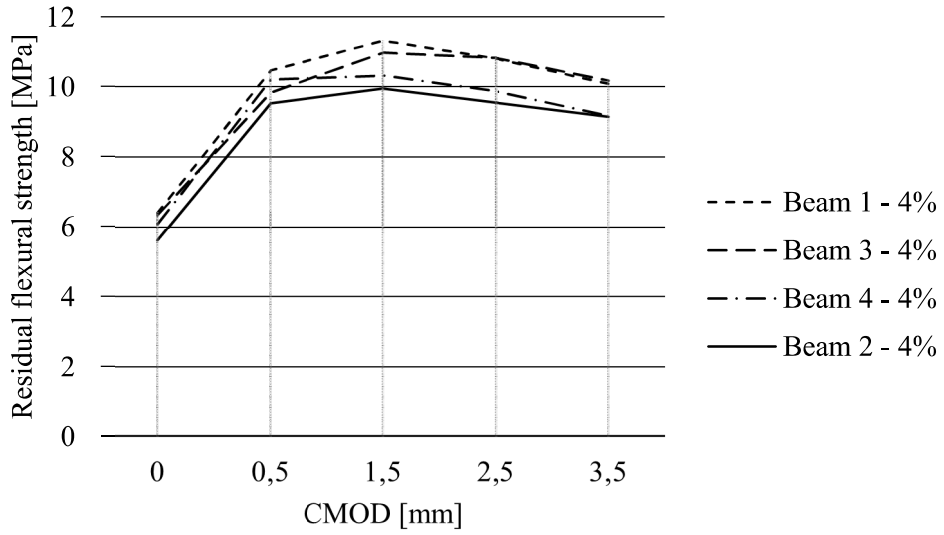

Figure 34 *Visualization of residual flexural strength from test result of 3PBT, according to (EN 14651 2005), on four beams with concrete class C25/30 and AR-glass MiniBar content 4%.*

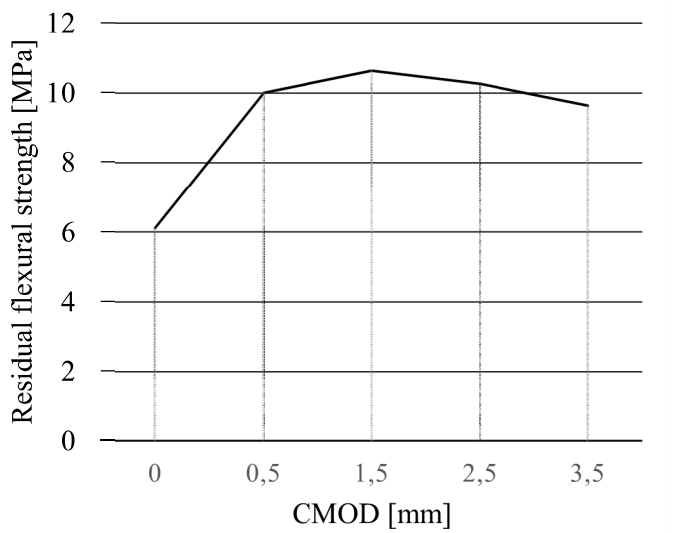

Figure 35 *Visualization of mean value of test results of 3PBT, according to (EN 14651 2005), on four beams with concrete class C25/30 and AR-glass MiniBar content 4%.*

Table 6 *Density of tested concrete C25/30 with different AR-glass MiniBar content.*

Fibre content [%]	Density [kg/m^3]
0.3	2244
2.5	2253
4	2271

The compressive strength from cube compression tests of concrete specimens with the same concrete class C25/30 and fibre volumes are shown in Table 7. The cube had a side length of 150 mm.

Table 7 *Test results from cube compression tests on concrete C25/30 with different AR-glass MiniBar content.*

Fibre content [%]	Max. load [kN]	Compressive strength [MPa]
0.3	1120.7	49.8
2.5	1063.0	47.2
4.0	1174.7	52.2

The residual flexural strength for concrete class C50/60 and AR-glass MiniBar content 0.3%, 2.5% and 4% respectively are shown in Table 8, Table 9 and Table 10. The same results are visualized in Figure 36, Figure 38 and Figure 40. The mean value of the

residual flexural strengths curves are show in Figure 37, Figure 39 and Figure 41. Moreover, the tested concrete had a density according to Table 11. Observe also at this concrete class, that the curves for the beams with fibre content 0.3% indicate a bending softening behaviour while the curves for the other fibre contents indicate bending hardening behaviour.

Table 8 *Residual flexural strength from test result of 3PBT, according to (EN 14651 2005), on four beams with concrete class C50/60 and AR-glass MiniBar content 0.3%.*

Beam	$f_{ct,L}^{f}$	$f_{R,1}$	$f_{R,2}$	$f_{R,3}$	$f_{R,4}$
	[MPa]				
1	4.514	1.164	1.161	0.948	0.775
2	4.850	1.798	1.765	1.308	1.031
3	5.062	1.752	1.456	1.266	1.002
4	5.171	1.874	1.807	1.435	1.202
Mean	4.900	1.647	1.547	1.239	1.003

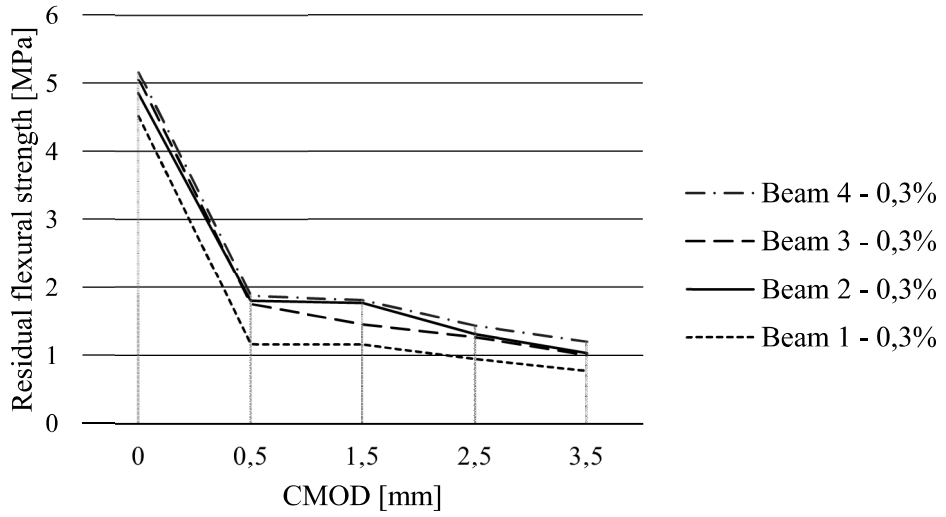

Figure 36 *Visualization of residual flexural strength from test result of 3PBT, according to (EN 14651 2005), on four beams with concrete class C50/60 and AR-glass MiniBar content 0.3%.*

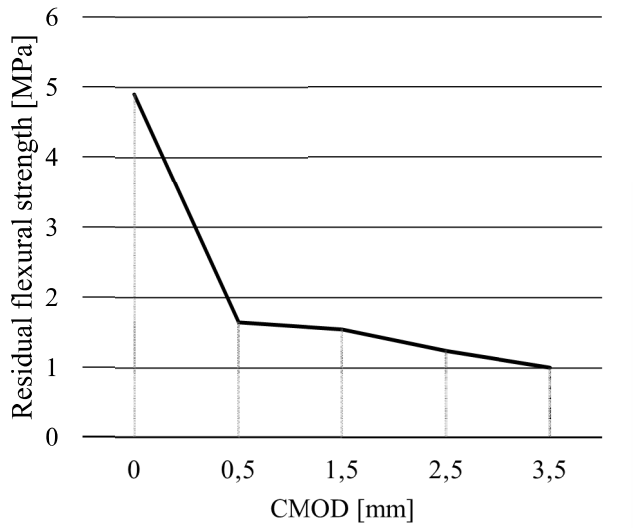

Figure 37 *Visualization of mean value of test results of 3PBT, according to (EN 14651 2005), on four beams with concrete class C50/60 and AR-glass MiniBar content 0.3%.*

Table 9 *Residual flexural strength from test result of 3PBT, according to (EN 14651 2005), on four beams with concrete class C50/60 and AR-glass MiniBar content 2.5%.*

Beam	$f_{ct,L}^{f}$	$f_{R,1}$	$f_{R,2}$	$f_{R,3}$	$f_{R,4}$
	[MPa]				
1	5.439	8.506	9.173	9.348	7.396
2	5.539	8.502	9.165	7.936	7.207
3	5.751	8.664	9.539	8.653	7.614
4	6.092	9.334	10.924	9.560	8.099
Mean	5.705	8.751	9.700	8.624	7.579

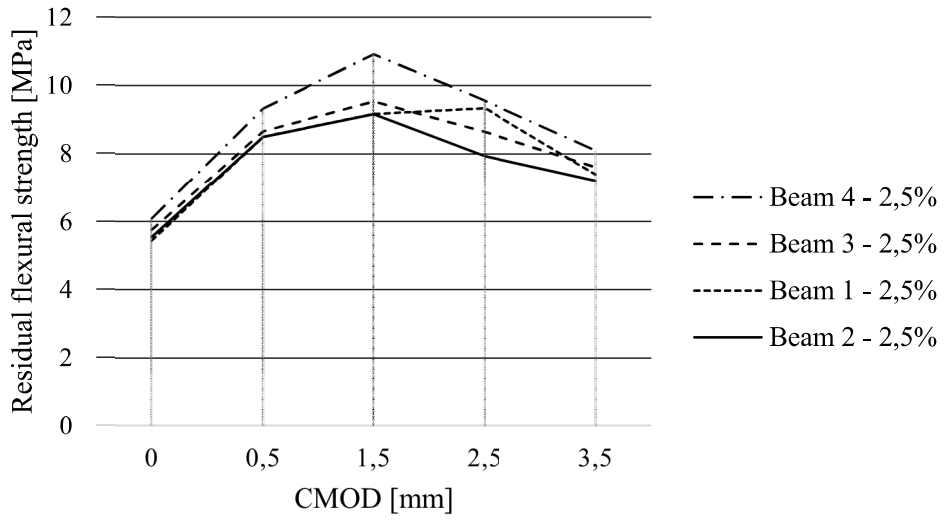

Figure 38 *Visualization of residual flexural strength from test result of 3PBT, according to (EN 14651 2005), on four beams with concrete class C50/60 and AR-glass MiniBar content 2.5%.*

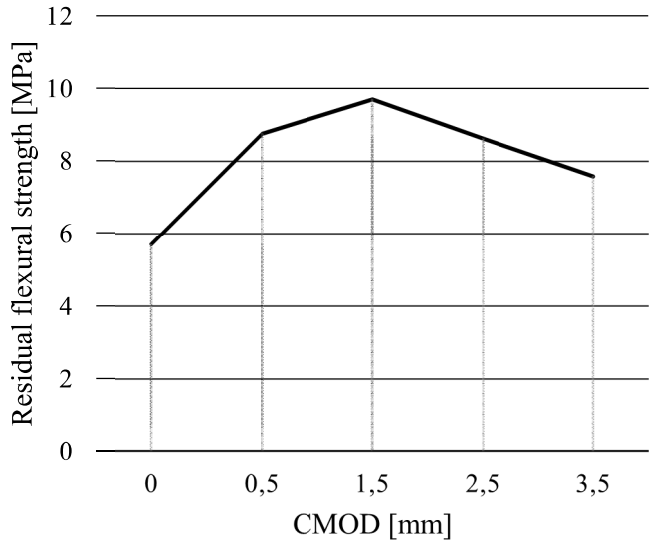

Figure 39 *Visualization of mean value of test results of 3PBT, according to (EN 14651 2005), on four beams with concrete class C50/60 and AR-glass MiniBar content 2.5%.*

Table 10 *Residual flexural strength from test result of 3PBT, according to (EN 14651 2005), on four beams with concrete class C50/60 and AR-glass MiniBar content 4%.*

Beam	$f_{ct,L}^{f}$	$f_{R,1}$	$f_{R,2}$	$f_{R,3}$	$f_{R,4}$
	[MPa]				
1	6.497	11.197	11.180	10.751	9.933
2	7.033	12.025	12.849	12.860	11.989
3	4.947	9.291	11.173	10.316	8.925
4	7.029	12.727	13.325	12.882	12.133
Mean	6.377	11.310	12.132	11.702	10.745

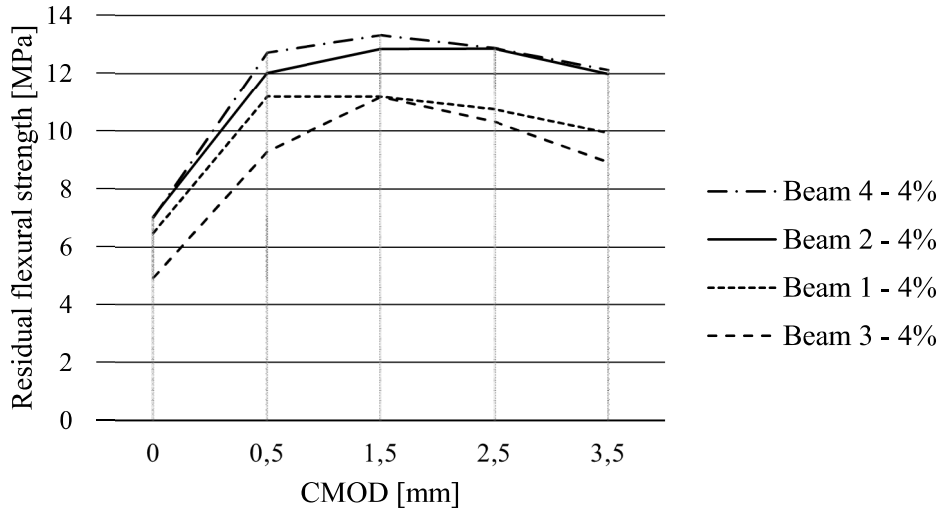

Figure 40 *Visualization of residual flexural strength from test result of 3PBT, according to (EN 14651 2005), on four beams with concrete class C50/60 and AR-glass MiniBar content 4%.*

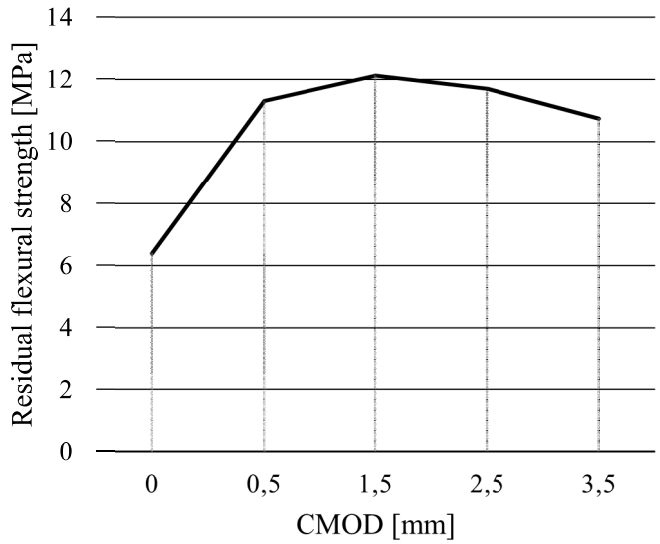

Figure 41 *Visualization of mean value of test results of 3PBT, according to (EN 14651 2005), on four beams with concrete class C50/60 and AR-glass MiniBar content 4%.*

Table 11 *Density of tested concrete C50/60 with different AR-glass MiniBar content.*

Fibre content [%]	Density [kg/m^3]
0.3	2258
2.5	2243
4	2250

The compressive strength from cube compression tests of concrete specimens with the same concrete class C50/60 and fibre contents are shown in Table 12. The cube had a side length of 150 mm.

Table 12 *Test results from cube compression tests on concrete C50/60 with different AR-glass MiniBar content.*

Fibre content [%]	Max. load [kN]	Compressive strength [MPa]
0.3	1707.5	76.6
2.5	1510.25	67.1
4.0	1649.9	73.6

2.5 Conclusions of literature study

The aim with the literature study was to find a theory based on the MCFT that is applicable on FRC.

The FRC-MCFT was chosen to be used in this study with basis on the great work within the area of FRC that had been done by the research group that developed the theory, as well as the validation of the theory itself. It shall be noted that the theory was based on SFRC tests.

The FRC-MCFT, which was used in the following partial study, only applies on material properties with tension softening response. According to Section 2.1.2 tension softening response does not necessarily mean that the FRC has a bending softening behaviour but it can also have bending hardening behaviour. On the other hand, bending softening behaviour indicates tension softening response directly. This would make it hard to find a unique result from inverse analysis if bending hardening curves would have been analysed.

The given bending test results received from ReforceTech showed bending softening response for AR-glass MiniBar volume 0.3% only. Thus fibre volumes of 2.5% and 4% showed bending hardening response. This meant that only concrete beams with fibre volume 0.3% could be studied further. Moreover this meant that only concrete beams with two different concrete classes (C25/30 and C50/60) and the same fibre volume (0.3%) were possible to study in the application of MCFT extended to SFRC.

Since the AR-glass and basalt MiniBars have the same fibre shape and a similar modulus of elasticity, the behaviour of the FRC made of the different materials can be assumed to be similar. In addition, this assumption can be made since the fibres are designed for bond failure between the fibre and concrete matrix. The difference in the maximum tensile strength of the two bare fibres will thus not contribute to a difference of the behaviour of the FRC since there will not be a failure of the fibre itself. Although, it shall be noted that it is an assumption. For this to be a fact, more experimental tests need to be made on both AR-glass and basalt MRC.

3 Inverse analysis of bending tests

In this chapter, the second partial study, the inverse analysis is presented. First the general methodology of inverse analysis is described, followed by the inverse analysis in this thesis work, including method, results and conclusions.

3.1 Methodology of inverse analysis

In structural calculations of fibre reinforced concrete (FRC) structures, the tensile strength of the concrete might be one of the needed input data. That was the case in the calculation of shear capacity according to Modified Compression Field Theory (MCFT) in this thesis work, see Chapter 4. The needed tensile strength input of MiniBar reinforced concrete (MRC) in this Master's thesis work was therefore received from inverse analysis in the Finite Element (FE)-software Abaqus.

Generally, an inverse analysis is performed on the basis of known or already executed tests. The test setup is modelled, for example in a FE-software, both with known and predicted input data. The predicted input is changed in iterations until the analysed result match the experimental result with a specified convergence criteria. When a match is received the predicted input can be used as the real value, see for inverse methodology. Another way of referring to these kinds of analyses is by back-calculation, which differs from inverse analysis because it does not require the use of FE-software. Instead it requires conventional calculation methods, i.e. mathematical relationships.

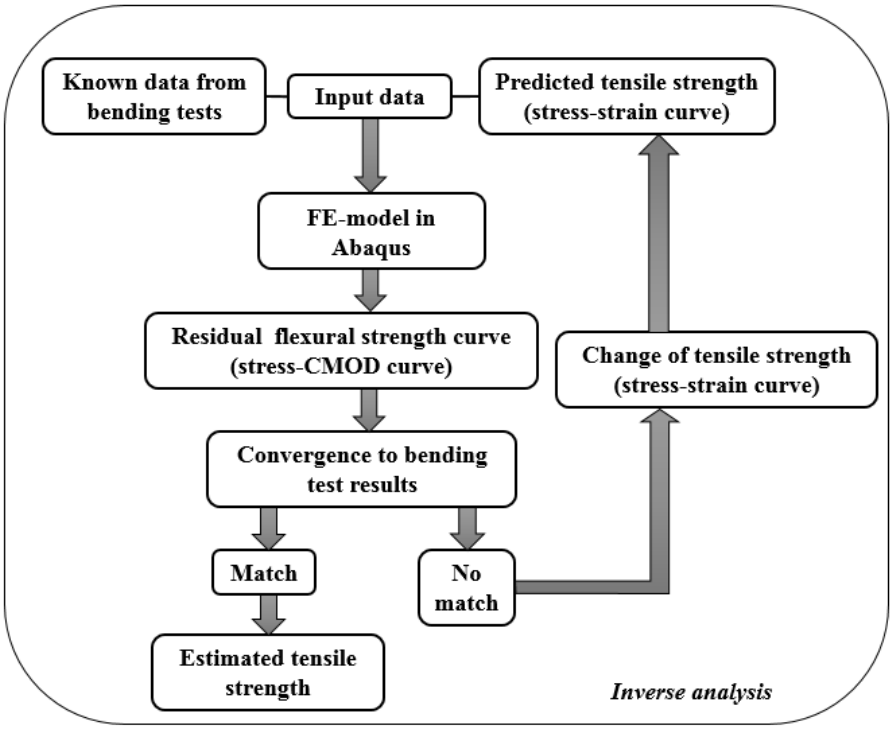

Figure 42 Inverse methodology in this thesis work.

The reason for choosing numerical analysis to receive the tensile strength curve was due to the fact that experimental tests on the tensile strength of FRC is not commonly done because of the difficulties in the operation of the tests according to (Ferreira &

Branco 2007). Difficulties by using uniaxial tension tests to receive the tensile strength curve of cementitious composites, such as FRC, is also confirmed by (Slowik et al. 2006) saying that these tests are time consuming and expensive. Even though there is another test which can give tensile behaviour in a direct way, i.e. the wedge splitting test, it can only give the fracture energy. Hence, the stress-strain curves for the tensile behaviour needs to be received from inverse analysis according to (Slowik et al. 2006).

Inverse analyses have been widely examined as a tool to predict unknown data from a set of already known data. Many authors have studied the methodology of receiving the tensile strength ($\sigma - w$ relationship) of reinforced concrete (RC) by doing an inverse analysis performed by for example an FE-analysis. According to (Löfgren 2005), inverse analysis can also be used for FRC.

Steel fibre reinforced concrete (SFRC) has been studied with inverse analysis of Three Point Bending Test (3PBT) and wedge splitting test by (Löfgren et al. 2005). In addition, inverse analysis of SFRC has also been executed by for example (Tlemat et al. 2006) and (de Oliveira e Sousa & Gettu 2006). However, some difficulties when using this method for FRC are reported in (Löfgren 2005):

- the shape of the $\sigma - w$ relationship is not as well defined as for regular concrete, but varies depending on the mix constituents
- with increasing fibre volumes, it becomes difficult to distinguish between the effect of the tensile strength and the first slope of the $\sigma - w$ relationship
- the inverse problem is often ill-posed, i.e. there exists no unique solution
- a large number of parameters may be required for describing the $\sigma - w$ relationship
- the response is influenced by the position of the fibres, which may be reflected on the determined $\sigma - w$ relationship as it is usually assumed that the properties are uniform over the section

FRC with other fibre reinforcement materials, such as Alkali Resistant glass (AR-glass) and polymeric, have also been studied with back-calculation. AR-glass and polymeric together with steel fibres are studied by (Mobasher et al. 2014).

Inverse analysis demands an iterative solution process. Therefore there exist studies proposing that the results from experimental testing shall be fitted to the numerical results with fitting algorithms to optimize the match (Slowik et al. 2006). Although, in this thesis work the fitting was done with manual iterations.

In the following sections, the inverse analysis methodology in this thesis work is presented followed by results and conclusions.

3.2 Inverse analysis of MRC

In this thesis work, inverse analysis were done to obtain tensile strength curves for MRC. The tensile curves were received by modelling already executed 3PBTs which were available for AR-glass MRC only, see Chapter 2.4. From the conclusions drawn in Section 2.5, only the bending tests corresponding to AR-glass MiniBar volume 0.3% were further analysed.

Four beams were tested for each AR-glass MiniBar volume from which a mean value of the residual flexural curve was calculated, as described in Chapter 2.4. To minimize the impact of the scatter in test results, only the mean value was analysed with the inverse method.

3.2.1 Modelling technique

In order to receive the tensile strength curves, the FE-program Abaqus was used. Choices made within the modelling, as well as the procedure to obtain the tensile strength curves, are presented.

3.2.1.1 Material properties

The result wanted from the inverse FE-analysis was a tensile strength curve for AR-glass MRC. The components of the modelled specimens were hence the concrete and the reinforcement fibres. To receive a curve corresponding to the concrete interacting with the fibres, the specimens were modelled as one material. This means that the material was seen as homogenous and hence the fibre distribution was smeared out over the concrete elements.

To model this interaction, the material was modelled with damaged plasticity. Damaged plasticity in Abaqus is based on the theories of scalar plastic damage and the models proposed by Lubliner in 1989 and by Lee and Fenves in 1998 (Abaqus 6.14 2014). Moreover, the plastic damage model for concrete failure is a model both considering the non-linear behaviour in tension and in compression. For more information about the plastic damage model see (Lubliner et al. 1989) and (Lee & Fenves 1998). Consequently, this material model makes it possible to define the compressive as well as the tensile stress-strain curves of concrete and thus the tension softening behaviour of MRC (Abaqus 6.14 2014).

Another material model evaluated in this thesis work was the concrete smeared cracking, also available in Abaqus. This model only account for the compressive strength in concrete does not take the tensile strength into account (Abaqus 6.14 2014). Because of this, the concrete damaged plasticity model was a better choice in this thesis work.

The response in compression was assumed linear elastic, going to infinite strength, with the modulus of elasticity and Poisson's ratio same as for concrete without added fibres. This assumption was made according to Model code, saying that the modulus of elasticity does not change significantly because of the addition of fibres (Fib 2013). The modulus of elasticity and Poisson's ratio for plain concrete were received from (SS-EN 1992-1-1 2008), see equation (3-1), (3-2) and (3-3).

$$E_{C25/30} = 31 \quad [\text{GPa}] \tag{3-1}$$

$$E_{C50/60} = 37 \quad [\text{GPa}] \tag{3-2}$$

$$\nu = 0.2 \tag{3-3}$$

Before cracking, the response in tension was assumed linear elastic with modulus of elasticity and poisons ratio similar to plain concrete, see equation (3-1), (3-2) and (3-3). This assumption was made for the same reason as for the response in compression.

After cracking, the response in tension can be simulated in different ways, i.e. with different shapes of the residual tensile strength curve. For example, the curve can be bi-linear, exponential or multilinear, see Figure 44 (Löfgren 2005). In (Tlemat et al. 2006), a multi-linear curve was used while (Mobasher et al. 2014) used a bi-linear curve to describe the stress-strain response in tension after crack initiation.

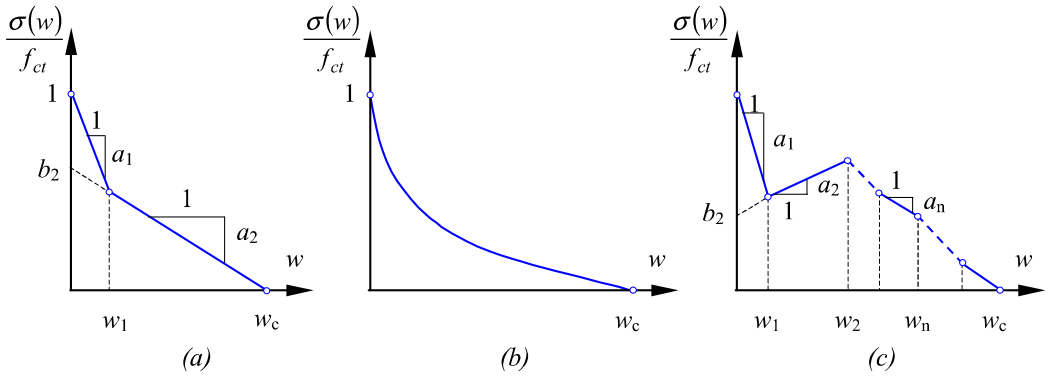

Figure 43 *Different σ-w relationships: (a) bi-linear, (b) exponential, and (c) polylinear (or multilinear)* (Löfgren 2005).

In this Master's thesis work, both a bi-linear and a tri-linear curve were evaluated. Hence, other shapes of the tensile strength curve were excluded in this work. The linear curve was for example excluded due to that it could not describe the tension softening response. This was because it did not simulate the stress drop from after crack initiation at f_{ct}. Therefore, two stresses (f_{ct} and f_A) and two strains ($\varepsilon_{A,cr}$ and ε_u) were received from the iteration process of the bi-linear curve, see Figure 44. For the tri-linear curve, three stresses (f_{ct}, f_A and f_B) and three strains ($\varepsilon_{A,cr}$, $\varepsilon_{B,cr}$ and ε_u) were to be received, see Figure 45. Moreover, the stresses f_{ct} and f_A in the tri-linear iteration were assumed equal.

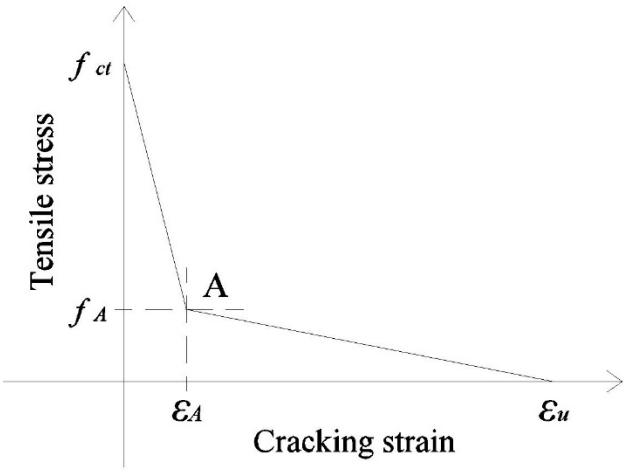

Figure 44 *Input bi-linear tensile strength curve (tensile stress-cracking strain) in FE-model.*

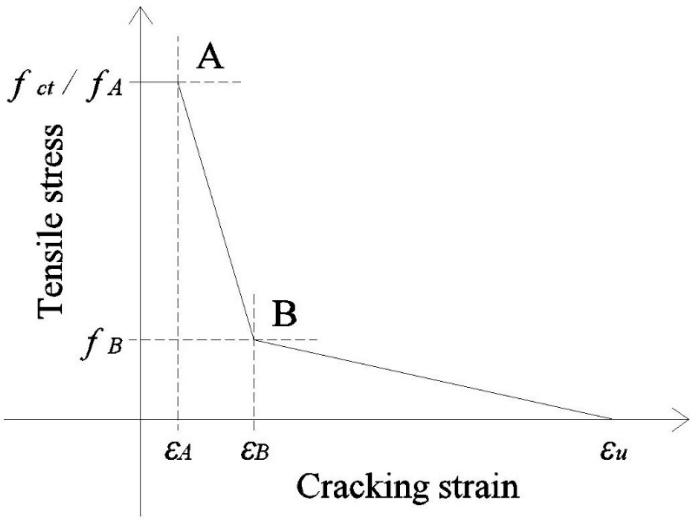

Figure 45 *Input tri-linear tensile strength curve (tensile stress-cracking strain) in FE-model.*

3.2.1.2 Finite element model

The whole geometry of the beam specimen, as described in Section 2.4.1, was modelled, i.e. no symmetry line in the middle of the beam. This choice did not require a significant increase in computational effort and the effort of modelling the symmetry line was avoided. If modelling the beam with a symmetry line, different element sizes would have been needed at the symmetry.

The two boundaries (point rolling supports), were both restrained in the vertical direction and one of the supports was restrained in the horizontal direction. The load in the bending tests was applied with deformation control in accordance to EN 14651. Therefore, the load in the FE-model was also applied as a deformation, increasing in small increments. See Figure 46 for geometry, boundary conditions and load application in the FE-model.

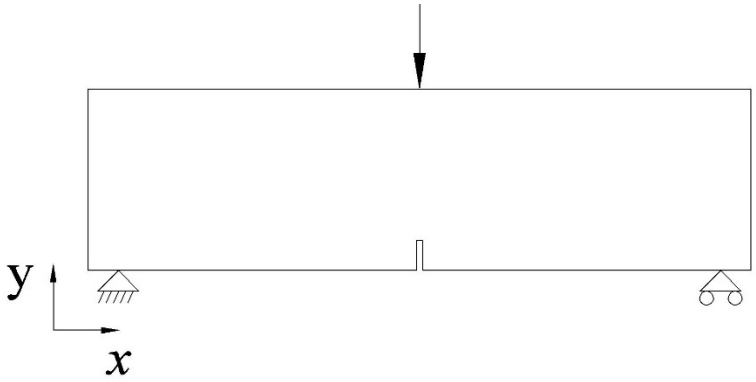

Figure 46 *FE-model for inverse analysis in Abaqus.*

The material properties of the beam were applied differently on different parts of the beam. Plastic material properties were applied on the middle part of the beam over a distance of the characteristic length, l_{cs}, see equation (3-4).

$$l_{cs} = 0.8h = 0.8 \cdot 0.25 = 0.2m \tag{3-4}$$

Elastic material properties were applied on the remaining parts of the beam. See Figure 47 for application of material properties (SS812310:2014 2014).

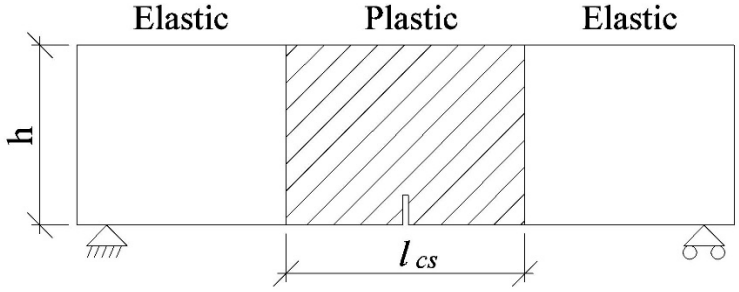

Figure 47 *Application of plastic and elastic material properties in FE-model,* (SS812310:2014 2014).

The beam specimen was modelled with solid, two dimensional (2D) elements and the element type was chosen to 8-node, biquadratic, plane stress and quadrilateral with reduced integration (CPS8R), see Figure 48. The analysis did not require out-of plane stresses, hence that was why a plane stress analysis was performed by choosing plane stress elements.

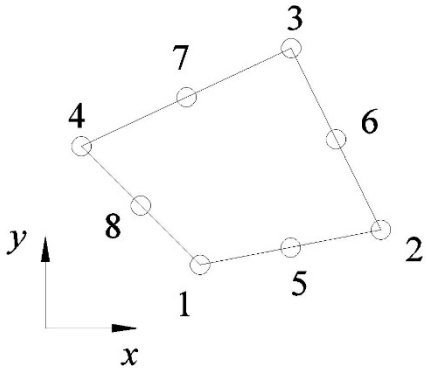

Figure 48 *Element geometry, 8-node isoparametric quadrilateral.*

A mesh sensitivity analysis was performed by trying different mesh densities, with element sizes of 2.5, 5, 7.5 and 15 mm, to analyse the convergence of the maximum load. For all mesh densities, the same input data for the material properties was used. See Table 13 and Figure 49 for mesh sensitivity analysis results.

Table 13 Results from mesh sensitivity analysis, convergence of maximum load.

Test	Element size [mm]	Number of elements	Maximum load [kN]	Convergence difference [‰]
1	2.5	12583	38.80	1.54
2	5	3372	38.86	1.80
3	7.5	1789	38.93	-0.51
4	15	608	38.91	

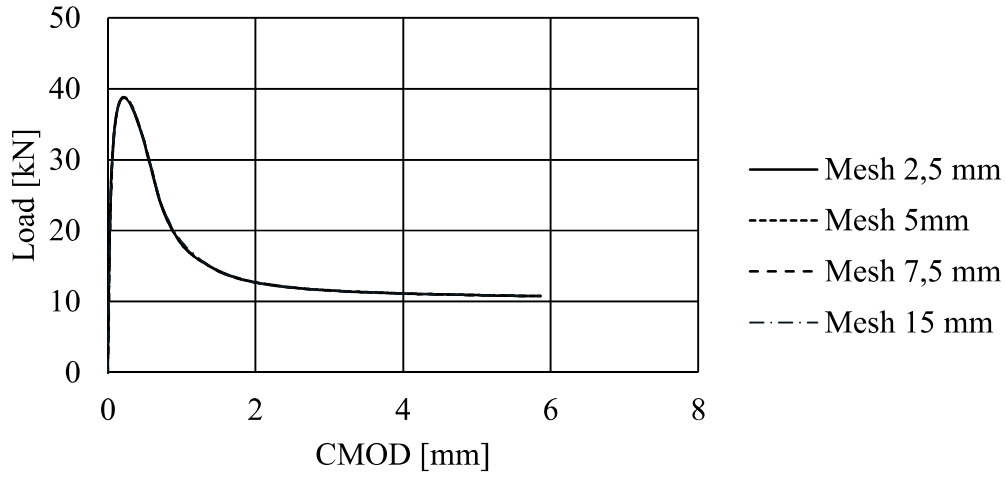

Figure 49 Mesh sensitivity: convergence of Load-crack mouth opening displacement (CMOD) curve.

As can be seen in Table 13, the convergence is very well fulfilled due to the small difference between the maximum loads in the different mesh densities. The mesh with the largest elements that was still verified for a denser mesh was hence the mesh with element size 7.5 mm. The final mesh with 7.5 mm element size is shown in Figure 50.

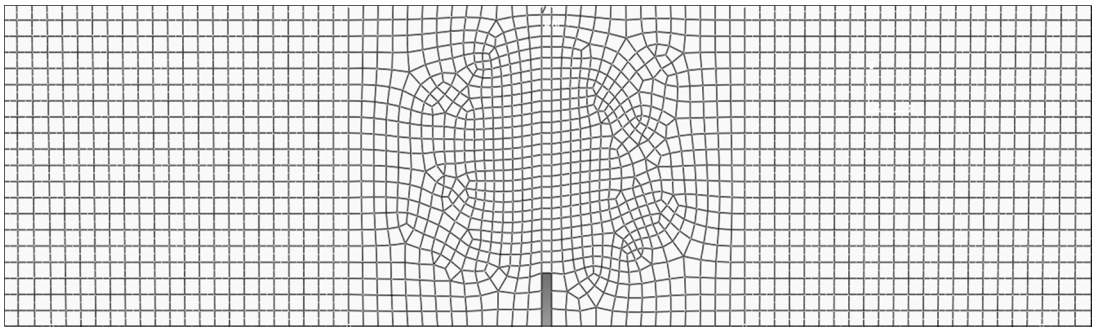

Figure 50 Final mesh of FE-model, 7.5 mm element size.

An additional observation of the final FE-model was that with the chosen mesh it always deformed in one single element row, i.e. in the element row at the notch. See Figure 51 for deformation of the FE-model.

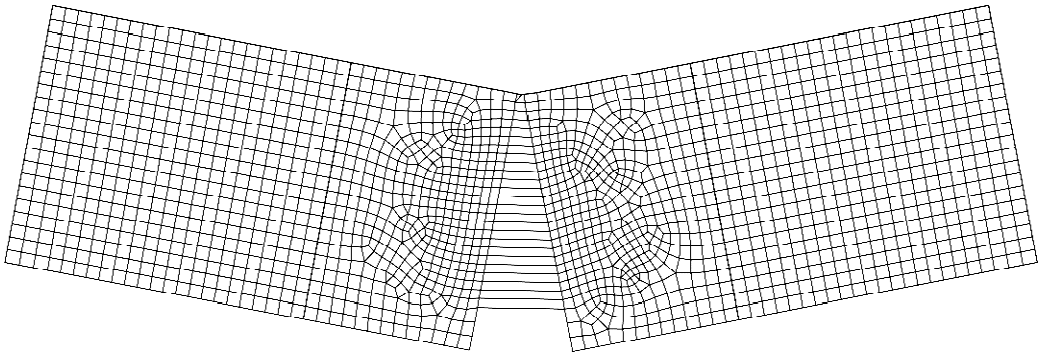

Figure 51 Deformation of the final FE-model.

3.2.1.3 Modelling steps

In accordance with the method for inverse analysis described in previous sections the bi-liner and the tri-linear curves for the tensile stress-strain behaviour were changed manually in the FE-model in iterations. The residual flexural strength-CMOD curves from the numerical analyses were then compared to the same curve from the 3PBT results. The stress values compared were the values corresponding to the residual strengths $f_{ct,L}^{f}$, $f_{R,1}$, $f_{R,2}$, $f_{R,3}$ and $f_{R,4}$. When the values matched with a satisfying factor and when the both curves matched visually, the final tensile stress-strain curves were received.

3.2.2 Assumptions and simplifications

The most important simplifications in the FE-model verified with mesh sensitivity analysis were the following;

- the results from the numerical analysis in Abaqus were compared to the mean value of the results from four beams tested in 3PBT
- the FE-model was modelled in 2D
- uniform distribution of fibres over the concrete section
- the input material data for the beam was the concrete with smeared fibres all over the section

3.3 Results from inverse analysis

The inverse analysis resulted in two different tensile stress-cracking strain curves for both the bi-linear analysis and the tri-linear analysis. For each analysis, one of the curves corresponded to concrete class C25/30 and another curve to concrete class C50/60. All curves had the same AR-glass MiniBar volume of 0.3%.

In this section, the results from the bi-linear analysis are presented followed by the results from the tri-linear analysis.

3.3.1 Bi-linear tensile curve

The results obtained from the inverse analysis when using a bi-linear tensile strength curve as input are presented. First, the tensile strength results from the concrete C25/30 are presented in Table 14 and can be seen in Figure 52.

Table 14 *Bi-linear analysis: Final stress-cracking strain values in tension for concrete class C25/30 and AR-glass MiniBar volume 0.3%.*

Tensile stress [MPa]		Cracking strain [-]	
f_{ct}	8.5	-	0
f_A	1.1	ε_A	0.035
-	0	ε_u	1

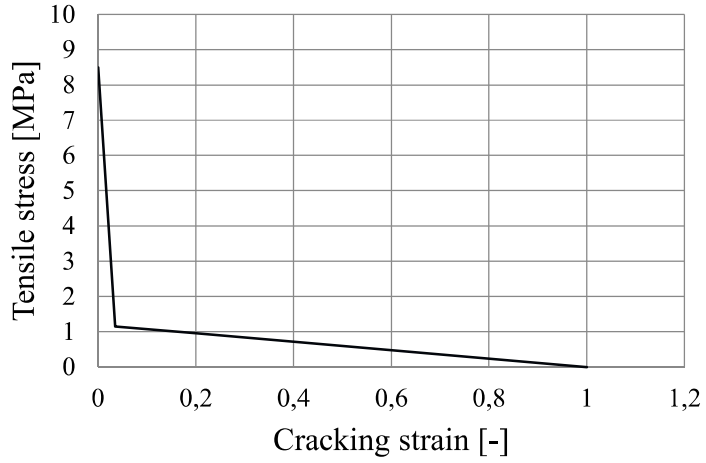

Figure 52 *Bi-linear analysis: Final stress-cracking strain curve in tension for concrete class C25/30 and AR-glass MiniBar volume 0.3%.*

The tensile strength results from the concrete C50/60 are presented in Table 15 and can be seen in Figure 53.

Table 15 *Bi-linear analysis: Final stress-cracking strain values in tension for concrete class C50/60 and AR-glass MiniBar volume 0.3%.*

Tensile stress [MPa]		Cracking strain [-]	
f_{ct}	9.2	-	0
f_A	1.7	ε_A	0.04
-	0	ε_u	1

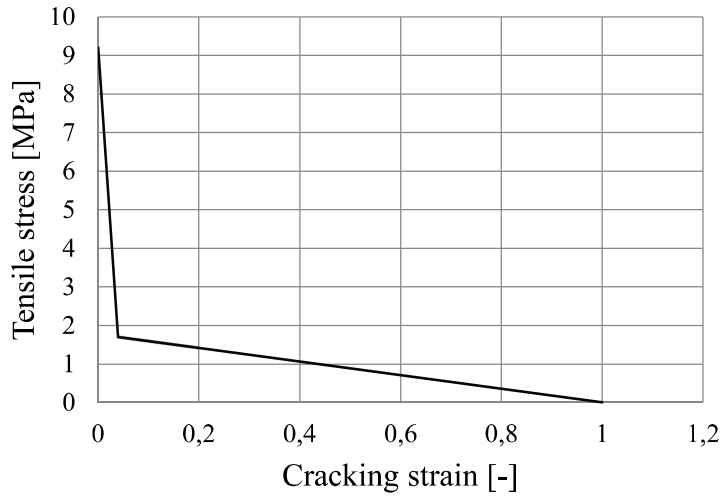

Figure 53 *Bi-linear analysis: Final stress-cracking strain curve in tension for concrete class C50/60 and AR-glass MiniBar volume 0.3%.*

The ultimate residual tensile strengths, f_{Ftu}, were received by plotting the tensile stress-CMOD relation in the inverse analysis and retrieve the values corresponding to $CMOD_{R,3}$, see Section 2.1.4. The ultimate residual strength together with the f_{Ftu} / f_{ct} ratios for the bi-linear analysis can be seen for both concretes in Table 16.

Table 16 *Bi-linear analysis: Ultimate residual tensile strength f_{Ftu} and ratio f_{Ftu} / f_{ct} for concrete class C25/30 and C50/60 and AR-glass MiniBar content 0.3%.*

Concrete class	Ultimate residual tensile strength, f_{Ftu} [MPa]	Ratio f_{Ftu} / f_{ct} [-]
C25/30	0.740	0.087
C50/60	1.087	0.118

A comparison between the numerical results and the experimental results from 3PBT for concrete class C25/30 and C50/60 are shown in Table 17 and Table 18 and Figure 54 and Figure 55.

Table 17 *Bi-linear analysis: Concrete class C25/30 and AR-glass MiniBar volume 0.3%. Comparison of residual strength values between results from numerical analysis and 3PBT.*

CMOD [mm]	Stress from numerical analysis [MPa]	Stress from experimental results [MPa]	Difference [%]
0	4.230	4.354	2.8
0.5	1.477	0.929	59.0
1.5	0.961	0.947	1.5
2.5	0.811	0.848	4.4
3.5	0.698	0.723	3.4

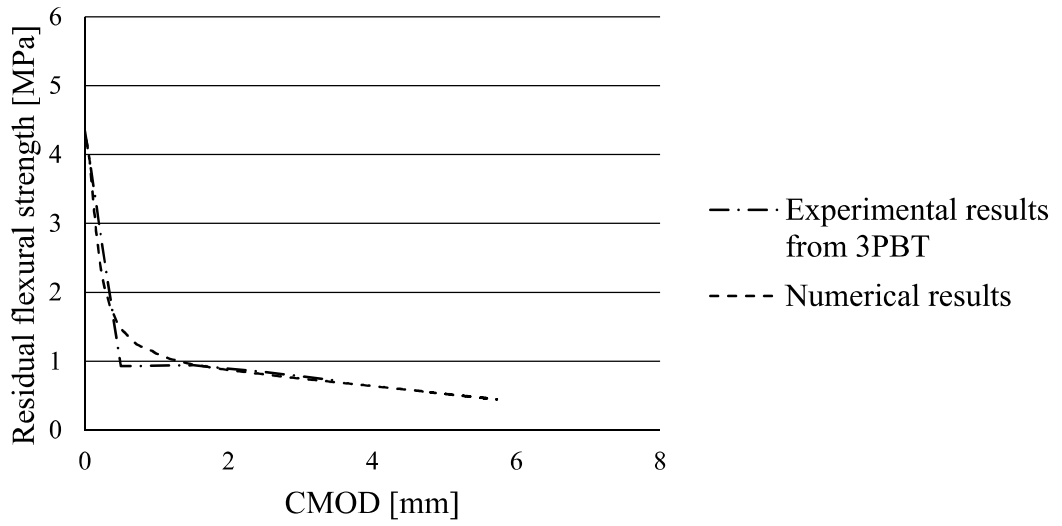

Figure 54 *Bi-linear analysis: Concrete class C25/30 and AR-glass MiniBar volume 0.3%. Comparison between stress-CMOD curves in bending for mean experimental results from 3PBT and numerical analysis.*

Table 18 *Bi-linear analysis: Concrete class C50/60 and AR-glass MiniBar volume 0.3%. Comparison of residual strength values between results from numerical analysis and 3PBT.*

CMOD [mm]	Stress from numerical analysis [MPa]	Stress from experimental results [MPa]	Difference [%]
0	4.841	4.900	1.2
0.5	2.070	1.647	25.7
1.5	1.413	1.547	8.7
2.5	1.194	1.239	3.7
3.5	1.019	1.003	1.6

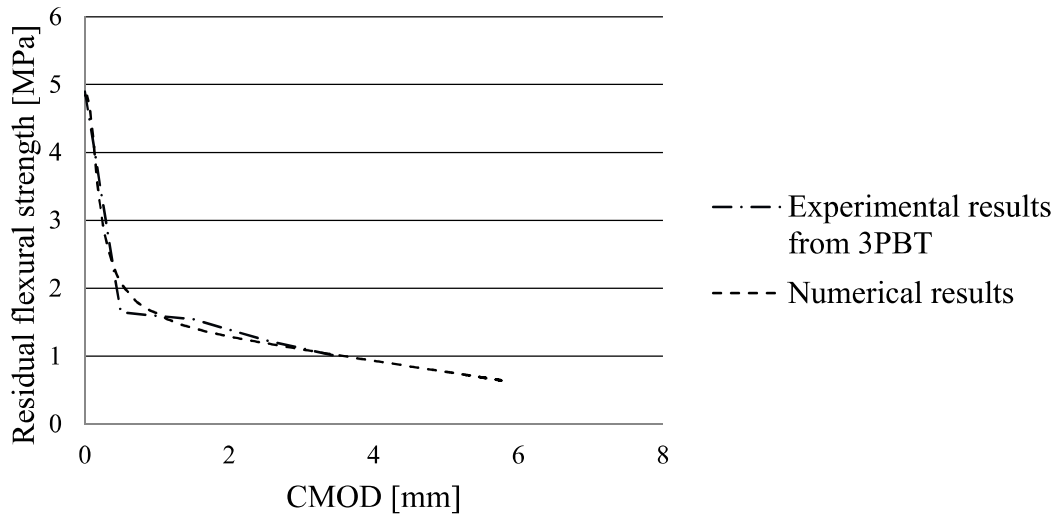

Figure 55 *Bi-linear analysis: Concrete class C50/60 and AR-glass MiniBar volume 0.3%. Comparison between stress-CMOD curves in bending for mean experimental results from 3PBT and numerical analysis.*

Finally, the maximum tensile strength from inverse analysis was compared to the maximum tensile strength of plain concrete for each concrete class C25/30 and C50/60, see Table 19. The average tensile strength of plain concrete, f_{ctm}, was retrieved from Eurocode 2 (SS-EN 1992-1-1 2008).

Table 19 *Bi-linear analysis: Comparison between maximum tensile strength for plain concrete and from inverse analysis.*

Concrete class	Maximum tensile strength, plain concrete, f_{ctm} [MPa]	Maximum tensile strength, inverse analysis, f_{ct} [MPa]	Difference [%]
C25/30	2.6	8.5	227
C50/60	4.1	9.2	124

3.3.2 Tri-linear tensile curve

The results obtained from the inverse analysis when using a tri-linear tensile strength curve as input are presented. First, the tensile strength results from the concrete C25/30 are presented in Table 20 and can be seen in Figure 56.

Table 20 *Tri-linear analysis: Final stress-cracking strain values in tension for concrete class C25/30 and AR-glass MiniBar volume 0.3%.*

Tensile Stress [MPa]		Cracking strain [-]	
f_{ct}	5	-	0
f_A	5	ε_A	0.04
f_B	1	ε_B	0.07
-	0	ε_u	1.2

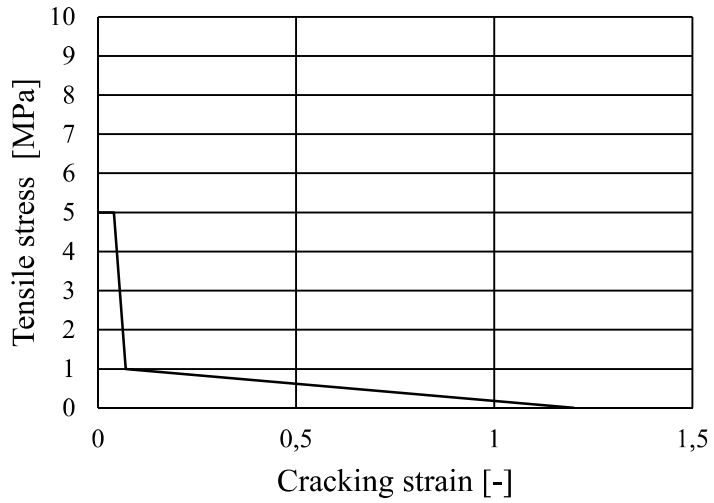

Figure 56 *Tri-linear analysis: Final stress-cracking strain curve in tension for concrete class C25/30 and AR-glass MiniBar volume 0.3%.*

The tensile strength results from the concrete C50/60 are presented in Table 21 and can be seen in Figure 57.

Table 21 *Tri-linear analysis: Final stress-cracking strain values in tension for concrete class C50/60 and AR-glass MiniBar volume 0.3%.*

Tensile stress [MPa]		Cracking strain [-]	
f_{ct}	6	-	0
f_A	6	ε_A	0.04
f_B	1.5	ε_B	0.07
-	0	ε_u	1.2

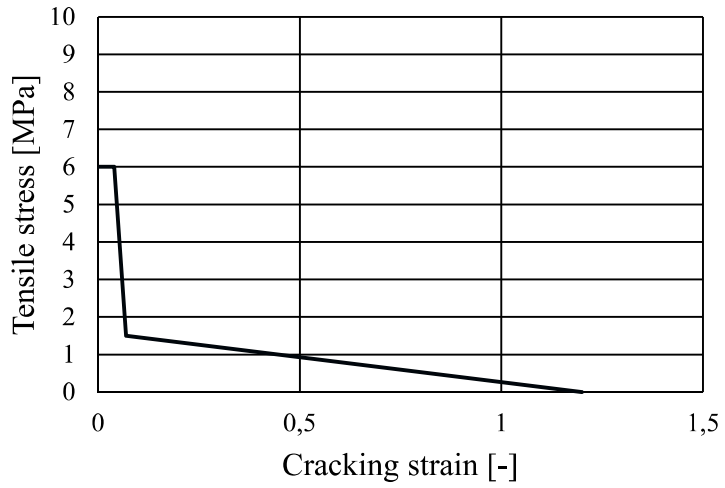

Figure 57 *Tri-linear analysis: Final stress-cracking strain curve in tension for concrete class C50/60 and AR-glass MiniBar volume 0.3%.*

The ultimate residual tensile strengths, f_{Ftu}, were received by plotting the tensile stress-CMOD relation in the inverse analysis and retrieving the values corresponding to $CMOD_{R,3}$, see Section 2.1.4. The ultimate residual tensile strength together with the the f_{Ftu} / f_{ct} ratios from the tri-linear analysis can be seen for both concretes in Table 22.

Table 22 *Tri-linear analysis: Ultimate residual tensile strength f_{Ftu} and ratio f_{Ftu} / f_{ct} for concrete class C25/30 and C50/60 and AR-glass MiniBar content 0.3%.*

Concrete class	Ultimate residual tensile strength, f_{Ftu} [MPa]	Ratio f_{Ftu} / f_{ct} [-]
C25/30	0.717	0.143
C50/60	1.070	0.178

A comparison between the numerical results and the experimental results from 3PBT for concrete class C25/30 and C50/60 are shown in Table 23 and Table 24 and Figure 58 and Figure 59.

Table 23 *Tri-linear analysis: Concrete class C25/30 and AR-glass MiniBar volume 0.3%. Comparison of residual flexural strength values between results from numerical analysis and 3PBT.*

CMOD [mm]	Stress from numerical analysis [MPa]	Stress from experimental results [MPa]	Difference [%]
0	4.230	4.354	2.8
0.5	1.477	0.929	59.0
1.5	0.961	0.947	1.5
2.5	0.811	0.848	4.4
3.5	0.698	0.723	3.4

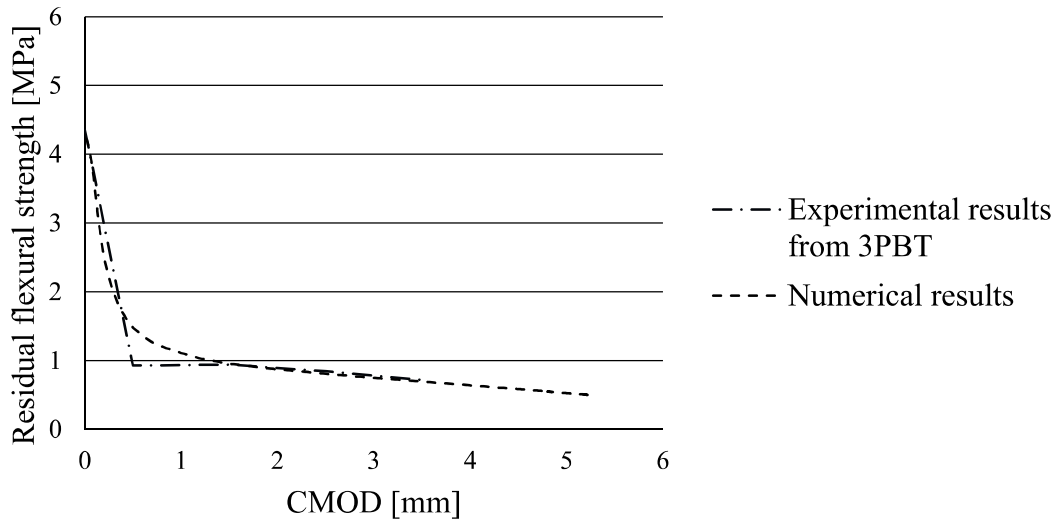

Figure 58 *Tri-linear analysis: Concrete class C25/30 and AR-glass MiniBar volume 0.3%. Comparison between stress-CMOD curves in bending for mean experimental results from 3PBT and numerical analysis.*

Table 24 *Tri-linear analysis: Concrete class C50/60 and AR-glass MiniBar volume 0.3%. Comparison of residual strength values between results from numerical analysis and 3PBT.*

CMOD [mm]	Stress from numerical analysis [MPa]	Stress from experimental results [MPa]	Difference [%]
0	4.649	4.900	5.1
0.5	2.440	1.647	48.2
1.5	1.476	1.547	4.6
2.5	1.198	1.239	3.3
3.5	1.023	1.003	2.0

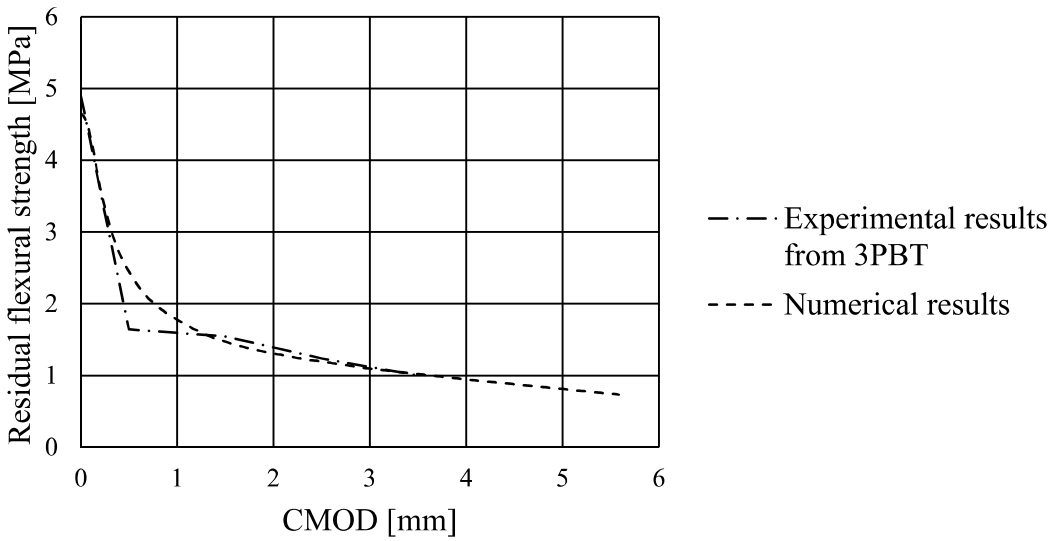

Figure 59 *Tri-linear analysis: Concrete class C50/60 and AR-glass MiniBar volume 0.3%. Comparison between stress-CMOD curves in bending for mean experimental results from 3PBT and numerical analysis.*

Finally, the maximum tensile strength from inverse analysis was compared to the maximum tensile strength of plain concrete for each concrete class C25/30 and C50/60, see Table 25. The average tensile strength of plain concrete, f_{ctm}, was retrieved from Eurocode 2 (SS-EN 1992-1-1 2008).

Table 25 Comparison between maximum tensile strength for plain concrete and from inverse analysis.

Concrete class	Maximum tensile strength, plain concrete, f_{ctm} [MPa]	Maximum tensile strength, inverse analysis, f_{ct} [MPa]	Difference [%]
C25/30	2.6	5	92
C50/60	4.1	6	46

3.3.3 Comparison of bi-linear and tri-linear tensile strength curves

Both the bi-linear and tri-linear analyses resulted in tensile strength curves for concrete C25/30 and C50/60. The curves are compared to each other with regard to their fracture energies in Table 26.

Table 26 Difference in fracture energy between bi-linear and tri-linear curves.

Fracture Energy	Bi-linear curve [N/m]	Tri-linear curve [N/m]	Difference [%]
C25/30	5323	5308	0.3
C50/60	8934	7414	20.5

The obtained tensile curves from the bi-linear and tri-linear analysis, for concrete class C25/30, are compared in Figure 60.

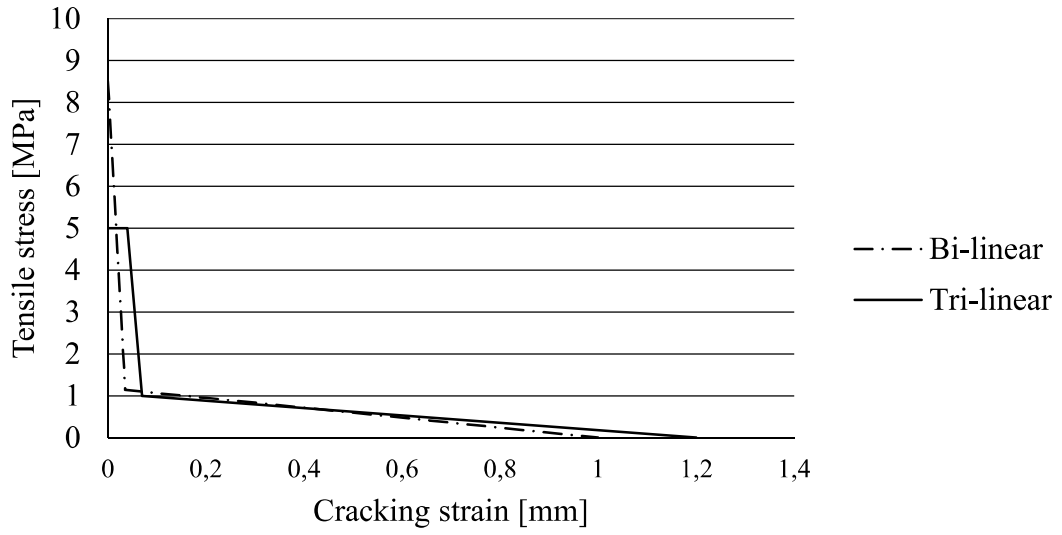

Figure 60 *Comparison between bi-linear and tri-linear tensile strength curves received from inverse analysis of concrete C25/30 with 0.3% fibre volume.*

The obtained tensile curves from the bi-linear and tri-linear analysis, for concrete class C50/60, are compared in Figure 61.

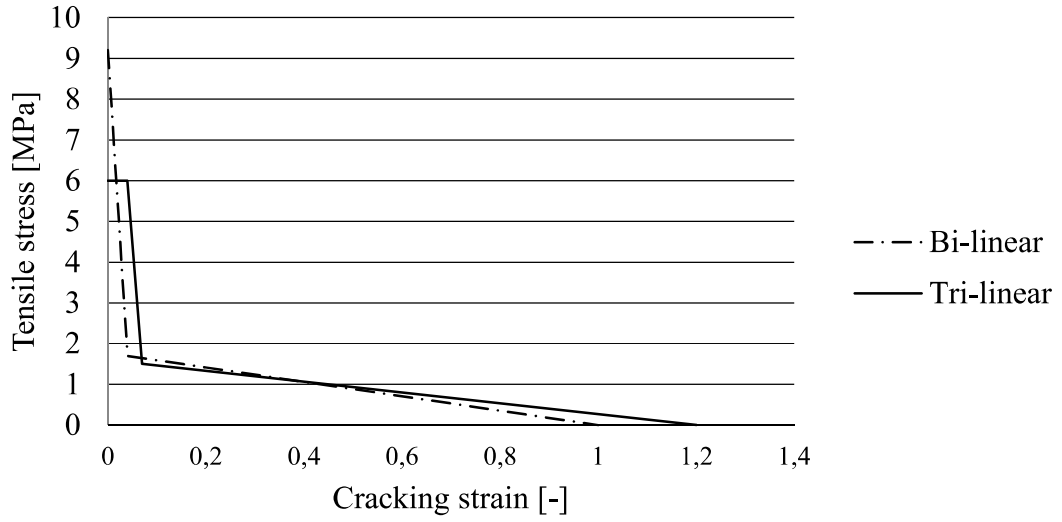

Figure 61 *Comparison between bi-linear and tri-linear tensile strength curves received from inverse analysis of concrete C50/60 with 0.3% fibre volume.*

3.4 Conclusions of inverse analysis

The aim of this partial study was to obtain tensile strength curves for glass and basalt FRC by doing an inverse analysis. Two tensile strength curves were received from both the bi-linear and the tri-linear analysis. These curves corresponded to concrete with low fibre volume, i.e. 0.3% and with two concrete classes, C25/30 and C50/60.

In the comparison between the residual flexural strength curves from numerical analysis and experimental testing, the numerical results were in good correlation to experimental testing. However, the residual flexural strength value that gave the largest strength difference was corresponding to CMOD 0.5 mm, which was the case for both the bi-linear and the tri-linear analysis and for both concrete classes. Based on these results, the inverse method both with bi-linear and tri-linear input curves was considered to work well. Although, an analysis method which better can capture the stress drop after crack initiation is needed.

The maximum tensile strength in concrete was greatly affected by the inclusion of AR-glass MiniBars according to the results from inverse analysis, even for the studied small fibre volume. This can be seen in the comparison of maximum tensile strength for plain concrete with the same concrete classes. For the bi-linear curves, the increase in maximum tensile strength was higher than for the tri-linear curves. For concrete class C25/30, the tri-linear curve had an increase of 92% instead of 227% as in the bi-linear analysis. In similar manner, for concrete class C50/60, the increase was 46% instead of 124%.

In the comparison between the bi-linear and tri-linear curves, the difference in fracture energy for concrete class C25/30 was small, while the difference for the concrete class C50/60 was around 20%. The comparisons are not giving the same result and therefore it is difficult to see any relationship between the fracture energy and type of input tensile strength curve used.

Even though the correlation to the bending test results was good, the large increase in maximum tensile strength from the inverse analysis compared to plain concrete can be concluded large due to the low fibre volume of 0.3%. The large increase in maximum tensile strength was seen by the authors of this thesis as unrealistic. This was important to have in mind in the following parts of the work, especially for the bi-linear analysis.

No test results from pure tensile tests of exactly the same MRC used in the inverse analysis were found in the literature, which could be compared to the received tensile strength curves. Therefore, a conclusion whether the received tensile curves for MRC from inverse analysis were in good correlation to the real strength could not be drawn on the basis of the work made in this thesis work. Hence further experimental studies are needed in order to investigate the real tensile response.

4 Analysis of FRC-MCFT

In this chapter, the third partial study, the analysis of the FRC-MCFT is presented. First, the methodology of the calculations is described, followed by the results from shear capacity calculations. To analyse the applicability of FRC-MCFT on different FRCs a sensitivity analysis was also performed which is presented with its results. Finally, the conclusions of this partial study are presented.

The inverse analysis resulted in two different tensile stress- cracking strain curves for the bi-linear analysis and two curves for the tri-linear. For each analysis, one of the curves corresponded to concrete class C25/30 and the other curve to concrete class C50/60. All curves had the same AR-glass MiniBar volume of 0.3%. These curves were named according to Figure 62 below.

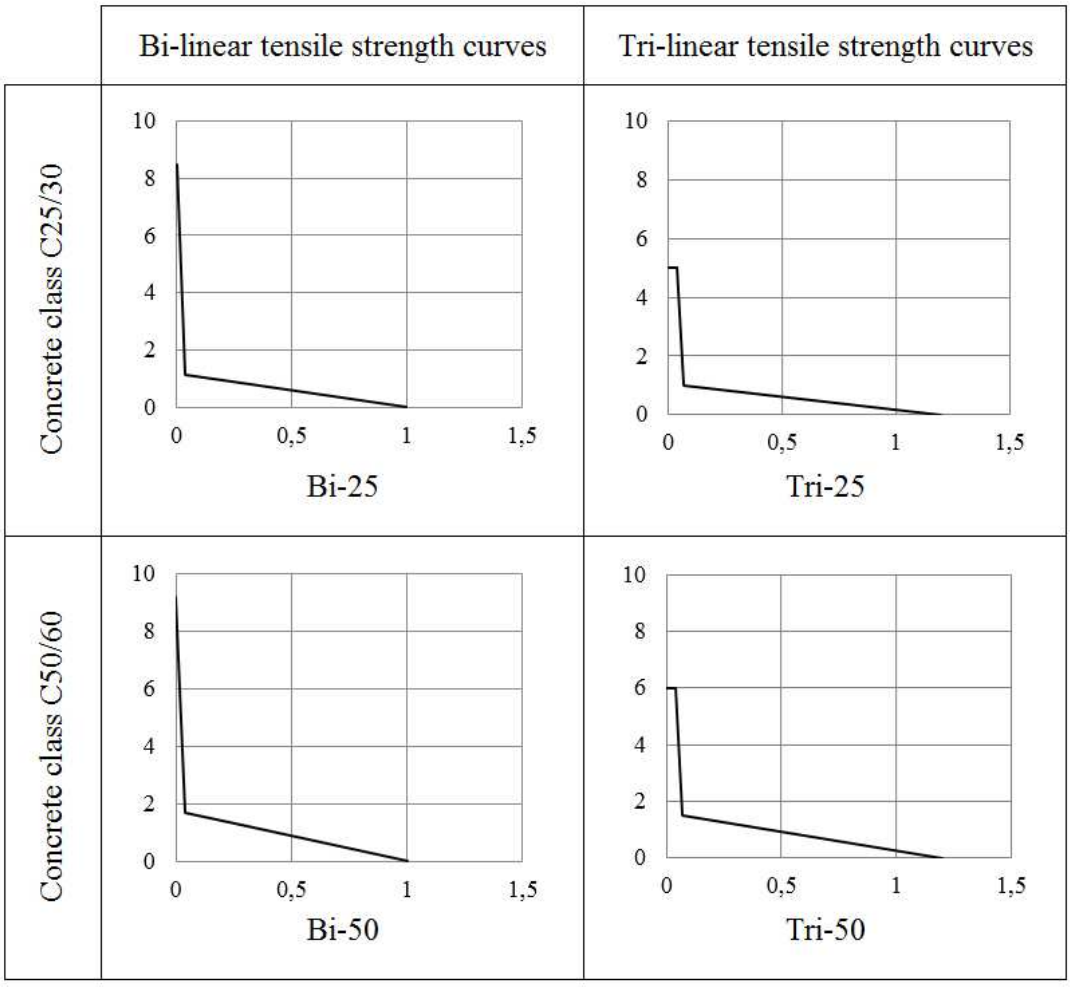

Figure 62 Names of the 4 tensile strength curves retrieved from inverse analysis.

4.1 Application of tensile strength curves

To analyse the possibilities to utilize the Modified Compression Field Theory (MCFT) on glass and basalt fibre reinforced concrete (FRC) by using the tensile strength curves of the materials, both a MCFT adopted for FRC and tensile strength

curves were needed. These were received from the literature study and the inverse analysis respectively.

The Simplified FRC-MCFT (FRC-MCFT) is a theory based on the MCFT to calculate the shear capacity of a structure that may include fibre reinforcement. This theory was thoroughly described in Section 2.3.6. In this study, the FRC-MCFT is used in the analysis of whether the tensile strength curves of glass fibre reinforced concrete (GFRC) and basalt fibre reinforced concrete (BFRC) could be applicable on the MCFT to calculate the shear capacity of a structure.

Tensile strength curves of GFRC were established in Chapter 3, by doing an inverse analysis of real bending tests of Alkali Resistant glass (AR-glass) MiniBars. The outcome of this became two tensile curves for the bi-linear analysis and two curves for the tri-linear analysis. All curves had the same fibre volume of 0.3% with different concrete classes and tension softening behaviour. Hence, the suitability of using the FRC-MCFT on GFRC and BFRC was going to be based on the result given by the results of the appliance of AR-glass MiniBars. The glass and basalt s were therefore assumed to have the same response, which is in accordance with the conclusions drawn in Section 2.5.

The shear calculations were done by developing a program in the software Matlab, based on the FCT-MCFT, see Appendix A. The iteration process of the program can be seen in Figure 63. The ultimate shear capacities were calculated when convergence was reached in the program, i.e. when equilibrium existed.

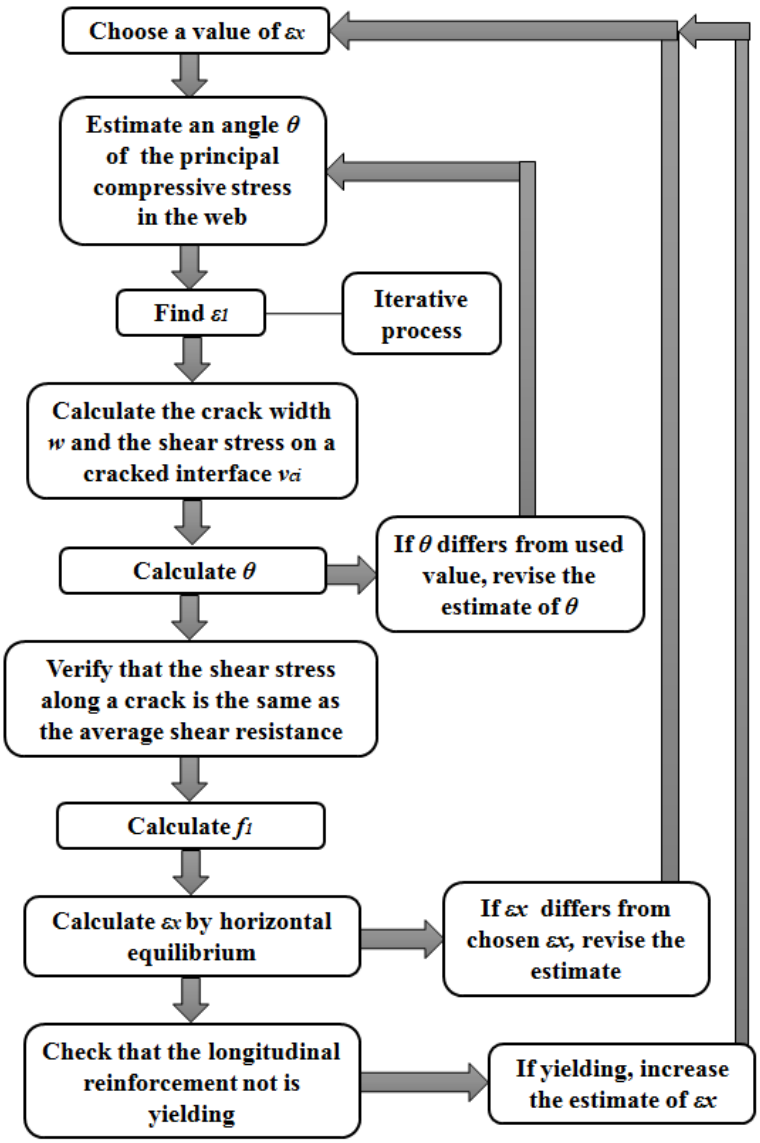

Figure 63 *The iterative process of the FRC-MCFT by* (Minelli & Plizzari 2011).

In the MCFT, as well as in the FRC-MCFT, the values are being iterated until compatibility exists between the strain ε and the angle θ of the compressive strut, in accordance with equilibrium conditions. It can be hard to find exact convergence since the equations are based on empirical data and are not analytically enclosed (Collins & Mitchell 1987).

The FRC-MCFT is based on structures with bars aligned in the longitudinal direction (x-direction) with or without stirrups (z-direction). Also, a cross section of the structure is needed. Therefore, to be able to apply the FRC-MCFT to calculate the shear response of the MRC, a fictitious beam was needed. With the fictitious beam, the reinforcement arrangement could be decided and changed. The beam was decided to be rectangular with a width of 220 mm and a height of 400 mm. This beam has nothing to do with the modelled beam in Abaqus. In all calculations, presented in the following sections, the beam was reinforced with stirrups, 4x3 bars as lower reinforcement and 7 bars with a spacing of 100 mm as skin reinforcement. See Figure 64 for visualization of the beam cross-section and the reinforcement arrangement.

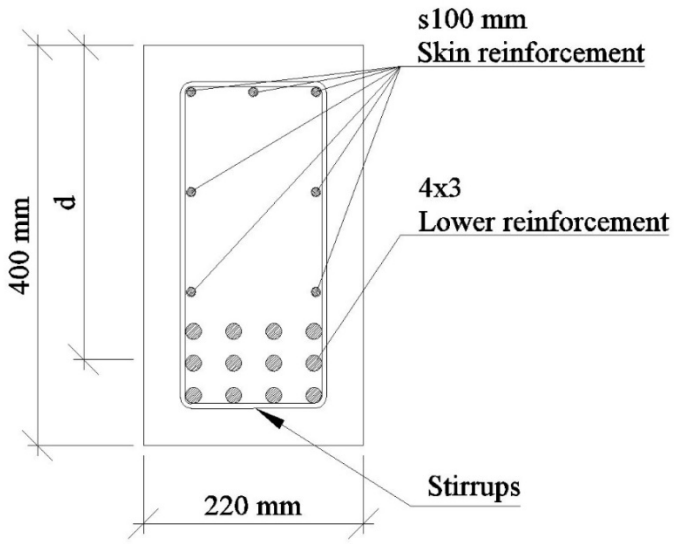

Figure 64 Beam cross-section used in the calculations according to FRC-MCFT.

Moreover, some changes were done in the program based on the FRC-MCFT in order to apply some of the parameters obtained from the inverse analysis of the concretes. The most important changes were;

- the maximum tensile strength, f_{ct}, was received from inverse analysis, hence not calculated according to the relationship in the FRC-MCFT
- the modulus of elasticity was assumed equal to that of plain concrete
- the value of the ultimate tensile strength was received from inverse analysis, thus not calculated according to the relationship given in the FRC-MCFT

The first of these changes was regarding the maximum tensile strength. In the FRC-MCFT, f_{ct} is being calculated from the concrete compressive strength, f_{ck}, in accordance with the MCFT (Minelli & Plizzari 2011). The relationship can be seen below:

$$f_{ct} = 0.33\sqrt{f_{ck}} \tag{4-1}$$

When using the FRC-MCFT in this study, the maximum tensile strengths received from the inverse analysis were used instead of the above relationship. The method used was therefore, to some extent, distinguished from the study by (Minelli & Plizzari 2011). It shall be noted again that the tensile strengths received from the inverse analysis showed, in comparison to plain concrete, very high maximum tensile strengths.

The second modification that was done of the FRC-MCFT within this study was regarding the modulus of elasticity, E_c. In the FRC-MCFT, E_c is calculated based on the compression strength, see equation (2-33) in Section 2.3.6. This relation was not used in this study. Instead, the values used in the inverse analysis were used in order to have the same modulus of elasticity in both the inverse analysis and in the FRC-MCFT. This resulted in lower modulus of elasticity than of the ones calculated based on f_{ck}. The values used were assumed to be the same as of ordinary concrete of the same concrete class since the modulus of elasticity does not change significantly, due to the addition of fibres (Fib 2013). For the values of the modulus of elasticity, see Table 27.

Table 27 Difference between used E_c and calculated from FRC-MCFT.

Concrete class	Modulus of elasticity [GPa]	
	Eurocode	$4950 \cdot \sqrt{f_{ck}}$
C25/30	31	34.9
C50/60	37	43.3

Moreover, in the FRC-MCFT, the only parameter taken into account for FRC is the ultimate residual tensile strength, f_{Ftu} (Minelli & Plizzari 2011). Since it is difficult to obtain the tension behaviour of concrete by experimental testing, it is also difficult to obtain the f_{Ftu}. According to (Fib 2013), for a rigid-plastic model a simplification can be used to receive the parameter f_{Ftu}. This simplification is based on the residual nominal bending strength, f_{R3}, and is presented in equation (4-2) below. In addition, equation (4-3) and Figure 65 show how this simplification is obtained. The relationship between f_{Ftu} and f_{R3} can be justified by calibration of a variety of specimen sizes and various types of fibres and fibre dosages (Mobasher et al. 2014).

$$f_{Ftu} = \frac{f_{R3}}{3} \tag{4-2}$$

$$M_u = \frac{f_{R3} b h_{sp}^2}{6} = \frac{f_{Ftu} b h_{sp}^2}{2} \tag{4-3}$$

where M_u is the ultimate moment, b is the width and h_{sp} is the distance between the notch tip and the top of the specimen.

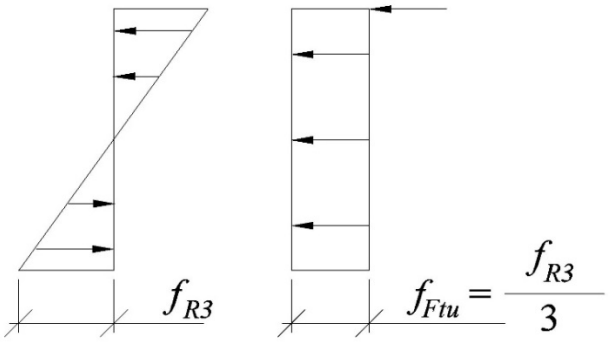

Figure 65 Simplified model used to calculate the ultimate residual tensile strength in uniaxial tension f_{Ftu} by using the residual nominal bending strength f_{R3}.

The third and last modification in this study was that the values of f_{Ftu} were obtained from the inverse analysis, thus not from the equation (4-2) above. Since the FRC-MCFT is only applicable on tension softening materials, it was important to obtain an ultimate residual tensile strength value, f_{Ftu}, lower than the maximum tensile strength, f_{ct}, obtained from the inverse analysis, i.e. the tension softening.

When calculating the crack width in the FRC-MCFT, a denser crack pattern is received when having a higher value of the ultimate residual tensile strength, f_{Ftu}. A denser crack pattern results in smaller cracks and higher shear resistance in the FRC-MCFT. The spacing of the cracks is reduced with the following ratio according to the FRC-MCFT:

$$1 - \frac{f_{Ftu}}{f_{ct}} \tag{4-4}$$

4.2 Shear capacity calculation of MRC

Shear capacity calculations were performed according to the FRC-MCFT and applied on both the bi-linear curves and the tri-linear curves, received from inverse analysis. In this section, the input data and the results from this calculations are presented.

4.2.1 Input data

The input data for the shear capacity calculations were received both from the inverse analysis in Section 3.3 and from the compression tests in Section 2.4.2.

In order to be able to apply the tensile strength curves of the materials, some values of the curves were distinguished. The values obtained from the inverse analysis were the maximum tensile strength, f_{ct}, and the ultimate residual tensile strength, f_{Ftu}. These parameters were further used to represent the tensile strength curves of the AR-glass MRC. In addition, the compressive strength, f_{ck}, was received from the compression tests and the modulus of elasticity, E, from Eurocode in accordance with the assumptions of E in Section 3.2.1.1. For input data to the shear capacity calculations applied on the bi-linear input curves, see Table 28, and on the tri-linear curves, see Table 29.

Table 28 Bi-linear curve: Input data to shear capacity calculations.

Bi-linear	f_{ct} [MPa]	f_{Ftu} [MPa]	f_{ck} [MPa]	E [GPa]
Bi-25	8.5	0.740	49.8	31
Bi-50	9.2	1.087	76.6	37

Table 29 Tri-linear curve: Input data to shear capacity calculations.

Tri-linear	f_{ct} [MPa]	f_{Ftu} [MPa]	f_{ck} [MPa]	E [GPa]
Tri-25	5	0.717	49.8	31
Tri-50	6	1.070	76.6	37

4.2.2 Results from shear capacity calculations

In this section, the results from the shear capacity calculations are presented. First, the results with the bi-linear curve as input are given, followed by the results with the tri-linear curve as input.

4.2.2.1 Bi-linear tensile strength input

In this section, the results from calculations according to FRC-MCFT on the two bi-linear tensile strength curves received from the inverse analysis in Section 3.3.1 and input data according to Table 28 are presented. First, the results for Bi-25 are presented followed by the results for Bi-50.

The calculation of shear capacity according to FRC-MCFT was an iterative process. In order for the shear capacity calculations to receive a value, all relationships (see Section 2.3.6) had to converge. Moreover, for the shear capacity to be reasonable, the calculation needs to converge for a possible reinforcement amount. With regard to unrealistic spacing of stirrups and minimum spacing of cracks, s_z and s_x are limited to a minimum of 100 mm according to Section 2.3.4.

For the calculations with Bi-25 as input, no convergence was received for a reasonable and possible shear reinforcement ratio/amount. To show this, different stirrup diameters and different distances between the stirrups were analysed when having constant longitudinal reinforcement ratio, ρ_x. In Table 30, the largest distance between stirrups for different stirrup diameter is presented together with the reinforcement ratio in the longitudinal and vertical direction respectively. The largest possible distance between stirrups was given due to that higher angles were needed for increasing distance, which gave negative longitudinal strain, see Appendix B for more results. As a consequence of the unreasonable result of reinforcement amount, the shear capacities from the calculations are not presented.

Table 30 *Bi-25 as input: Results from shear capacity calculations according to FRC-MCFT for AR-glass MRC with concrete class C25/30 and AR-glass MiniBar content 0.3%.*

Stirrup diameter [mm]	Reinforcement ratio of stirrups, ρ_z [-]	Reinforcement ratio of longitudinal reinforcement, ρ_x [-]	Largest possible distance between stirrups, s_z [mm]
8	0.0183	0.0625	25*
10	0.0178		40*
12	0.0228		45*

** With regard to unrealistic spacing of stirrups and minimum spacing of cracks, s_z and s_x, were limited to a minimum of 100 mm according to Section 2.3.4.*

With Bi-50 as input, the calculations according to FRC-MCFT did converge for some reasonable reinforcement ratios/amounts. Although, the maximum spacing between the stirrups was limited to very short spacing. Therefore, the calculations for Bi-50 were

performed in the same way as for Bi-25, i.e. with varying diameter of stirrups and spacing. Thus, from this calculation, the largest possible distance between the stirrups for different diameters is presented in Table 31. For more results see Appendix C.

Table 31 *Bi-50 as input: Results from shear capacity calculations according to FRC-MCFT for AR-glass MRC with concrete class C50/60 and AR-glass MiniBar content 0.3%.*

Stirrup diameter [mm]	Reinforcement ratio of stirrups, ρ_z [-]	Reinforcement ratio of longitudinal reinforcement, ρ_x [-]	Largest possible distance between stirrups, s_z [mm]
8	0.00762	0.0625	60*
10	0.00793		90*
12	0.00935		110

* *With regard to unrealistic spacing of stirrups and minimum spacing of cracks, s_z and s_x, were limited to a minimum of 100 mm according to Section 2.3.4.*

The most reasonable stirrup placing from this analysis was hence stirrup diameter 12 mm and distance between stirrups 110 mm. To analyse how the reinforcement ratio of the longitudinal reinforcement affected the results, the transversal reinforcement ratio was kept constant while the longitudinal reinforcement ratio was changed. The longitudinal reinforcement ratios was changed by changing the diameter of the bars in the longitudinal direction while the number of bars was kept constant. This resulted in different possible bar diameters, received when convergence in the calculations according to FRC-MFT was reached, see Table 32.

Table 32 *Bi-50 input: Possible longitudinal bar diameters for shear calculations, according to FRC-MCFT for AR-glass MRC with concrete class C50/60, constant reinforcement ratio of stirrups.*

Possible longitudinal bar diameter [mm]	Transversal reinforcement ratio, ρ_z [-]	Longitudinal reinforcement ratio, ρ_x [-]
12	0.00935	0.0276
16		0.04287
20		0.0625

The shear capacity for plain concrete with concrete class C50/60 was calculated according to FRC-MCFT for the possible longitudinal bar diameters in Table 33. Moreover the calculations were performed with stirrup diameter 12 mm and distance between stirrups 110 mm, which was the most reasonable stirrup amount as can be seen in Table 31 above. The shear capacity for plain concrete is shown in a comparison to the calculations with Bi-50 as input in Table 33. See Appendix C for more results.

Table 33 *Bi-50 as input: Comparison between shear capacity calculations according to FRC-MCFT for plain concrete C50/60 and AR-glass MRC C50/60.*

Possible lower longitudinal bar diameter [mm]	Shear capacity of plain concrete, C50/60 [kN]	Shear capacity with Bi-50 [kN]	Difference [%]
12	579	665	14.9
16	620	674	8.7
20	645	668	3.6

4.2.2.2 Tri-linear tensile strength input

In this section, the results from calculations according to FRC-MCFT on the two tri-linear tensile strength curves received from the inverse analysis in Section 3.3.2 and input data according to Table 29 are presented.

In the calculations with the tri-linear curves as input, there were no obvious problems with convergence. The calculations converged for varying stirrup amounts as well as varying longitudinal reinforcement amounts. For more results of the calculations of Tri-25 and Tri-50, see Appendix D respectively E.

To be able to compare the results from calculations between the bi-linear curve and the tri-linear curves as input, the shear capacities were calculated with the same reinforcement amount as in the shear capacity calculations with Bi-50 as input. These results are presented in Table 33. In similar manner, the shear capacities with tri-linear curves were compared to the shear capacities for plain concrete with concrete class C25/30 and C50/60. For the shear capacities, including comparison to plain concrete, see Table 34 for Tri-25 and Table 35 for Tri-50.

Table 34 *Tri-25 as input: Comparison between shear capacity calculations according to FRC-MCFT for plain concrete C25/30 and AR-glass MRC C25/30.*

Lower longitudinal bar diameter [mm]	Shear capacity of plain concrete, C25/30 [kN]	Shear capacity with Tri-25 [kN]	Difference [%]
12	557	-*	-
16	595	689	15.8
20	625	720	15.2

* *The shear capacity calculation with this specific reinforcement amount led to that the steel stress in the longitudinal reinforcement exceeded its yield strength.*

Table 35 *Tri-50 as input: Comparison between shear capacity calculations according to FRC-MCFT for plain concrete C50/60 and AR-glass MRC C50/60.*

Lower longitudinal bar diameter [mm]	Shear capacity of plain concrete, C50/60 [kN]	Shear capacity with Tri-50 [kN]	Difference [%]
12	579	-*	-
16	620	775	25.0
20	645	817	26.7

* *The shear capacity calculation with this specific reinforcement amount led to that the steel stress in the longitudinal reinforcement exceeded its yield strength.*

4.3 Sensitivity analysis of FRC-MCFT

A sensitivity analysis was performed on the calculations according to FRC-MCFT due to the following reasons;

- the results from the inverse analysis were concluded to show a very large increase in the maximum tensile strength, f_{ct}. These results could not be concluded to be realistic without validation against real experimental testing of the tensile strength of the materials
- the calculations according to the FRC-MCFT, with Bi-25 as input, did not converge for reasonable reinforcement amounts
- the calculations according to the FRC-MCFT, with Bi-50 as input, did only converge for some reasonable reinforcement amounts

The sensitivity analysis was performed with a parameter study, where the constant input data was;

- the modulus of elasticity E
- the compressive strength f_{ck}
- beam cross section
- reinforcement arrangement

The reinforcement arrangement is shown in Table 36.

Table 36 Reinforcement arrangement, input data in sensitivity analysis.

Longitudinal reinforcement				Stirrups	
Lower		Skin		ϕ [mm]	s_z [mm]
ϕ [mm]	Amount	ϕ [mm]	s_x [mm]		
20	12	10	100	10	100

The sensitivity was analysed by changing the input of the maximum tensile strength f_{ct} and the ultimate residual tensile strength f_{Ftu}. The inputs of the f_{ct} were in a range from 2 MPa up to 9 MPa with steps of 1 MPa. For every value of the maximum tensile strength, f_{ct}, shear capacity calculations were performed for different values of f_{Ftu}, which was changed by changing the ratio of f_{Ftu} / f_{ct} from 0.1 to 0.9 with a step of 0.1. The resulting possible range of f_{Ftu} for different values of f_{ct} are shown in Table 37. The corresponding possible range of the ratio of f_{Ftu} / f_{ct} are visualized in Figure 66. More calculation results are shown in Appendix F.

Table 37 *Results from sensitivity analysis, possible range of ultimate residual tensile strength, f_{Ftu}, for different maximum tensile strengths, f_{ct}.*

Maximum tensile strength input, f_{ct} [MPa]	Possible range of ultimate residual tensile strength, f_{Ftu} [MPa]
2	0.2
3	0.3 - 0.9
4	0.4 – 1.2
5	0.5 - 2
6	0.6 – 2.4
7	0.7 – 2.8
8	1.6 - 4
9	2.7 – 4.5

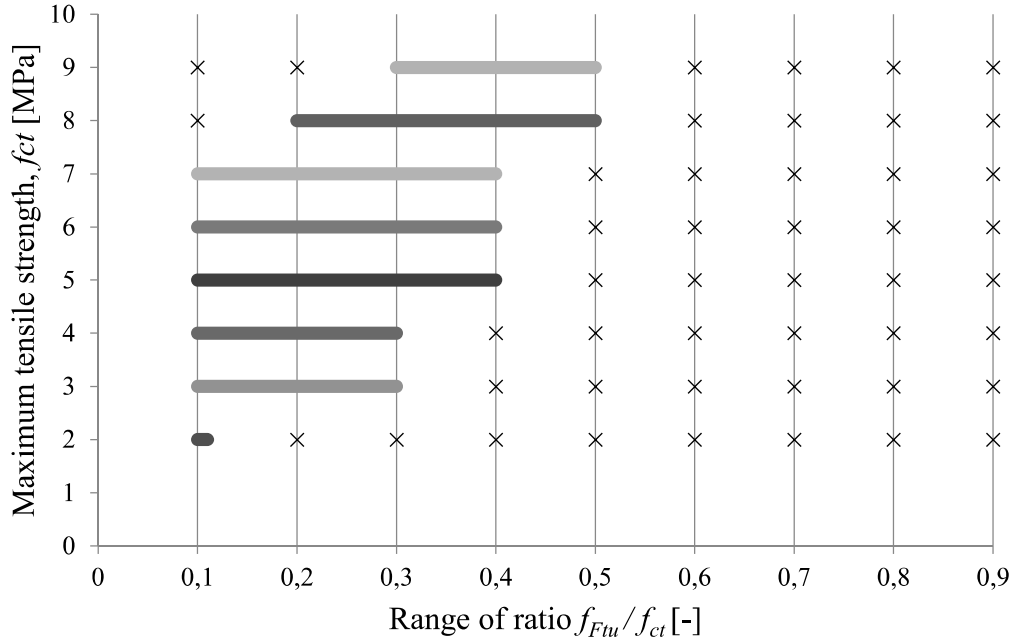

Figure 66 *Results from sensitivity analysis, possible range of ratio f_{Ftu} / f_{ct} for different maximum tensile strengths, f_{ct}. The x-symbol means no convergence.*

The lower limit of the f_{Ftu} / f_{ct} ratios was given due to no convergence. The method needs convergence of the longitudinal strain and of the angle of the principal compressive stress at the same time. For low values of the f_{Ftu} / f_{ct} ratio, a high angle was needed

which could give negative longitudinal strain. Therefore, at these specific f_{Ftu} / f_{ct} ratios, where convergence was not found, the lower limits for the different f_{ct} values were given.

If the longitudinal reinforcement yielded in the last check of the method, the longitudinal strain should be increased. This was not performed since equilibrium was found only at certain values. The yielding of the longitudinal reinforcement was therefore seen as an upper limit of the f_{Ftu} / f_{ct} ratios.

4.4 Conclusions of analysis of FRC-MCFT

The aim with the shear capacity calculation according to FRC-MCFT was, if it was found applicable on the tensile strength curves received from inverse analysis, to investigate how the shear capacity is influenced by the addition of fibres.

The calculations resulted in shear capacity results for all tensile strength curves, i.e. convergence was found for all curves for at least one reinforcement arrangement. Although, the results for Bi-25 and Bi-50 did not converge for reasonable reinforcement arrangements due to small spacing between stirrups. Therefore, the FRC-MCFT is said to be applicable on only the Tri-25 and Tri-50 curves.

The increases in shear capacity, compared to plain concrete, were for the tri-linear analysis 15.8% and 15.2% for curve Tri-25 respectively 25.0% and 26.7% for curve Tri-50, corresponds to two different reinforcement arrangements. In the same calculation for the Bi-50 curve, the increases in shear capacity did not give as collected increase as for the tri-linear analysis.

In addition to the shear capacity calculation, a sensitivity analysis was performed in order to point out the observed difficulties and obstacles with the FRC-MCFT when applying it on the tensile strength curves received from inverse analysis. From the results of the sensitivity analysis it could be concluded that the FRC-MCFT can be applied with reasonable reinforcement amounts on many f_{Ftu} / f_{ct} ratios.

The Bi-25 curve gave a f_{ct} of 8.5 MPa with a f_{Ftu} / f_{ct} ratio of 0.087. The other bilinear curve, Bi-50, gave a f_{ct} of 9.2 MPa with a f_{Ftu} / f_{ct} ratio of 0.118. According to the sensitivity analysis, which is made with a reasonable reinforcement arrangement, see Figure 66, these values are not giving convergence. In comparison, if applying the same values from the tri-linear analysis convergence is received.

The observed difficulties with applying the FRC-MCFT on the tensile strength curves received from inverse analysis were as follows;

- For high f_{ct} values (as 8.5 MPa and 9.2 MPa for the bi-linear curves), the method did not find convergence for low ratios of f_{Ftu} / f_{ct} for reasonable reinforcement amounts.
- For all tried values of f_{ct}, upper limitations of f_{Ftu} / f_{ct} ratios were received. These were given when the stress in the longitudinal reinforcement exceeded yielding, which should not be the case according to the FRC-MCFT.

5 Results

In this study, the MCFT was represented by the FRC-MCFT which is an extended theory which is developed for SFRC. The FRC-MCFT is not dealing with tensile hardening behaviour, which excluded the curves of MRC with fibre volume 2.5% and 4%.

From the second partial study in this thesis work, the inverse analysis, tensile strength curves were received for AR-glass MRC with concrete class C25/30 and 50/60 with 0.3% fibre volume, both by a bi-linear and a tri-linear analysis. This resulted in four curves: Bi-25, Bi-50, Tri-25 and Tri-50. The maximum tensile strength f_{ct} and ultimate residual tensile strength f_{Ftu} for these curves are presented in Table 38 below.

Table 38 Maximum tensile strength values and ultimate residual tensile strength values for the four tensile strength curves from inverse analysis.

	Bi-25	Bi-50	Tri-25	Tri-50
f_{ct} [MPa]	8.5	9.2	5	6
f_{Ftu} [MPa]	0.74	1.087	0.717	1.070

In the third partial study, where shear calculations were made according to the FRC-MCFT by using the above input from the four curves together with other input data, the appliance of the curves was analysed.

The curves that were applicable in the FRC-MCFT to calculate the shear capacity of a randomly chosen beam were curve Tri-25 and Tri-50. The two curves represent concrete class C25/30 and C50/60, both with a fibre volume of 0.3%. The two tensile strength curves, Tri-25 and tri-50, can be seen in Figure 67 and Figure 68, respectively.

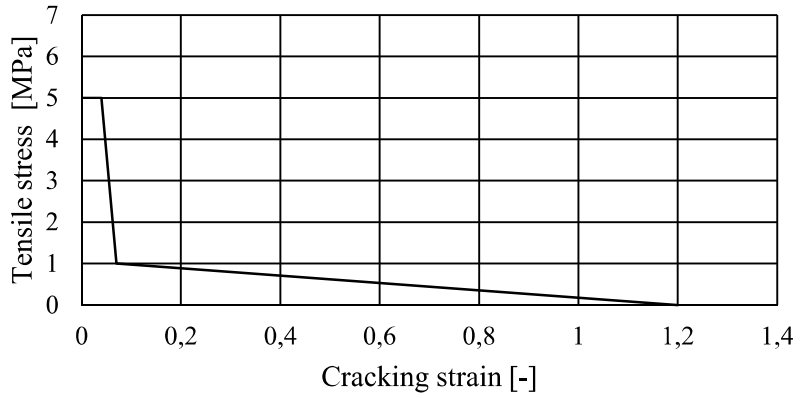

Figure 67 Tensile strength curve Tri-25.

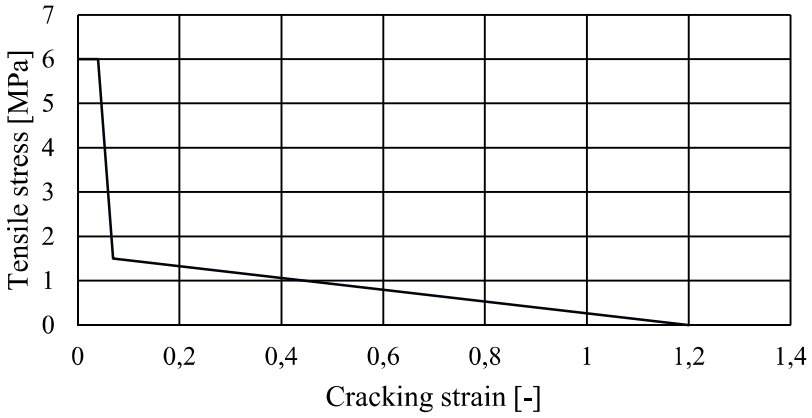

Figure 68 Tensile strength curve, Tri-50.

The curves that were not applicable in the analysis of the FRC-MCFT, to calculate the shear capacity of a randomly chosen beam were curve Bi-25 and Bi-50. The two curves represent concrete class C25/30 and C50/60, both with a fibre volume of 0.3%. The two tensile strength curves, Bi-25 and Bi-50, can be seen in Figure 69 and Figure 70, respectively.

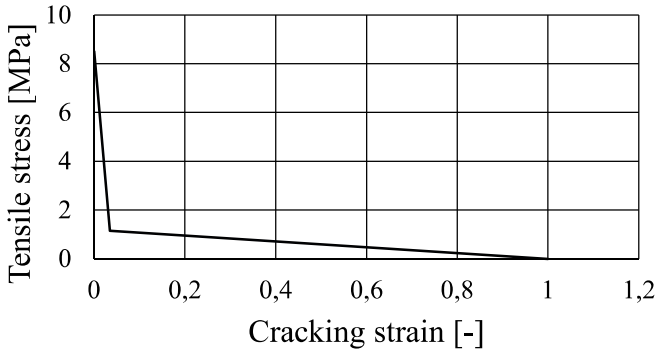

Figure 69 Tensile strength curve, Bi-25.

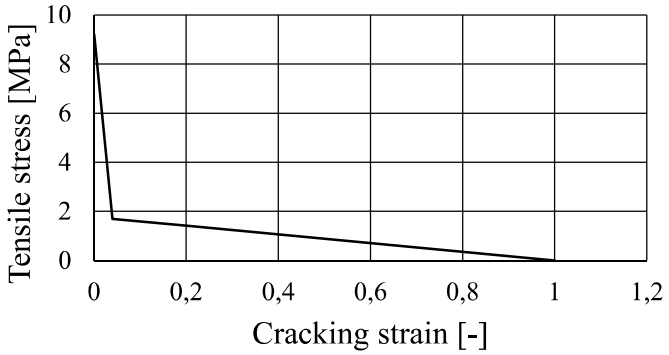

Figure 70 Tensile strength curve, Bi-50.

6 Discussion

The Modified Compression Field Theory (MCFT) is one of many theories for calculation of the shear capacity in concrete. The most advantageous property of this theory, when analysing fibre reinforced concrete (FRC), is that it takes the tensile strength of concrete into account. Therefore the MCFT was preferred before available other theories on the shear capacity of concrete.

Moreover, there exist extended MCFTs which are developed further for shear calculations of FRC, mostly for SFRC. One such theory was chosen from the literature to be used in this study, which was validated and seemed suitable for SFRC.

Furthermore, it would have been interesting to test other MCFT extended to SFRC, to see if these methods would have given the same result as the one used in this study. Namely, the Simplified FRC-MCFT.

The FRC-MCFT has one limitation that affects the result in this thesis work to a large extent, i.e. that it only deals with tension softening behaviour. This is a limitation that excludes a lot of FRCs which have tension hardening response, for example some of the Alkali Resistant glass (AR-glass) MiniBar reinforced concrete (MRC) curves studied in this thesis work. The received experimental results from Three Point Bending Test (3PBT) which had bending hardening behaviour could either have had tension hardening or tensioning softening behaviour. The procedure of finding the right tensile curves for the bending hardening curves was evaluated to be difficult and problematic. These curves were therefore decided to be excluded from the study since it did not fit in the scope of this master's thesis. Thus, the tests corresponding to 2.5% and 4% fibres were excluded from the shear capacity analysis. This made the work much less extensive and the change in shear capacity for different fibre volumes could not be studied. The developers of the FRC-MCFT also stated that more theories dealing with tensioning hardening needs to be developed.

It was assumed in this thesis work that the AR-glass and basalt MRC had the same mechanical behaviour. This was due to the similar fibre shape and similar modulus of elasticity of the fibres. In addition, the fact that they are designed to fail in bond-slip also indicates the similarities of their mechanical behaviour. These are important properties which point in the same direction; that both fibres act the same when dispersed in concrete. Although, for this to be a reliable assumption, more experimental tests regarding e.g. material properties, mechanical behaviour of hardened concrete, durability aspects and rheology etc. need to be executed both for AR-glass and basalt MRC. In addition, it is important for the experimental tests to be executed with the same conditions regarding parameters, such as fibre amount, concrete class, water-cement ratio etc. for the results to be comparable.

The MiniBar, which can be produced both in AR-glass and basalt, was chosen to represent glass and basalt FRC in this thesis work. This choice was made to limit the work and because different glass and basalt fibre reinforcement products have a large scatter in their properties. Therefore, no general conclusions could be drawn including all glass and basalt fibre reinforcement products. Moreover, the assumption of the AR-glass and basalt MiniBar to have the same response when added to concrete is due to its designed shape and not only due to the material properties. Hence, a general assumption that glass and basalt fibres can be studied as the same material cannot be made.

In order to have tensile strength curves for the material, inverse analysis was performed since no such curves were found in the literature of different fibre volumes and concrete classes of MRC. The inverse method is often made by a Finite Element (FE)-analysis and there are many possible choices to make when establishing a FE-model. In this thesis work, choices and assumptions have been made in the modelling, where the most important were;

- it was modelled in two dimensions (2D)
- the tensile strength input was evaluated both as a bi-linear and a tri-linear curve
- the mean value of four tested beams were modelled and
- the fibres were assumed to be smeared out over the whole model as well as the material properties

Other possibilities in the model could for example have been a three dimensional (3D) model, to take any possible 3D effects into account. Also, the tensile strength input could have been interpreted with other shapes, as for example exponential. All these modelling choices could possibly have given a different result of tensile curve. However, two models with good agreement with the received experimental flexural strength were analysed in this thesis work.

The tensile strength curves received from the inverse analysis indicated large increases, for both the bi- and tri-linear curves, in the maximum tensile strength, f_{ct}, from plain concrete to AR-glass MRC. The tri-linear curves had a less increase in the f_{ct} compared to the bi-linear curve. When using a tri-linear curve, the curve could be manipulated to begin with a lower and constant f_{ct}. This shape of the tensile curve, with a plateau of f_{ct}, might represent the MRC better. Since both the bi- and tri-linear input tensile strength curves gave good correlation to bending test results, it is difficult to evaluate if one curve represents MRC better than the other.

The high tensile strength results were not expected, and in addition, a test executed by (Adhikari 2013) at the University of Akron on the tensile strength of basalt MRC with fibre volume 0.5% (>0.3%) did not indicate any significant increase in the tensile strength. Even though the results are not directly comparable, they indicated that the received strengths were unrealistically high.

Thus, more studies needs to be made both regarding the inverse methodology, by trying other modelling choices, and regarding more experimental testing on the tensile strength, to verify the results and calibrate the FE-model.

The inverse methodology has been applied successfully by many authors on SFRC, but not as many on glass and basalt FRC. Therefore, whether this is a good method for receiving tensile strength curves for glass and basalt FRC is not well known. Perhaps this methodology overestimates the tensile input or maybe the FE-model demands other modelling choices in order to describe the real tensile strength. Even though the inverse analysis gave somewhat unrealistic results, the tensile curves obtained were studied further in the calculation of shear capacity. During the analysis of the results from the calculation of shear capacity, the accuracy of the results from the inverse analysis was taken into account. Consequently, the shear capacity received in the analysis of FRC-MCFT cannot be more accurate than the results from the inverse analysis.

From the bi-linear curves with concrete classes C25/30 and C50/60, results of the shear capacity were obtained but not for realistic reinforcement amounts. Therefore, the FRC-MCFT was not considered applicable on the bi-linear curves. In comparison, when

using the f_{ct} and f_{Ftu} values obtained with a tri-linear curve, the FRC-MCFT converged for almost all tried reinforcement arrangements.

The convergence problem with the bi-linear curves, when using the FRC-MCFT, might be based on the low f_{Ftu} / f_{ct} ratio and the high f_{ct}. Since the original MCFT is based on empirical data, the extreme case in this study may be too different and therefore convergence problem occurred. The tri-linear tensile strength values, together with the f_{Ftu}, seemed to be more suitable values for the FRC-MCFT.

The shear capacities of the concretes C25/30 and C50/60 were calculated and compared to ordinary concrete, for both the bi- and tri-linear curve. The tri-linear curves gave similar increases in shear capacity even though the reinforcement amount was changed. In contrast, the values used from the bi-linear gave shear capacity increases of 3.6-14.9%, depending which reinforcement was used. This might also indicate on that the FRC-MCFT is more balanced for values of f_{ct}.

The shear capacities obtained from the tri-linear curves, gave for concrete C25/30 and C50/60, with fibre volume 0.3%, increases of the shear capacity of around 15% and 26% respectively. These results indicated that the fibre volume of 0.3% affect the shear capacity. In contrast, the developer of the FRC-MCFT used in this study, (Minelli & Plizzari 2011), stated in their study that no significant increase of the shear resistance could be concluded for toughness f_{Ftu} lower than 1.5 MPa in a member with stirrups.

The whole material strength curves, retrieved from inverse analysis, were never used as input in the FRC-MCFT. Instead, it was the f_{ct} and f_{Ftu} values together with other properties of the materials that were used as input data. The FRC-MCFT did therefore not take into account the whole tensile behaviour of the materials.

It is important to notice that the SFRC and glass and basalt FRC are completely different materials with different mechanical properties. It is not possible to compare the different fibres themselves. Instead, it is the final material and its behaviour that is important, i.e. the behaviour of the final FRC.

In the same manner, saying that the response before cracking is not affected by the incorporated fibres (Section 2.1.2) may not apply for the MRC since most studies have been executed on SFRC. Maybe the incorporated MiniBars are influencing the pre-cracking response of the concrete more than the post-cracking response. This would give a contrast to the SFRC and empirical relationships based on SFRC experiments may not apply for the MRC.

As presented in Section 2.2, (Naaman 2003) stated some properties for the fibres to have a reinforcing effect on the concrete; the modulus of elasticity of the fibre needs to be greater than that of the concrete (3 times greater) and the fibre shall have a ductile behaviour, i.e. to increase the fracture toughness of the material. If this would be the case, the MiniBars would not have a reinforcing effect on the concrete since the bare fibre has a brittle failure and the modulus of elasticity of the fibre is almost the same as the one of concrete.

The FRC-MCFT may suit better for SFRC compared to MRC. Therefore, further studies are needed on the glass and basalt FRCs in order to obtain validated behaviours and relationships since there can be a significant difference compared to the SFRC. Generally, when talking about FRC, the mechanical behaviour is adopted to SFRC, since this is the most common fibre and the most studied.

In this study, the analysis whether the MCFT is applicable on glass and basalt FRC was analysed by using the FRC-MCFT. Moreover, one specific FRC product was chosen, i.e. the AR-glass and basalt MRC. Even though results have been presented regarding this specific FRC, no general conclusions can be made regarding all types of glass and basalt FRC. This is also due to the big spectra of existing products which may give other mechanical properties to the final concrete material. The same point of view can be applied on the used FRC-MCFT. This theory represents one of many MCFT extended to FRC. The results of the appliance of the tensile strength curves may be different if using another method.

In order to support the calculated shear capacity results when using the FRC-MCFT, real experiments of the shear capacity are needed. Therefore, the results of the shear capacity calculations are not well supported.

There is a low significance in the obtained shear capacities since they are based on high and not validated maximum tensile strength values and on limited tests, where other parameters influencing the results are not included. Despite that, this study has significance within the scientific area of FRC, since it is an attempt to increase the knowledge within the mechanical properties and design of glass and basalt FRC members.

Finally, if a theory which would be able to take tension hardening behaviour into consideration were to be developed in the future, a more comprehensive study of the shear capacity of AR-glass and basalt MRC can be executed. Because with the method in this study, it was not possible to account for variation in fibre volumes, even though bending test results were received for these conditions.

7 Conclusions and further studies

As described by the method in Section 1.5, this thesis work was divided in three partial studies. The conclusions of the literature study can be found in Section 2.5, of the inverse analysis in Section 3.4 and of the analysis of the FRC-MCFT in Section 4.4. In this chapter, the final conclusions of this thesis work are presented together with recommendations for further studies.

7.1 Conclusion

The purpose of this Master's thesis work was to analyse the possibilities to apply the Modified Compression Field Theory (MCFT) on tensile strength curves of glass and basalt fibre reinforced concrete (FRC) received from inverse analysis.

From the results of this Master's thesis work it could be concluded that;

- Bi-linear and tri-linear tensile strength curves of AR-glass MiniBar reinforced concrete (MRC) of concrete class C25/30 and C50/60 with fibre volume 0.3% could be retrieved by inverse analysis of real flexural bending tests.
- The FRC-MCFT could be applied on the tri-linear tensile strength curves of the AR-glass MRC to calculate shear capacity of a beam. The tensile strength curves of the materials were represented by the maximum tensile strength f_{ct} and the ultimate residual tensile strength f_{Ftu}.
- The FRC-MCFT could not be applied on the bi-linear curves received from inverse analysis. This was probably due to high maximum tensile strengths compared to plain concrete together with low f_{Ftu} / f_{ct} ratios compared to SFRC tests.
- The inverse analysis resulted in both bi-linear and tri-linear tensile strength curves for the same material and concrete strength. Both analyses had good correlation to real flexural bending tests and it was difficult to evaluate which tensile strength curve represented the tensile behaviour of the AR-glass MRC best.
- The FRC-MCFT could not be utilized on tensile strength curves with tensioning hardening behaviour, i.e. many glass and basalt FRCs could not be used in this theory due to their tension hardening response.
- Even though the FRC-MCFT could be applied on AR-glass MRC according to the tensile strength curves obtained, the curves have not been validated against real tensile strength curves of the same material.
- Due to the assumed similar behaviour of AR- glass and basalt MRC, the same conclusions regarding the AR-glass MRC above applies for basalt MRC.
- The conclusions in this thesis work could only be drawn regarding AR-glass- and basalt MRC. Other glass and basalt FRCs may have different mechanical behaviours due to other fibre shapes and bond properties. Therefore, the results cannot be generalised on all glass and basalt FRCs.
- The MCFT has in this study been represented by the FRC-MCFT, which is developed for shear capacity calculations of SFRC. Therefore, the results are based on this theory and do not apply for all shear capacity theories based on the MCFT.

7.2 Further studies

Glass and basalt FRCs are relatively new building materials in comparison to SFRC. SFRC has been investigated and used in application to a much larger extent and is thus a more reliable material to choose for structural applications.

The research of glass fibre reinforced concrete (GFRC) and basalt fibre reinforced concrete (BFRC) is an ongoing process. Much more studies regarding for example mechanical properties, rheology, possible applications and durability need to be made in order for the materials to be seen as safe and reliable in the construction industry.

The list of further studies can be long due to the novel state of the research of GFRC and BFRC. The most important studies according to the authors of this study are as follows;

- Development of MCFT extended to FRC, which can take tension hardening response into account
- Experimental studies of the mechanical properties of hardened concrete, such as tensile strength and shear capacity for concrete with varying fibre content, concrete class, water-cement ratio etc.
- Comparative experimental testing of AR-glass and basalt MRC
- Experimental studies on durability aspects of GFRC and BFRC, such as alkali resistance
- Development of Finite Element (FE)-model for inverse analysis of GFRC and BFRC, calibrated against the real response in tension and in bending
- Assessment of sectional models for shear failure calculations with a comparison between existing shear models for FRC with shear failure tests
- Perform shear tests of glass and basalt FRC specimens

8 References

Abaqus 6.14, 2014. Abaqus 6.14 Online Documentation. Available at: http://50.16.225.63/v6.14/index.html [Accessed January 1, 2015].

Adhikari, S., 2013. *Mechanical and structural characterization of mini-bar reinforced concrete beams*, Akron.

Alwan, J., Naaman, A. & Guerrero, P., 1999. Effect of mechanical clamping on the pull-out response of hooked steel fibers embedded in cementitious matrices. *Concrete Science and Engineering*, 1(March), pp.15–25. Available at: http://rilem.net/gene/main.php?base=600026&id_publication=391&id_papier=7278.

Bentz, E.C., Vecchio, F.J. & Collins, M.P., 2006. Simplified modified compression field theory for calculating shear strength of reinforced concrete elements. *ACI Structural Journal*, 103(65), pp.614–624.

Bernardi, P. et al., 2015. Experimental and numerical study on cracking process in RC and R/FRC ties. *Materials and Structures*. Available at: http://link.springer.com/10.1617/s11527-014-0494-1.

Blanco, A. et al., 2013. Application of constitutive models in European codes to RC-FRC. *Construction and Building Materials*, 40, pp.246–259. Available at: http://dx.doi.org/10.1016/j.conbuildmat.2012.09.096.

Brandt, A.M., 2008. Fibre reinforced cement-based (FRC) composites after over 40 years of development in building and civil engineering. *Composite Structures*, 86, pp.3–9.

CEN, 2006. *SS-EN 14889-1:2006, Fibres for concrete - Part 1: Steel fibres - Definitions, specifications and conformity*, SIS Förlag AB.

Chen, F., 2013. An Experimental Study on Mechanical Properties of Basalt Fiber Reinforced Concrete. , 405-408, pp.2767–2770.

Chugh, P. et al., 2013. Improvement of punching shear resistance of RC slabs using GFRC : An experimental study. In S.-Y. Chang, S. K. Al Bahar, & J. Zhao, eds. *Advances in Civil Engineering and Building Materials*. London: Taylor & Francis Group, pp. 739–743.

Collins, M.P. & Mitchell, D., 1987. *Prestressed conrete basics* First edit., Ottawa: Canadian Prestressed Concrete Institute.

Criado, M. et al., 2014. Effect of recycled glass fiber on the corrosion behavior of reinforced mortar. *Construction and Building Materials*, 64, pp.261–269.

Dhand, V. et al., 2014. A short review on basalt fiber reinforced polymer composites. *Composites Part B: Engineering*, 73, pp.166–180.

Ding, Y. et al., 2012. Shear behaviour of steel fibre reinforced self-consolidating concrete beams based on the modified compression field theory. *Composite Structures*, 94(8), pp.2440–2449. Available at: http://dx.doi.org/10.1016/j.compstruct.2012.02.025.

EN 14651, 2005. *Test method for metallic fibred concrete — Measuring the flexural tensile strength (limit of proportionality (LOP), residual)*.

Ferreira, J.P.J.G. & Branco, F. a. B., 2007. The use of glass fiber-reinforced concrete as a structural material. *Experimental Techniques*, 31(June), pp.64–73. Available at: http://doi.wiley.com/10.1111/j.1747-1567.2007.00153.x.

Fib, 2013. *Fib Model Code for Concrete Structures 2010: A landmark in an ongoing development*.

Fiore, V. et al., 2014. A review on basalt fibre and its composites. *Composites Part B: Engineering*, 74, pp.74–94.

Fischer, G. & Li, V.C., 2007. Effect of fiber reinforcement on the response of structural members. *Engineering Fracture Mechanics*, 74, pp.258–272.

Gardiner, G., 2009. The making of glass fiber. *CompositesWorld*. Available at: http://www.compositesworld.com/articles/the-making-of-glass-fiber [Accessed March 23, 2015].

Jansson, A. et al., 2012. Experimental investigation of surface crack initiation, propagation and tension stiffening in self-compacting steel–fibre-reinforced concrete. *Materials and Structures*, 45, pp.1127–1143.

Kabay, N., 2013. Abrasion resistance and fracture energy of concretes with basalt fiber. *Construction and Building materials*, 50, pp.95 – 101.

Karbhari, V.M. et al., 2003. Durability Gap Analysis for Fiber-Reinforced Polymer Composites in Civil Infrastructure. *Journal of Composites for Construction*, 7(3), pp.238–247.

Katzer, J., 2006. Steel Fibers and Steel Fiber Reinforced Concrete in Civil Engineering. *The Pacific Journal of Science and Technology*, 7(1), pp.53–58.

Knudsen, E. & Lie Skadal, K., 2012. *Basalt reinforced concrete in load carrying structures*, Trondheim.

Kooiman, A.G., 2000. *Modelling Steel Fibre Reinforced Concrete for Structural Design*. Delft University of Technology.

Lee, J.H. & Fenves, G.L., 1998. Plastic-damage model for cyclic loading of concrete structures. *J. Eng. Mech. (ASCE)*, 124, pp.892–900.

Li, V.C., Stang, H. & Krenchel, H., 1993. Micromechanics of crack bridging in fibre-reinforced concrete. *Materials and Structures*, 26, pp.486–494.

Lipatov, Y.V. et al., 2015. High alkali-resistant basalt fiber for reinforcing concrete. *Materials & Design*, 73, pp.60–66. Available at: http://linkinghub.elsevier.com/retrieve/pii/S0261306915000680.

Loberg, B., 2015. Basalt. *Nationalencyklopedin*. Available at: http://www.ne.se.proxy.lib.chalmers.se/uppslagsverk/encyklopedi/enkel/basalt.

Lubliner, J. et al., 1989. A plastic-damage model for concrete. *International Journal of Solids and Structures*, 25, pp.299–326.

Löfgren, I., 2005. *Fibre-reinforced Concrete for Industrial Construction - a fracture mechanics approach to material testing and structural analysis*. Göteborg: Chalmers University of technology.

Löfgren, I., Stang, H. & Olesen, J.F., 2005. Fracture Properties of FRC Determined through Inverse Analysis of Wedge Splitting and Three-Point Bending Tests. *Journal of Advanced Concrete Technology*, 3(3), pp.423–434.

Miedlar, P.C. et al., 2002. Residual strength methodology. In *Damage tolerant design handbook: Guidelines for the analysis and design of damage tolerant aircraft structures*. Dayton. Available at: http://www.afgrow.net/applications/DTDHandbook/sections/page2_3.aspx.

Minelli, F., 2005. *Plain and fiber reinforced concrete beams under shear loading: Structural behavior and design aspects*. Brescia University.

Minelli, F. & Plizzari, G.A., 2011. On the role of fibre-reinforced concrete in improving the shear resistance of R/C beams. *Studi e ricerche - Politecnico di Milano. Scuola di specializzazione in costruzioni in cemento armato*, (31), pp.63–89. Available at: http://cat.inist.fr/?aModele=afficheN&cpsidt=26385781 [Accessed March 9, 2015].

Minelli, F. & Vecchio, F.J., 2006. Compression Field Modeling of Fiber-Reinforced Concrete Members Under Shear Loading. *ACI Structural Journal*, 103(2), pp.244–252.

Mobasher, B., Bakhshi, M. & Barsby, C., 2014. Backcalculation of residual tensile strength of regular and high performance fiber reinforced concrete from flexural tests. *Construction and Building Materials*, 70, pp.243–253. Available at: http://www.sciencedirect.com/science/article/pii/S0950061814007612.

Mondo, E., 2011. *Shear Capacity of Steel Fibre Reinforced Concrete Beams without Conventional Shear Reinforcement*. Royal Institute of Technology (KTH).

Musmar, M., 2013. Tensile Strength of Steel Fiber Reinforced Concrete. *Contemporary Engineering Scienes*, 6(5), pp.225–237.

Naaman, A.E., 2003. Engineered Steel Fibers with Optimal Properties for Reinforcement of Cement Composites. *Journal of Advanced Concrete Technology*, 1(3), pp.241–252.

De Oliveira e Sousa, J.L.A. & Gettu, R., 2006. Determining the Tensile Stress-Crack Opening Curve of Concrete by Inverse Analysis. *Journal of Engineering Mechanics*, 132(February), pp.141–148.

Olivito, R.S. & Zuccarello, F. a., 2010. An experimental study on the tensile strength of steel fiber reinforced concrete. *Composites Part B: Engineering*, 41(3), pp.246–255. Available at: http://dx.doi.org/10.1016/j.compositesb.2009.12.003.

Parnas, R., Shaw, M. & Liu, Q., 2007. *Basalt Fiber Reinforced Polymer Composites*.

Peterson, P.E., 1980. Fracture energy of concrete: Method of determination. *Cement and Concrete research*, 10(1), pp.79–89.

Plos, M., 2000. *Finite element analyses of reinforced concrete structures*, Göteborg.

Prisco, M., Plizzari, G. & Vandewalle, L., 2009. Fibre reinforced concrete: new design perspectives. *Materials and Structures*, 42, pp.1261–1281.

Purnell, P. & Beddows, J., 2005. Durability and simulated ageing of new matrix glass fibre reinforced concrete. *Cement and Concrete Composites*, 27, pp.875–884.

ReforceTech, 2015. Basalt fiber process. Available at: www.reforcetech.com [Accessed March 12, 2015].

Rybin, V. a., Utkin, a. V. & Baklanova, N.I., 2013. Alkali resistance, microstructural and mechanical performance of zirconia-coated basalt fibers. *Cement and Concrete Research*, 53, pp.1–8. Available at: http://dx.doi.org/10.1016/j.cemconres.2013.06.002.

Scheffler, C. et al., 2009. Aging of alkali-resistant glass and basalt fibers in alkaline solutions: Evaluation of the failure stress by Weibull distribution function. *Journal of Non-Crystalline Solids*, 355(52-54), pp.2588–2595. Available at: http://dx.doi.org/10.1016/j.jnoncrysol.2009.09.018.

Shan, L. & Zhang, L., 2012. Experimental Study on Mechanical Properties of steel and polypropylene fibre-reinforced concrete. *Applied Mechanics and Materials*, 584-586, pp.1355–1361.

Skarendahl, Å., 1990. Fiberbetong. In *Betonghandboken - Material*. Solna: AB Svensk Byggtjänst, pp. 965 – 976.

Slowik, V. et al., 2006. Computational aspects of inverse analyses for determining softening curves of concrete. *Computer Methods in Applied Mechanics and Engineering*, 195, pp.7223–7236.

Spinella, N., Colajanni, P. & La Mendola, L., 2012. Nonlinear analysis of beams reinforced in shear with stirrups and steel fibers. *ACI Structural Journal*, 109(06), pp.53–64.

SS812310:2014, 2014. *SS 812310:2014: Fibre Concrete - Design of Fibre Concrete Structures*, SIS Förlag AB.

SS-EN 1992-1-1, 2008. *Eurocode 2: Design of concrete structures - Part 1-1: General rules and rules for buildings* 1st ed., SIS Förlag AB.

Stupishin, L.U. et al., 2014. Retain of Fine Dispersed Basalt Fiber Reinforcement in Cement Matrix. *Applied Mechanics and Materials*, 584-586, pp.1691–1694. Available at: http://www.scopus.com/inward/record.url?eid=2-s2.0-84905181393&partnerID=tZOtx3y1 [Accessed February 16, 2015].

Tlemat, H., Pilakoutas, K. & Neocleous, K., 2006. Modelling of SFRC using inverse finite element analysis. *Materials and Structures*, 39(May 2005), pp.221–233. Available at: http://dx.doi.org/10.1617/s11527-005-9010-y.

Wang, X. et al., 2014. Shear behavior of basalt fiber reinforced polymer (FRP) and hybrid FRP rods as shear resistance members. *Construction and Building Materials*, 73, pp.781–789.

Vecchio, F.J. & Collins, M.P., 1986. The modified compression-field theory for reinforced concrete elements subjected to shear. *ACI Journal*, 83, pp.219–231. Available at: http://www.concrete.org/Publications/ACIMaterialsJournal/ACIJournalSearch.aspx?m=details&ID=10416.

Zhang, J. & Li, V.C., 2004. Simulation of crack propagation in fiber-reinforced concrete by fracture mechanics. *Cement and Concrete Research*, 34, pp.333–339.

Zych, T. & Krasodomski, W., 2012. Study on the properties of cement mortars with basalt fibres. In *Brittle Matrix Composites 10*. Woodhead Publishing Limited, pp. 155–166. Available at: http://www.sciencedirect.com/science/article/pii/B9780857099884500323.

LIST OF APPENDICES

APPENDIX A	Matlab code	A-1 - A-3
APPENDIX B	Shear capacity calculations Bi-25	B-1 - B-4
APPENDIX C	Shear capacity calculations Bi-50	C-1 - C-5
APPENDIX D	Shear capacity calculations Tri-25	D-1 - D-3
APPENDIX E	Shear capacity calculations Tri-50	E-1 - E-3
APPENDIX F	Sensitivity analysis	F-1 - F-8

APPENDIX A MATLAB CODE

```
clc;
clear all;
save all;

INFORMATION
USED STUDY: Are steel fibre able to mitigate or eliminate the size effect
in shear? (Minelli & Plizzari 2014)
USED METHOD: Simplified FRC-MCFT by (Minelli & Plizzari 2014)

CONCRETE FROM REFORCETECH:
Vf = 0.3 %
AR-glass MiniBar reinforced concrete
Concrete class C25/30
INPUT DATA CONCRETE

% PARAMETERS OBTAINED FROM TENSILE STRESS-STRAIN CURVE BY INVERSE ANALYSIS
fct=9;                          % Tensile strength of FRC Abaqus [MPa]
f_Ftu=4.5;                      % Ultimate residual tensile strength [MPa]

% PARAMETERS FROM TESTS
fck=49.8;                       % Characteristic compressive strength [mPa]

% PARAMETER FROM EUROCODE
E=31000;                        % Modulus of elasticity C25/30 [MPA]

% EXAMPLE BEAM
% DIMENSIONS
a=16;                           % Maximum aggregate size [m]
bw=220;                         % Smallest width of element [m]
d=314;                          % Effective depth [mm]
m=1000;                         % 1 meter [mm]

% STEEL
Es=200000;                      % Modulus of elasticity of steel [MPa]
fsy=500;                        % Yielding strength of steel [MPa]

%% INPUT DATA REINFORCEMENT
% LONGITUDINAL REINFORCEMENT
fi_long=20;                     % Diameter of long. bars in bottom [mm]
nr_long=12;                     % Number of longitudinal bars [-]

fi_min=10;                      % Diameter of long. bars around beam [mm]
nr_min=7;                       % Number of long. bars around beam [-]
sx=100;                         % Vertical spacing of long. bars around beam
[mm]

Asx=pi*((fi_long/2)^2*nr_long+(fi_min/2)^2*nr_min); % Cross section area of
long. bars [mm2]
rho_x=Asx/(bw*d)                % Longitudinal reinforcement ratio [-]

% TRANSVERSAL REINFORCEMENT / STIRRUPS
fi_sti=10;                      % Diameter of stirrups [mm]
```

Matlab code

```
sz=100;                          % Horizontal spacing between stirrups [mm]

Asz=2*(fi_sti/2)^2*pi;           % Cross section area of two stirrups [mm2]
rho_z=Asz/(sz*bw)                % Reinforcement ratio of stirrups [-]

%% CALCULATING SHEAR CAPACITY
% Chosen begin values which are being iterated into konvergence

eps_x=0.0025                     % Chosen value of longitudinal strain [-]

theta_deg=27;                    % Estimated angle of the principal compressive
stress [degrees]

theta=theta_deg*pi/180;          % Angle being transformed into radians

eps_1=0;                         % Start walue of loop [-]
eps_11=1;
i=0.000001;

while (eps_11-eps_1)>0.00001
eps_1=eps_1+i;
eps_11=eps_x*(1+(cot(theta))^2)+((f_Ftu+((fct-
f_Ftu)/(1+sqrt(500*eps_1))))*(cot(theta))^4)/(E);  % Eq. 21
end

sxFRC=sx*(1-(f_Ftu/fct));        % FRC crack spacing (with crack-spacing
reduction factor) Eq. 24
szFRC=sz*(1-(f_Ftu/fct));

s_theta=1/((sin(theta)/sxFRC)+(cos(theta)/szFRC));

w=s_theta*eps_1;                 % Crack width

vci=(0.18*sqrt(fck))/(0.31+((24*w)/(a+16)));       % Shear stress on cracked
interface for plain concrete (in crack direction)

vs=rho_z*fsy*cot(theta);         % Eq. 10

theta_2=acot(vci*(1+sqrt(500*eps_1))/(fct-f_Ftu));  % Angle of the principal
compressive stresses, Eq. 17

theta_deg2=theta_2*180/pi;       % Angle being transformed into radians

v_crack=f_Ftu*cot(theta)+vci+vs;    % Eq. 13

v_avg=(f_Ftu+(fct-f_Ftu)/(1+sqrt(500*eps_1)))*cot(theta)+vs; % Eq. 15

f1=f_Ftu+((fct-f_Ftu)/(1+sqrt(500*eps_1))); % Eq. 12

v=v_avg;

eps_x2=(v*cot(theta)-f1)/(Es*rho_x); % Eq. 12
```

```
fsxcr=((v+vci)*cot(theta)-f_Ftu)/rho_x; % Eq. 26

fsz=fsy;                        % Assuming yielding in stirrups

fszcr=fsy;                      % Assuming yielding in stirrups

V_btw_cracks=Asz*fsz*((d*cot(theta))/sz)+f1*cot(theta)*bw*d; % Eq. 2

V_at_crack=Asz*fszcr*((d*cot(theta))/sz)+f_Ftu*cot(theta)*bw*d+vci*bw*d; % Eq.
4

w_tot=w*(m/szFRC);              % Total crack width over one meter beam

nr_cracks=(m/szFRC);
```

APPENDIX B SHEAR CAPACITY CALCULATIONS BI-25

Varying transversal reinforcement ratio

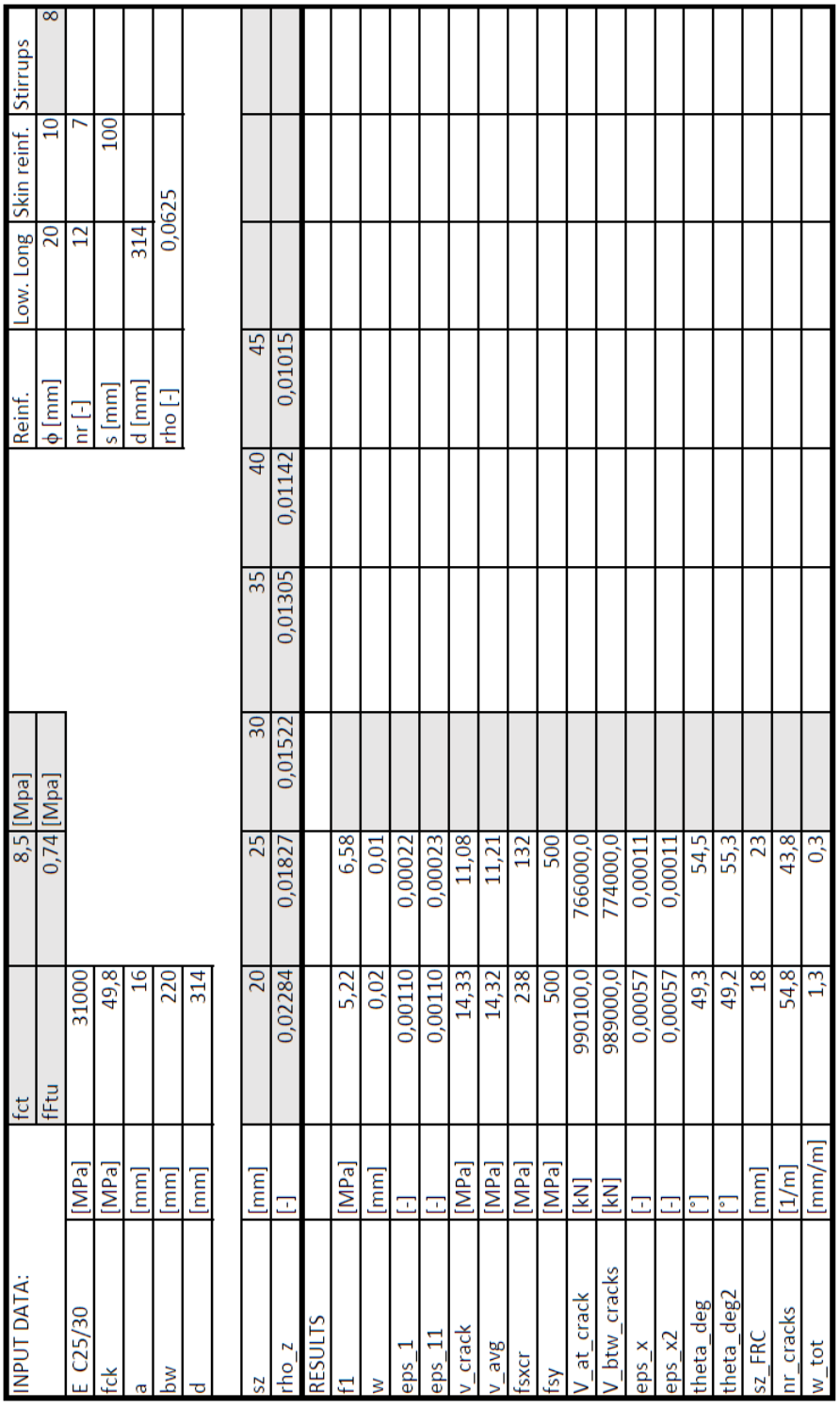

INPUT DATA:		fct		8,5	[Mpa]				Reinf.	Low. Long	Skin reinf.	Stirrups
		fFtu		0,74	[Mpa]				ϕ [mm]	20	10	8
E_C25/30	[MPa]		31000						nr [-]	12	7	
fck	[MPa]		49,8						s [mm]		100	
a	[mm]		16						d [mm]	314		
bw	[mm]		220						rho [-]	0,0625		
d	[mm]		314									
sz	[mm]	20		25		30	35	40	45			
rho_z	[-]	0,02284		0,01827		0,01522	0,01305	0,01142	0,01015			
RESULTS												
f1	[MPa]	5,22		6,58								
w	[mm]	0,02		0,01								
eps_1	[-]	0,00110		0,00022								
eps_11	[-]	0,00110		0,00023								
v_crack	[MPa]	14,33		11,08								
v_avg	[MPa]	14,32		11,21								
fsxcr	[MPa]	238		132								
fsy	[MPa]	500		500								
V_at_crack	[kN]	990100,0		766000,0								
V_btw_cracks	[kN]	989000,0		774000,0								
eps_x	[-]	0,00057		0,00011								
eps_x2	[-]	0,00057		0,00011								
theta_deg	[°]	49,3		54,5								
theta_deg2	[°]	49,2		55,3								
sz_FRC	[mm]	18		23								
nr_cracks	[1/m]	54,8		43,8								
w_tot	[mm/m]	1,3		0,3								

INPUT DATA:		fct	8,5	[Mpa]				Reinf.	Low. Long	Skin reinf.	Stirrups
		fFtu	0,74	[Mpa]				ϕ [mm]	20	10	10
E C25/30	[MPa]	31000						nr [-]	12	7	
fck	[MPa]	49,8						s [mm]		100	
a	[mm]	16						d [mm]	314		
bw	[mm]	220						rho [-]	0,0625		
d	[mm]	314									
sz	[mm]	20	25	30	35	40	45				
rho_z	[-]	0,03568	0,02855	0,02379	0,02039	0,01784	0,01586				
RESULTS											
f1	[MPa]	4,16	4,67	5,18	5,90	6,83					
w	[mm]	0,07	0,05	0,03	0,02	0,01					
eps_1	[-]	0,00320	0,00190	0,00110	0,00051	0,00015					
eps_11	[-]	0,00320	0,00190	0,00110	0,00052	0,00016					
v_crack	[MPa]	22,62	17,72	14,69	12,30	10,81					
v_avg	[MPa]	22,62	17,74	14,69	12,33	11,03					
fsxcr	[MPa]	418	308	242	187	500					
fsy	[MPa]	500	500	500	500	500					
V_at_crack	[kN]	1560000,0	1224000,0	1012000,0	850000,0	746000,0					
V_btw_cracks	[kN]	1562000,0	1226000,0	1015000,0	852000,0	762000,0					
eps_x	[-]	0,00150	0,00096	0,00060	0,00028	0,00072					
eps_x2	[-]	0,00150	0,00095	0,00060	0,00028	0,00072					
theta_deg	[°]	44,2	46,9	49,3	52,6	55,0					
theta_deg2	[°]	44,2	47,1	49,6	52,8	56,5					
sz_FRC	[mm]	18	23	27	32	37					
nr_cracks	[1/m]	54,8	43,8	36,5	31,3	27,4					
w_tot	[mm/m]	3,8	2,2	1,3	0,6	0,2					

INPUT DATA:		fct	8,5	[Mpa]				Reinf.	Low. Long	Skin reinf.	Stirrups
		fFtu	0,74	[Mpa]				ϕ [mm]	20	10	12
E_C25/30	[MPa]	31000						nr [-]	12	7	
fck	[MPa]	49,8						s [mm]		100	
a	[mm]	16						d [mm]	314		
bw	[mm]	220						rho [-]	0,0625		
d	[mm]	314									
sz	[mm]	20	25	30	35	40	45	50			
rho_z	[-]	0,0514	0,0411	0,0343	0,0294	0,0257	0,0228	0,0206			
RESULTS											
f1	[MPa]	3,59	4,07	4,46	4,92	5,20	5,63				
w	[mm]	0,12	0,09	0,07	0,05	0,04	0,03				
eps_1	[-]	0,00560	0,00360	0,00240	0,00150	0,00110	0,00069				
eps_11	[-]	0,00600	0,00360	0,00240	0,00150	0,00110	0,00070				
v_crack	[MPa]	32,42	24,95	20,29	17,11	15,12	13,35				
v_avg	[MPa]	32,42	24,85	20,29	17,10	15,15	13,35				
fsxcr	[MPa]	618	443	345	278	241	203				
fsy	[MPa]	500	500	500	500	500	500				
V_at_crack	[kN]	2240000,0	1720000,0	1401000,0	1180000,0	1040000,0	922000,0				
V_btw_cracks	[kN]	2240000,0	1720000,0	1401000,0	1180000,0	1046000,0	922000,0				
eps_x	[-]	0,00260	0,00170	0,00120	0,00079	0,00060	0,00039				
eps_x2	[-]	0,00260	0,00170	0,00120	0,00080	0,00060	0,00039				
theta_deg	[°]	42,1	44,7	46,8	48,9	50,0	52,0				
theta_deg2	[°]	42,1	44,8	46,8	48,9	50,2	52,0				
sz_FRC	[mm]	18	23	27	32	37	41				
nr_cracks	[1/m]	54,8	43,8	36,5	31,3	27,4	24,3				
w_tot	[mm/m]	6,8	4,0	2,6	1,6	1,2	0,7				

Varying diameter of lower longitudinal reinforcement

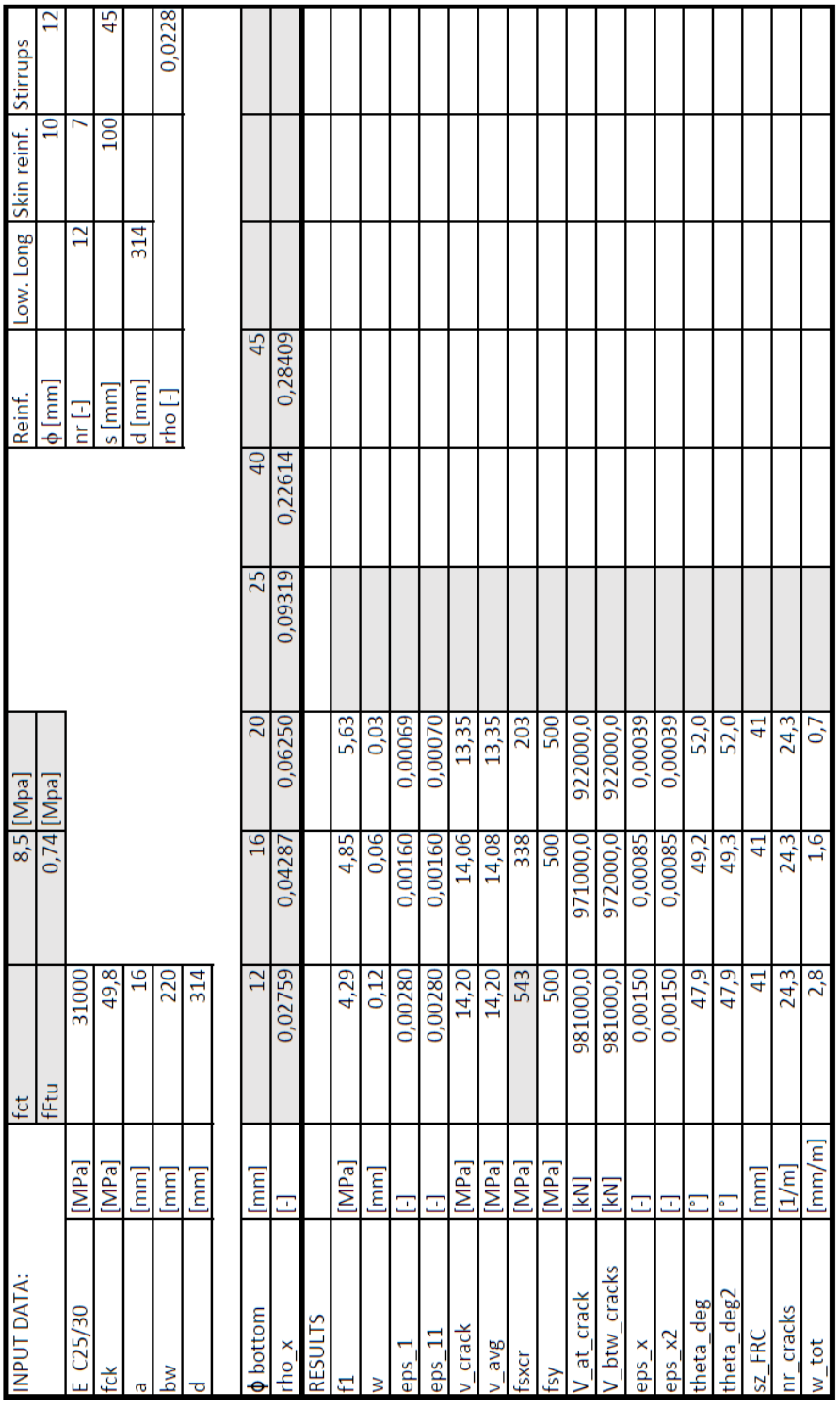

INPUT DATA:		fct	8,5	[Mpa]			Reinf.	Low. Long	Skin reinf.	Stirrups
		ffTu	0,74	[Mpa]			ϕ [mm]		10	12
E_C25/30	[MPa]	31000					nr [-]	12	7	
fck	[MPa]	49,8					s [mm]		100	45
a	[mm]	16					d [mm]	314		
bw	[mm]	220					rho [-]			0,0228
d	[mm]	314								
ϕ bottom	[mm]	12	16	20	25	40	45			
rho_x	[-]	0,02759	0,04287	0,06250	0,09319	0,22614	0,28409			
RESULTS										
f1	[MPa]	4,29	4,85	5,63						
w	[mm]	0,12	0,06	0,03						
eps_1	[-]	0,00280	0,00160	0,00069						
eps_11	[-]	0,00280	0,00160	0,00070						
v_crack	[MPa]	14,20	14,06	13,35						
v_avg	[MPa]	14,20	14,08	13,35						
fsxcr	[MPa]	543	338	203						
fsy	[MPa]	500	500	500						
V_at_crack	[kN]	981000,0	971000,0	922000,0						
V_btw_cracks	[kN]	981000,0	972000,0	922000,0						
eps_x	[-]	0,00150	0,00085	0,00039						
eps_x2	[-]	0,00150	0,00085	0,00039						
theta_deg	[°]	47,9	49,2	52,0						
theta_deg2	[°]	47,9	49,3	52,0						
sz_FRC	[mm]	41	41	41						
nr_cracks	[1/m]	24,3	24,3	24,3						
w_tot	[mm/m]	2,8	1,6	0,7						

APPENDIX C SHEAR CAPACITY CALCULATIONS BI-50

Varying transversal reinforcement ratio

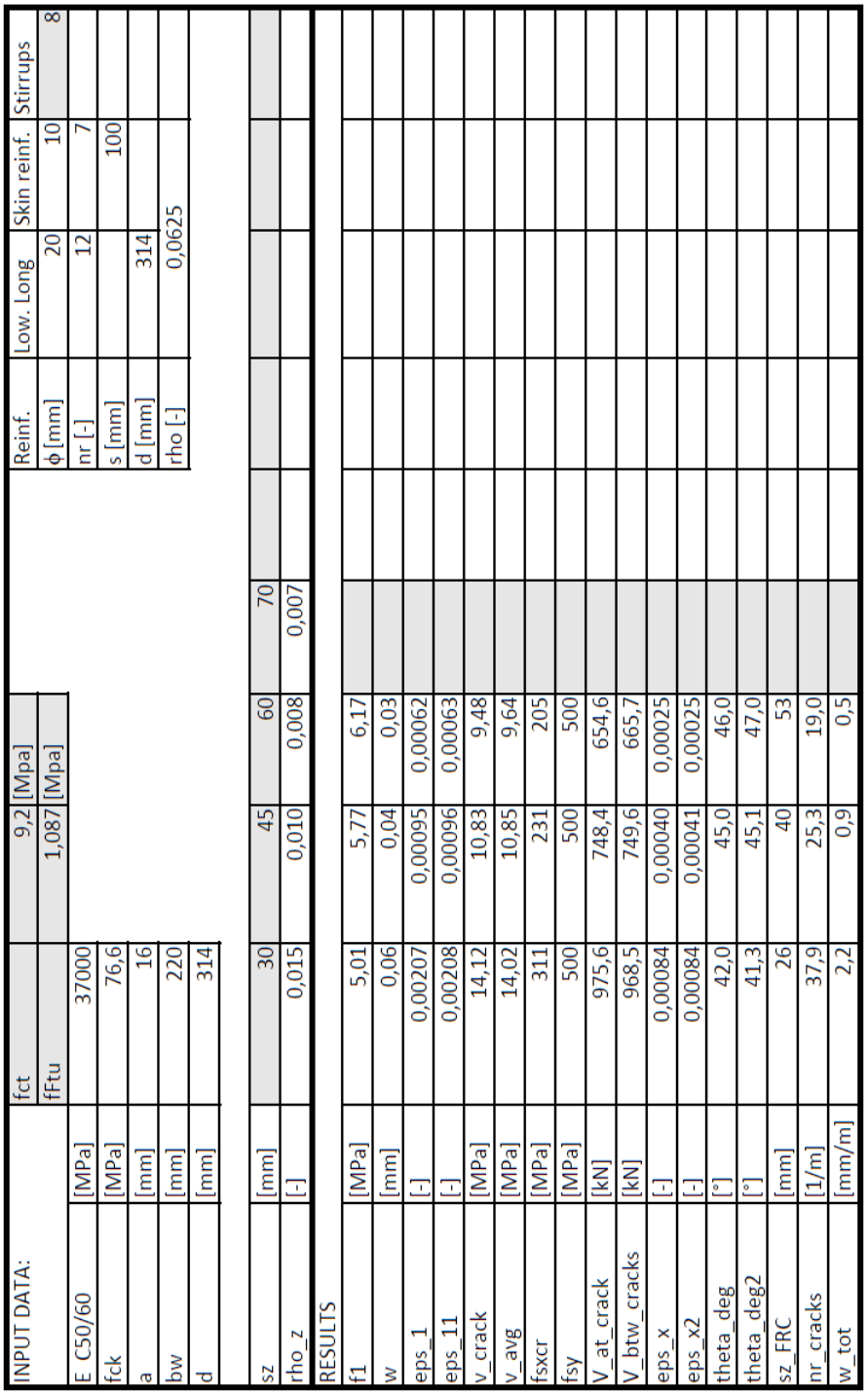

INPUT DATA:		fct	9,2	[Mpa]		Reinf.	Low. Long	Skin reinf.	Stirrups
		fFtu	1,087	[Mpa]		ϕ [mm]	20	10	8
E C50/60	[MPa]	37000				nr [-]	12	7	
fck	[MPa]	76,6				s [mm]		100	
a	[mm]	16				d [mm]	314		
bw	[mm]	220				rho [-]	0,0625		
d	[mm]	314							
sz	[mm]	30	45	60	70				
rho_z	[-]	0,015	0,010	0,008	0,007				
RESULTS									
f1	[MPa]	5,01	5,77	6,17					
w	[mm]	0,06	0,04	0,03					
eps_1	[-]	0,00207	0,00095	0,00062					
eps_11	[-]	0,00208	0,00096	0,00063					
v_crack	[MPa]	14,12	10,83	9,48					
v_avg	[MPa]	14,02	10,85	9,64					
fsxcr	[MPa]	311	231	205					
fsy	[MPa]	500	500	500					
V_at_crack	[kN]	975,6	748,4	654,6					
V_btw_cracks	[kN]	968,5	749,6	665,7					
eps_x	[-]	0,00084	0,00040	0,00025					
eps_x2	[-]	0,00084	0,00041	0,00025					
theta_deg	[°]	42,0	45,0	46,0					
theta_deg2	[°]	41,3	45,1	47,0					
sz_FRC	[mm]	26	40	53					
nr_cracks	[1/m]	37,9	25,3	19,0					
w_tot	[mm/m]	2,2	0,9	0,5					

INPUT DATA:		fct		9,2	[Mpa]		Reinf.	Low. Long	Skin reinf.	Stirrups
		fFtu		1,087	[Mpa]		ϕ [mm]	20	10	10
E_C50/60	[MPa]		37000				nr [-]	12	7	
fck	[MPa]		76,6				s [mm]		100	
a	[mm]		16				d [mm]	314		
bw	[mm]		220				rho [-]	0,0625		
d	[mm]		314							
sz	[mm]	70		80	90	100				
rho_z	[-]	0,010		0,009	0,008	0,007				
RESULTS										
f1	[MPa]	6,12		6,23	6,60					
w	[mm]	0,03		0,03	0,02					
eps_1	[-]	0,00066		0,00058	0,00038					
eps_11	[-]	0,00067		0,00059	0,00039					
v_crack	[MPa]	10,47		9,89	9,37					
v_avg	[MPa]	10,46		9,97	9,51					
fsxcr	[MPa]	209		202	189					
fsy	[MPa]	500		500	500					
V_at_crack	[kN]	723,1		683,3	647,3					
V_btw_cracks	[kN]	722,7		689,0	657,2					
eps_x	[-]	0,00029		0,00025	0,00015					
eps_x2	[-]	0,00029		0,00025	0,00016					
theta_deg	[°]	47,0		47,0	48,0					
theta_deg2	[°]	47,0		47,5	48,8					
sz_FRC	[mm]	62		70	79					
nr_cracks	[1/m]	16,2		14,2	12,6					
w_tot	[mm/m]	0,5		0,5	0,3					

INPUT DATA:		fct	9,2	[Mpa]					Reinf.	Low. Long	Skin reinf.	Stirrups
		fFtu	1,087	[Mpa]					ϕ [mm]	20	10	12
E_C50/60	[MPa]	37000							nr [-]	12	7	
fck	[MPa]	76,6							s [mm]		100	
a	[mm]	16							d [mm]	314		
bw	[mm]	220							rho [-]	0,0625		
d	[mm]	314										
sz	[mm]	110	115									
rho_z	[-]	0,0093	0,0089									
RESULTS												
f1	[MPa]	6,85	7,28									
w	[mm]	0,02	0,01									
eps_1	[-]	0,00033	0,00019									
eps_11	[-]	0,00034	0,00020									
v_crack	[MPa]	9,66	9,51									
v_avg	[MPa]	9,67	9,69									
fsxcr	[MPa]	258	175									
fsy	[MPa]	500	500									
V_at_crack	[kN]	667,5	657,0									
V_btw_cracks	[kN]	668,2	669,4									
eps_x	[-]	0,00015	0,00007									
eps_x2	[-]	0,00015	0,00006									
theta_deg	[°]	50,0	50,5									
theta_deg2	[°]	50,1	51,5									
sz_FRC	[mm]	97	101									
nr_cracks	[1/m]	10,3	9,9									
w_tot	[mm/m]	0,2	0,1									

Varying diameter of lower longitudinal reinforcement

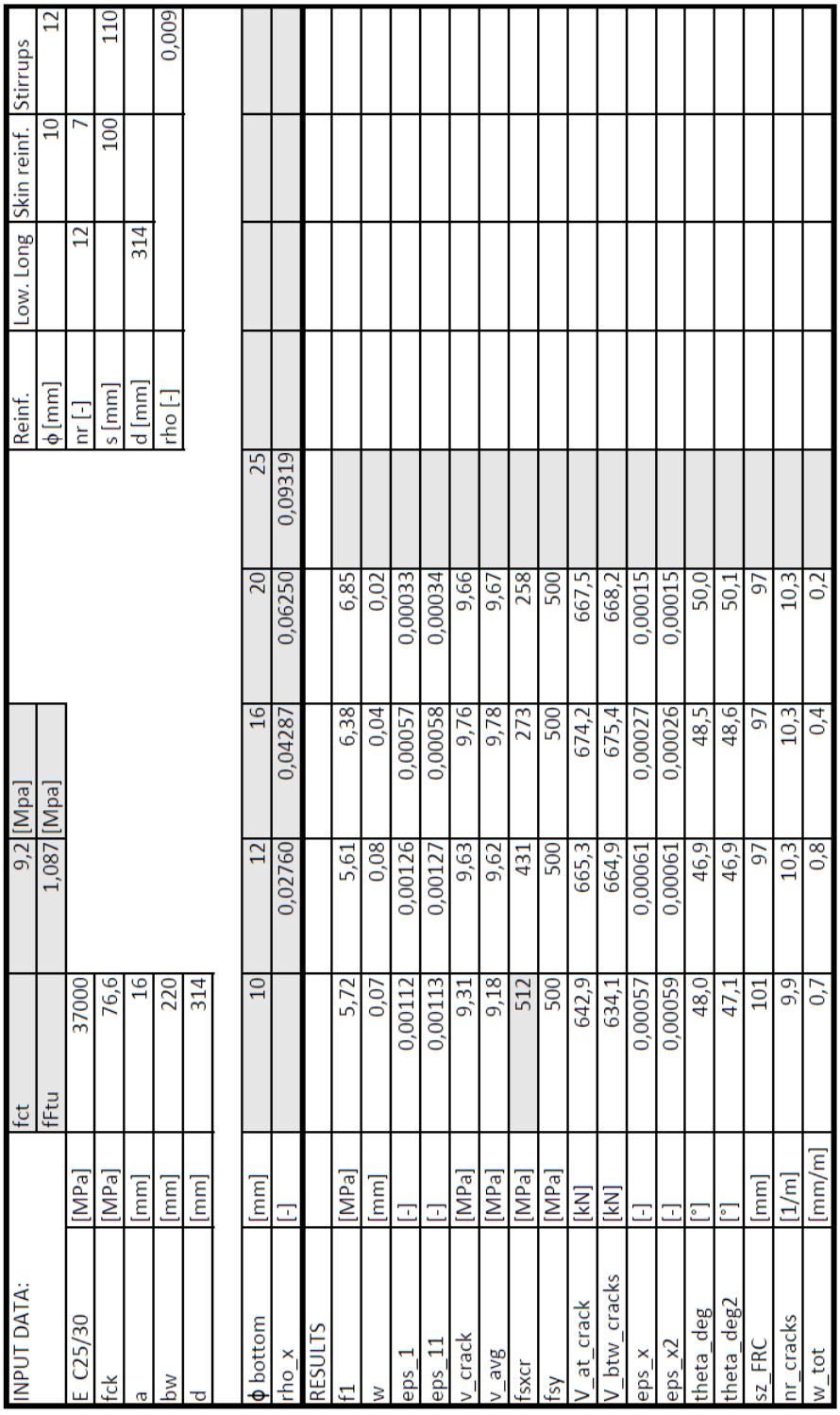

INPUT DATA:		fct	9,2	[Mpa]			Reinf.	Low. Long	Skin reinf.	Stirrups
		fFtu	1,087	[Mpa]			ϕ [mm]		10	12
E C25/30	[MPa]	37000					nr [-]	12	7	
fck	[MPa]	76,6					s [mm]		100	110
a	[mm]	16					d [mm]	314		
bw	[mm]	220					rho [-]			0,009
d	[mm]	314								
ϕ bottom	[mm]	10	12		16	20	25			
rho_x	[-]		0,02760		0,04287	0,06250	0,09319			
RESULTS										
f1	[MPa]	5,72	5,61		6,38	6,85				
w	[mm]	0,07	0,08		0,04	0,02				
eps_1	[-]	0,00112	0,00126		0,00057	0,00033				
eps_11	[-]	0,00113	0,00127		0,00058	0,00034				
v_crack	[MPa]	9,31	9,63		9,76	9,66				
v_avg	[MPa]	9,18	9,62		9,78	9,67				
fsxcr	[MPa]	512	431		273	258				
fsy	[MPa]	500	500		500	500				
V_at_crack	[kN]	642,9	665,3		674,2	667,5				
V_btw_cracks	[kN]	634,1	664,9		675,4	668,2				
eps_x	[-]	0,00057	0,00061		0,00027	0,00015				
eps_x2	[-]	0,00059	0,00061		0,00026	0,00015				
theta_deg	[°]	48,0	46,9		48,5	50,0				
theta_deg2	[°]	47,1	46,9		48,6	50,1				
sz_FRC	[mm]	101	97		97	97				
nr_cracks	[1/m]	9,9	10,3		10,3	10,3				
w_tot	[mm/m]	0,7	0,8		0,4	0,2				

Comparison to plain concrete

INPUT DATA:

fct	9,2	[Mpa]
fFtu	1,087	[Mpa]
E C25/30	[MPa]	37000
fck	[MPa]	76,6
a	[mm]	16
bw	[mm]	220
d	[mm]	314

ϕ Low. Long	[mm]	12	16	20
rho_x	[-]	0,02760	0,04287	0,06250

RESULTS

f1	[MPa]	5,61	6,38	6,85
w	[mm]	0,08	0,04	0,02
eps_1	[-]	0,00126	0,00057	0,00033
eps_11	[-]	0,00127	0,00058	0,00034
v_crack	[MPa]	9,63	9,76	9,66
v_avg	[MPa]	9,62	9,78	9,67
fsxcr	[MPa]	431	273	258
fsy	[MPa]	500	500	500
V_at_crack	[kN]	665,3	674,2	667,5
V_btw_cracks	[kN]	664,9	675,4	668,2
eps_x	[-]	0,00061	0,00027	0,00015
eps_x2	[-]	0,00061	0,00026	0,00015
theta_deg	[°]	46,9	48,5	50,0
theta_deg2	[°]	46,9	48,6	50,1
sz_FRC	[mm]	97	97	97
nr_cracks	[1/m]	10,3	10,3	10,3
w_tot	[mm/m]	0,8	0,4	0,2

fct	4,1	[Mpa]
fFtu	0	[Mpa]
E C25/30	[MPa]	37000
fck	[MPa]	50
a	[mm]	16
bw	[mm]	220
d	[mm]	314

12	16	20
0,02760	0,04289	0,06253

1,57	1,71	1,84
0,39	0,30	0,23
0,00517	0,00391	0,00301
0,00518	0,00392	0,00302
8,38	8,98	9,34
8,38	9,00	9,34
510	374	275
500	500	500
579,1	620,4	645,4
578,9	621,6	645,1
0,00180	0,00125	0,00092
0,00175	0,00128	0,00092
36,7	35,4	34,9
36,6	35,6	34,8
110	110	110
9,1	9,1	9,1
3,5	2,7	2,1

Reinf.	Low. Long	Skin reinf.	Stirrups
ϕ [mm]		10	12
nr [-]	12	7	
s [mm]		100	110
d [mm]	314		
rho [-]			0,009

APPENDIX D SHEAR CAPACITY CALCULATIONS Tri-25

Varying transversal reinforcement ratio

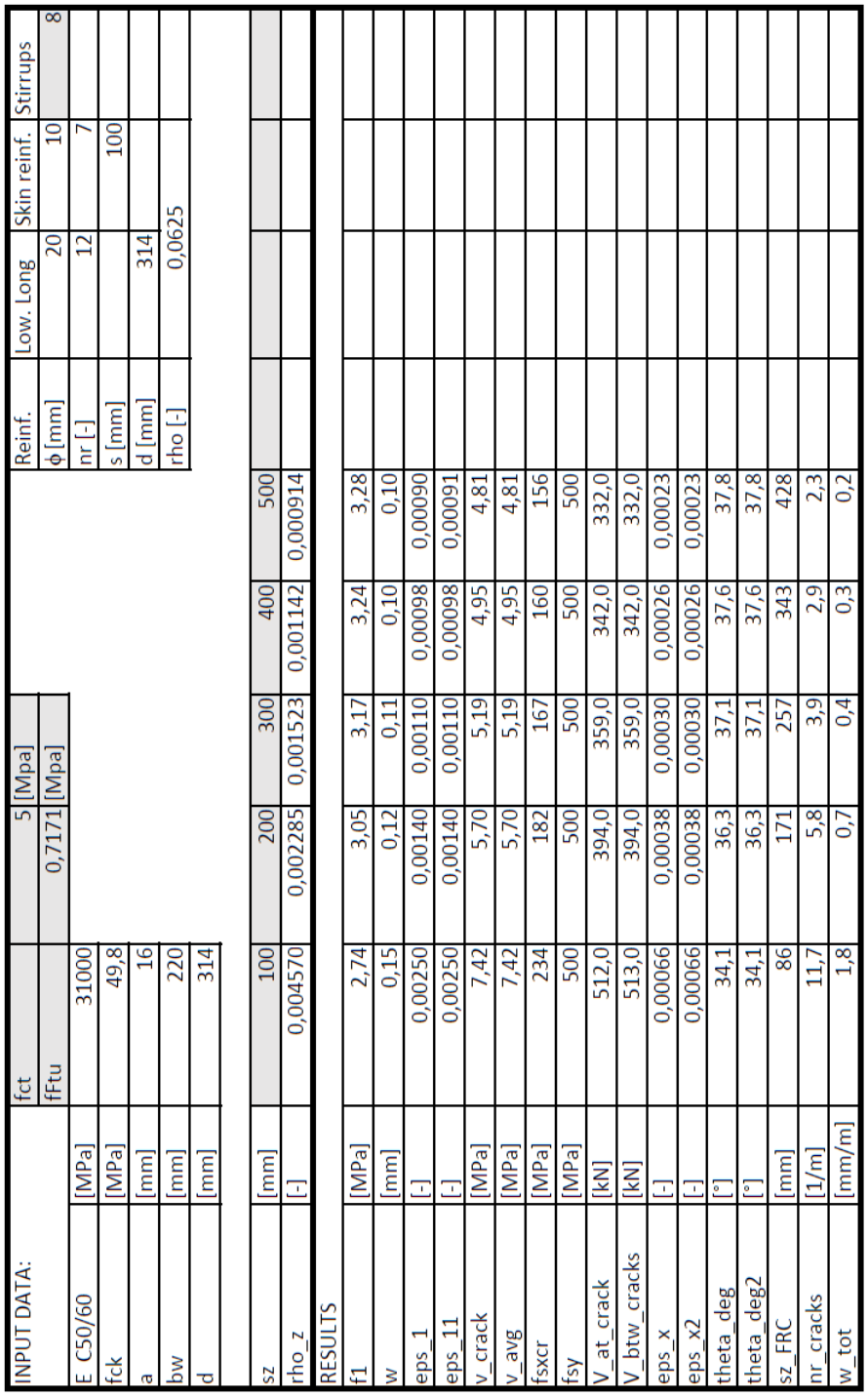

INPUT DATA:		fct	5	[Mpa]		Reinf.	Low. Long	Skin reinf.	Stirrups
		fFtu	0,7171	[Mpa]		ϕ [mm]	20	10	8
E C50/60	[MPa]	31000				nr [-]	12	7	
fck	[MPa]	49,8				s [mm]		100	
a	[mm]	16				d [mm]	314		
bw	[mm]	220				rho [-]	0,0625		
d	[mm]	314							
sz	[mm]	100	200	300	400	500			
rho_z	[-]	0,004570	0,002285	0,001523	0,001142	0,000914			
RESULTS									
f1	[MPa]	2,74	3,05	3,17	3,24	3,28			
w	[mm]	0,15	0,12	0,11	0,10	0,10			
eps_1	[-]	0,00250	0,00140	0,00110	0,00098	0,00090			
eps_11	[-]	0,00250	0,00140	0,00110	0,00098	0,00091			
v_crack	[MPa]	7,42	5,70	5,19	4,95	4,81			
v_avg	[MPa]	7,42	5,70	5,19	4,95	4,81			
fsxcr	[MPa]	234	182	167	160	156			
fsy	[MPa]	500	500	500	500	500			
V_at_crack	[kN]	512,0	394,0	359,0	342,0	332,0			
V_btw_cracks	[kN]	513,0	394,0	359,0	342,0	332,0			
eps_x	[-]	0,00066	0,00038	0,00030	0,00026	0,00023			
eps_x2	[-]	0,00066	0,00038	0,00030	0,00026	0,00023			
theta_deg	[°]	34,1	36,3	37,1	37,6	37,8			
theta_deg2	[°]	34,1	36,3	37,1	37,6	37,8			
sz_FRC	[mm]	86	171	257	343	428			
nr_cracks	[1/m]	11,7	5,8	3,9	2,9	2,3			
w_tot	[mm/m]	1,8	0,7	0,4	0,3	0,2			

Shear capacity calculations Tri-25

Varying diameter of lower longitudinal reinforcement

INPUT DATA:		fct	5	[Mpa]			Reinf.	Low. Long	Skin reinf.	Stirrups
		fFtu	0,7171	[Mpa]			ϕ [mm]		10	12
E_C25/30	[MPa]	31000					nr [-]	12	7	
fck	[MPa]	49,8					s [mm]		100	110
a	[mm]	16					d [mm]	314		
bw	[mm]	220					rho [-]			0,0093
d	[mm]	314								
ϕ Low. Long	[mm]	12	16	20						
rho_x	[-]	0,02759	0,04287	0,06250						
RESULTS										
f1	[MPa]	2,31	2,44	2,58						
w	[mm]	0,37	0,29	0,22						
eps_1	[-]	0,00570	0,00440	0,00340						
eps_11	[-]	0,00570	0,00450	0,00340						
v_crack	[MPa]	9,51	9,97	10,42						
v_avg	[MPa]	9,51	9,97	10,42						
fsxcr	[MPa]	550	388	289						
fsy	[MPa]	500	500	500						
V_at_crack	[kN]	557,0	689,0	720,0						
V_btw_cracks	[kN]	557,0	689,0	720,0						
eps_x	[-]	0,00190	0,00140	0,00099						
eps_x2	[-]	0,00190	0,00130	0,00099						
theta_deg	[°]	36,3	35,5	34,8						
theta_deg2	[°]	36,3	35,5	34,8						
sz_FRC	[mm]	94	92	94						
nr_cracks	[1/m]	10,6	10,6	10,6						
w_tot	[mm/m]	3,9	3,1	2,3						

Comparison to plain concrete

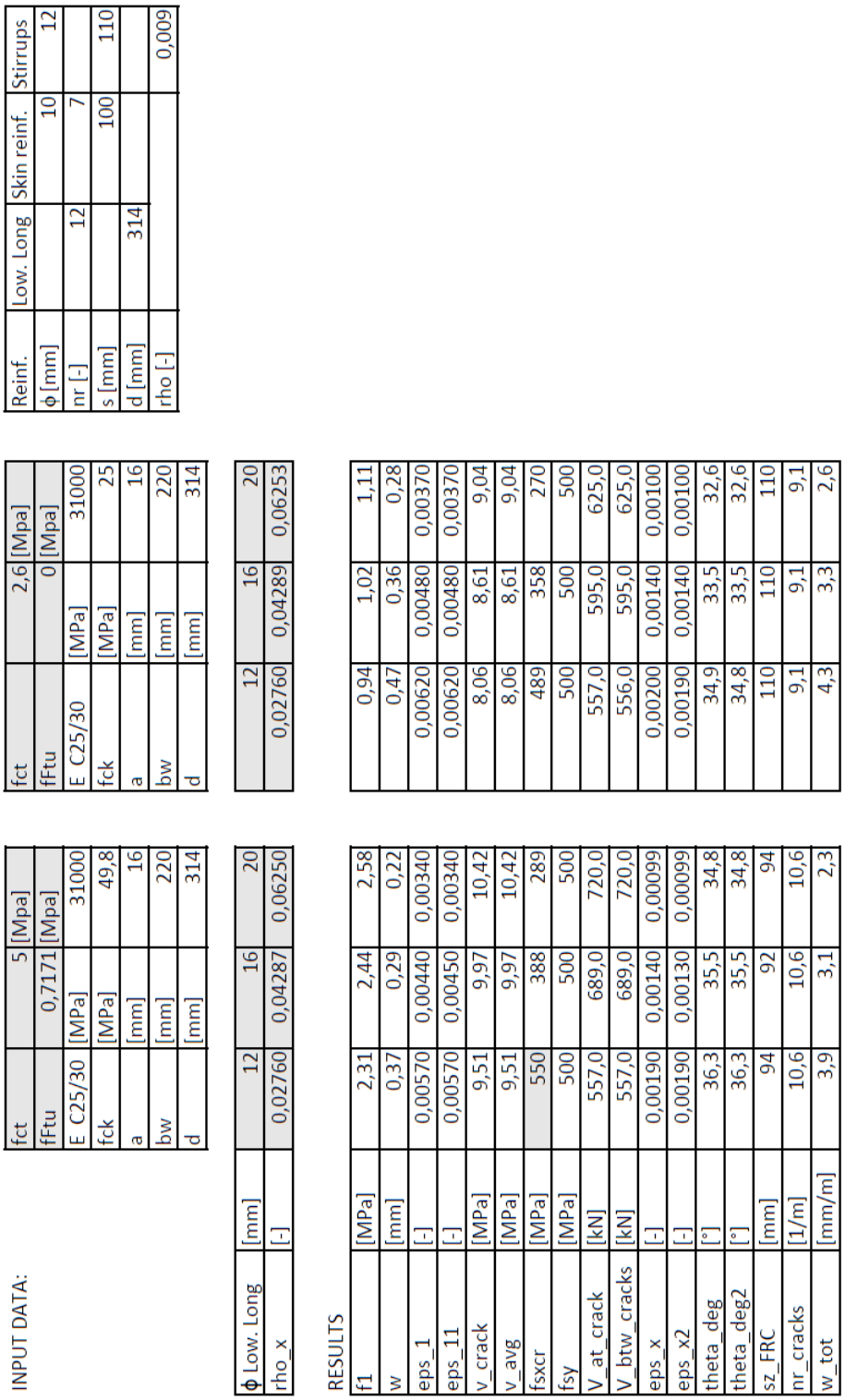

INPUT DATA:

fct	5	[Mpa]
fFtu	0,7171	[Mpa]
E C25/30	[MPa]	31000
fck	[MPa]	49,8
a	[mm]	16
bw	[mm]	220
d	[mm]	314

ϕ Low. Long	[mm]	12	16	20
rho_x	[-]	0,02760	0,04287	0,06250

RESULTS

f1	[MPa]	2,31	2,44	2,58
w	[mm]	0,37	0,29	0,22
eps_1	[-]	0,00570	0,00440	0,00340
eps_11	[-]	0,00570	0,00450	0,00340
v_crack	[MPa]	9,51	9,97	10,42
v_avg	[MPa]	9,51	9,97	10,42
fsxcr	[MPa]	550	388	289
fsy	[MPa]	500	500	500
V_at_crack	[kN]	557,0	689,0	720,0
V_btw_cracks	[kN]	557,0	689,0	720,0
eps_x	[-]	0,00190	0,00140	0,00099
eps_x2	[-]	0,00190	0,00130	0,00099
theta_deg	[°]	36,3	35,5	34,8
theta_deg2	[°]	36,3	35,5	34,8
sz_FRC	[mm]	94	92	94
nr_cracks	[1/m]	10,6	10,6	10,6
w_tot	[mm/m]	3,9	3,1	2,3

fct	2,6	[Mpa]
fFtu	0	[Mpa]
E C25/30	[MPa]	31000
fck	[MPa]	25
a	[mm]	16
bw	[mm]	220
d	[mm]	314

12	16	20
0,02760	0,04289	0,06253

0,94	1,02	1,11
0,47	0,36	0,28
0,00620	0,00480	0,00370
0,00620	0,00480	0,00370
8,06	8,61	9,04
8,06	8,61	9,04
489	358	270
500	500	500
557,0	595,0	625,0
556,0	595,0	625,0
0,00200	0,00140	0,00100
0,00190	0,00140	0,00100
34,9	33,5	32,6
34,8	33,5	32,6
110	110	110
9,1	9,1	9,1
4,3	3,3	2,6

Reinf.	Low. Long	Skin reinf.	Stirrups
ϕ [mm]		10	12
nr [-]	12	7	
s [mm]		100	110
d [mm]	314		
rho [-]			0,009

APPENDIX E SHEAR CAPACITY CALCULATIONS Tri-50

Varying transversal reinforcement ratio

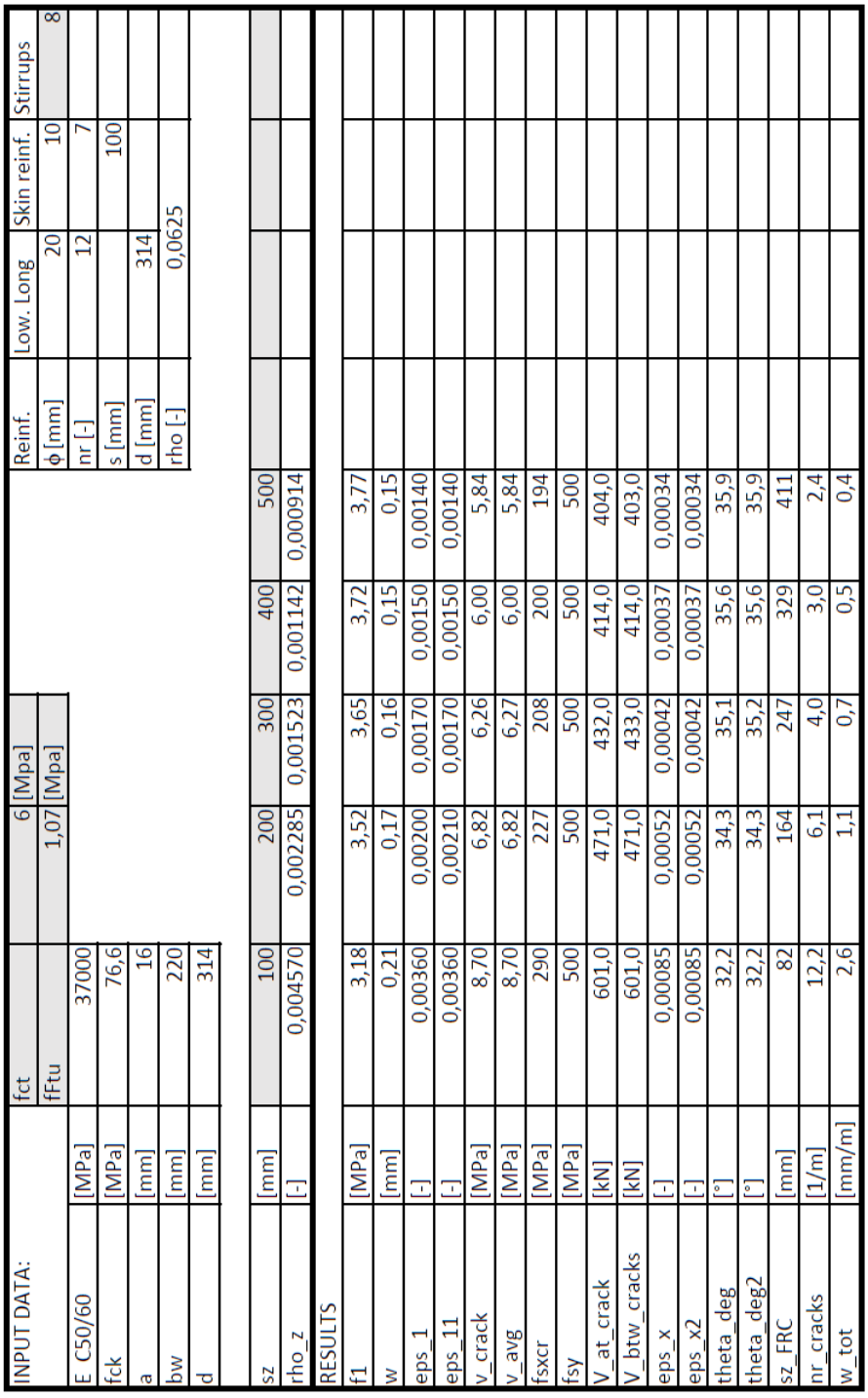

INPUT DATA:		fct	6 [Mpa]				Reinf.	Low. Long	Skin reinf.	Stirrups
		fFtu	1,07 [Mpa]				Φ [mm]	20	10	8
E C50/60	[MPa]	37000					nr [-]	12	7	
fck	[MPa]	76,6					s [mm]		100	
a	[mm]	16					d [mm]	314		
bw	[mm]	220					rho [-]	0,0625		
d	[mm]	314								
sz	[mm]	100	200	300	400	500				
rho_z	[-]	0,004570	0,002285	0,001523	0,001142	0,000914				
RESULTS										
f1	[MPa]	3,18	3,52	3,65	3,72	3,77				
w	[mm]	0,21	0,17	0,16	0,15	0,15				
eps_1	[-]	0,00360	0,00200	0,00170	0,00150	0,00140				
eps_11	[-]	0,00360	0,00210	0,00170	0,00150	0,00140				
v_crack	[MPa]	8,70	6,82	6,26	6,00	5,84				
v_avg	[MPa]	8,70	6,82	6,27	6,00	5,84				
fsxcr	[MPa]	290	227	208	200	194				
fsy	[MPa]	500	500	500	500	500				
V_at_crack	[kN]	601,0	471,0	432,0	414,0	404,0				
V_btw_cracks	[kN]	601,0	471,0	433,0	414,0	403,0				
eps_x	[-]	0,00085	0,00052	0,00042	0,00037	0,00034				
eps_x2	[-]	0,00085	0,00052	0,00042	0,00037	0,00034				
theta_deg	[°]	32,2	34,3	35,1	35,6	35,9				
theta_deg2	[°]	32,2	34,3	35,2	35,6	35,9				
sz_FRC	[mm]	82	164	247	329	411				
nr_cracks	[1/m]	12,2	6,1	4,0	3,0	2,4				
w_tot	[mm/m]	2,6	1,1	0,7	0,5	0,4				

Varying diameter of lower longitudinal reinforcement

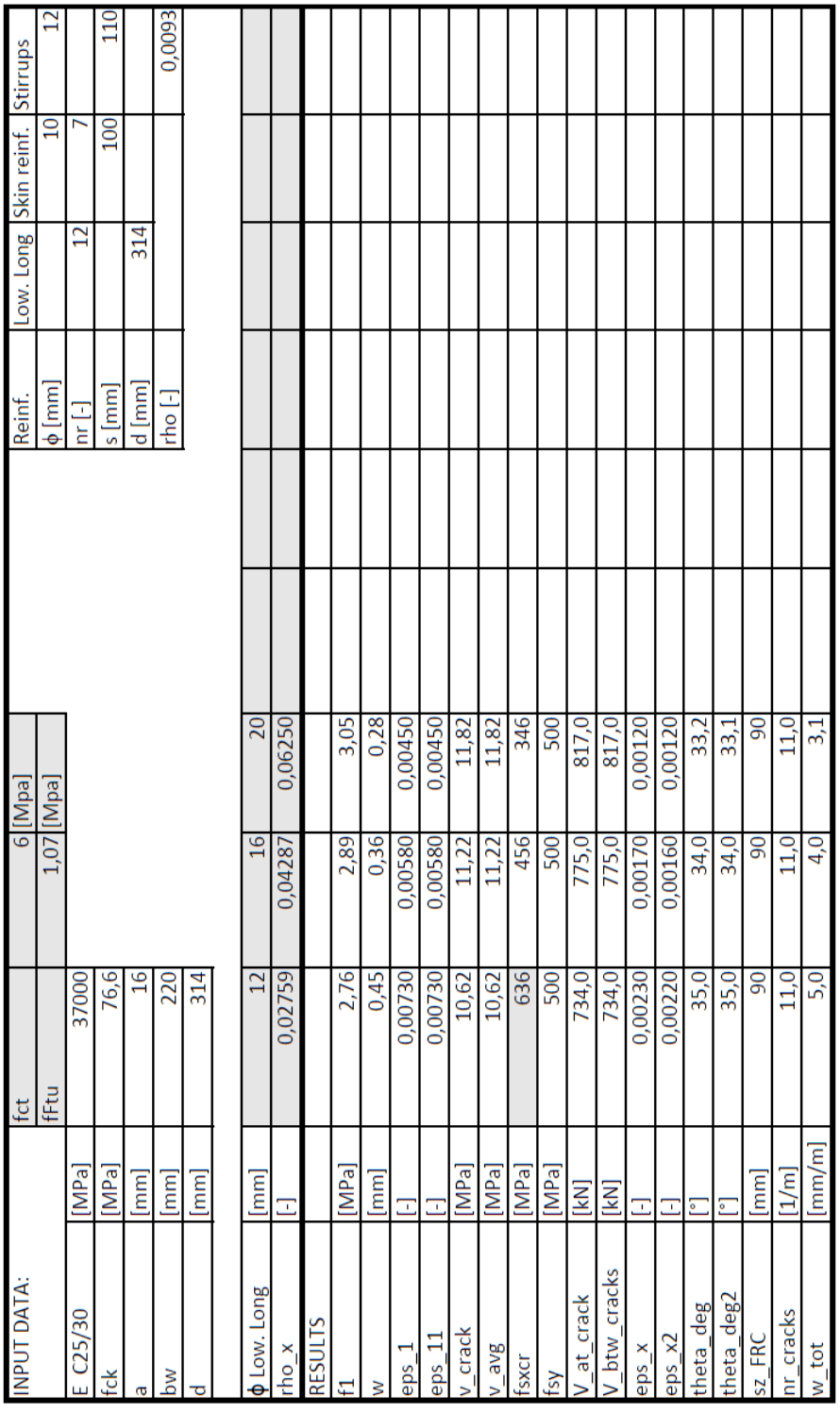

INPUT DATA:		fct	6	[Mpa]		Reinf.	Low. Long	Skin reinf.	Stirrups
		fFtu	1,07	[Mpa]		ϕ [mm]		10	12
E_C25/30	[MPa]	37000				nr [-]	12	7	
fck	[MPa]	76,6				s [mm]		100	110
a	[mm]	16				d [mm]	314		
bw	[mm]	220				rho [-]			0,0093
d	[mm]	314							
ϕ Low. Long	[mm]	12	16	20					
rho_x	[-]	0,02759	0,04287	0,06250					
RESULTS									
f1	[MPa]	2,76	2,89	3,05					
w	[mm]	0,45	0,36	0,28					
eps_1	[-]	0,00730	0,00580	0,00450					
eps_11	[-]	0,00730	0,00580	0,00450					
v_crack	[MPa]	10,62	11,22	11,82					
v_avg	[MPa]	10,62	11,22	11,82					
fsxcr	[MPa]	636	456	346					
fsy	[MPa]	500	500	500					
V_at_crack	[kN]	734,0	775,0	817,0					
V_btw_cracks	[kN]	734,0	775,0	817,0					
eps_x	[-]	0,00230	0,00170	0,00120					
eps_x2	[-]	0,00220	0,00160	0,00120					
theta_deg	[°]	35,0	34,0	33,2					
theta_deg2	[°]	35,0	34,0	33,1					
sz_FRC	[mm]	90	90	90					
nr_cracks	[1/m]	11,0	11,0	11,0					
w_tot	[mm/m]	5,0	4,0	3,1					

Comparison to plain concrete

INPUT DATA:

fct	6	[Mpa]
fFtu	1,07	[Mpa]
E C25/30	[MPa]	37000
fck	[MPa]	76,6
a	[mm]	16
bw	[mm]	220
d	[mm]	314

ϕ Low. Long	[mm]	12	16	20
rho_x	[-]	0,02760	0,04287	0,06250
RESULTS				
f1	[MPa]	2,76	2,89	3,05
w	[mm]	0,45	0,36	0,28
eps_1	[-]	0,00730	0,00580	0,00450
eps_11	[-]	0,00730	0,00580	0,00450
v_crack	[MPa]	10,62	11,22	11,82
v_avg	[MPa]	10,62	11,22	11,82
fsxcr	[MPa]	636	456	346
fsy	[MPa]	500	500	500
V_at_crack	[kN]	734,0	775,0	817,0
V_btw_cracks	[kN]	734,0	775,0	817,0
eps_x	[-]	0,00230	0,00170	0,00120
eps_x2	[-]	0,00220	0,00160	0,00120
theta_deg	[°]	35,0	34,0	33,2
theta_deg2	[°]	35,0	34,0	33,1
sz_FRC	[mm]	90	90	90
nr_cracks	[1/m]	11,0	11,0	11,0
w_tot	[mm/m]	5,0	4,0	3,1

fct	4,1	[Mpa]
fFtu	0	[Mpa]
E C25/30	[MPa]	37000
fck	[MPa]	50
a	[mm]	16
bw	[mm]	220
d	[mm]	314

12	16	20
0,02760	0,04289	0,06253
1,57	1,71	1,84
0,39	0,30	0,23
0,00517	0,00391	0,00301
0,00518	0,00392	0,00302
8,38	8,98	9,34
8,38	9,00	9,34
510	374	275
500	500	500
579,1	620,4	645,4
578,9	621,6	645,1
0,00180	0,00125	0,00092
0,00175	0,00128	0,00092
36,7	35,4	34,9
36,6	35,6	34,8
110	110	110
9,1	9,1	9,1
3,5	2,7	2,1

Reinf.	Low. Long	Skin reinf.	Stirrups
ϕ [mm]		10	12
nr [-]	12	7	
s [mm]		100	110
d [mm]	314		
rho [-]			0,009

APPENDIX F SENSITIVITY ANALYSIS

INPUT DATA:		fct	2	[Mpa]
E_C25/30	[MPa]	31000		
fck	[MPa]	49,8		
a	[mm]	16		
bw	[mm]	220		
d	[mm]	314		
fFtu	[Mpa]	0,2	0,4	0,6

Reinf.	Low. Long	Skin reinf.	Stirrups
ϕ [mm]	20	10	10
nr [-]	12	7	
s [mm]		100	100
d [mm]	314		
rho [-]	0,0625		0,0071

0,8	1	1,2	1,4	1,6	1,8									

RESULTS														
fFtu/fct	[-]	0,1	0,2	0,3	0,4	0,5	0,6	0,7	0,8	0,9				
fFtu	[MPa]	0,2	0,4											
fct	[MPa]	2	2											
f1	[MPa]	0,68	0,79											
w	[mm]	1,04	1,18											
eps_1	[-]	0,01507	0,01907											
eps_11	[-]	0,01508	0,01908											
v_crack	[MPa]	10,50	11,40											
v_avg	[MPa]	10,52	11,36											
fsxcr	[MPa]	459	511											
fsy	[MPa]	500	500											
V_at_crack	[kN]	725,0	787,8											
V_btw_cracks	[kN]	726,8	784,9											
eps_x	[-]	0,00200	0,00230											
eps_x2	[-]	0,00203	0,00230											
theta_deg	[°]	22,0	21,0											
theta_deg2	[°]	22,4	20,2											
sz_FRC	[mm]	90	80											
nr_cracks	[1/m]	11,1	12,5											
w_tot	[mm/m]	11,6	14,8											

INPUT DATA:		fct	3	[Mpa]			Reinf.	Low. Long	Skin reinf.	Stirrups
							ϕ [mm]	20	10	10
E C25/30	[MPa]	31000					nr [-]	12	7	
fck	[MPa]	49,8					s [mm]		100	100
a	[mm]	16					d [mm]	314		
bw	[mm]	220					rho [-]	0,0625		0,0071
d	[mm]	314								
fFtu	[Mpa]	0,3	0,6	0,9	1,2	1,5	1,8	2,1	2,4	2,7

RESULTS										
fFtu/fct	[-]	0,1	0,2	0,3	0,4	0,5	0,6	0,7	0,8	0,9
fFtu	[MPa]	0,3	0,6	0,9	1,2					
fct	[MPa]	3	3	3	3					
f1	[MPa]	1,22	1,33	1,46	1,59					
w	[mm]	0,49	0,63	0,81	1,19					
eps_1	[-]	0,00737	0,01042	0,01519	0,02545					
eps_11	[-]	0,00738	0,01043	0,01520	0,02546					
v_crack	[MPa]	9,46	10,57	11,91	13,82					
v_avg	[MPa]	9,41	10,51	11,85	13,81					
fsxcr	[MPa]	349	407	484	617					
fsy	[MPa]	500	500	500	500					
V_at_crack	[kN]	653,8	730,2	823,0	954,4					
V_btw_cracks	[kN]	650,1	726,1	818,4	954,1					
eps_x	[-]	0,00140	0,00170	0,00210	0,00280					
eps_x2	[-]	0,00138	0,00170	0,00212	0,00283					
theta_deg	[°]	27,0	25,0	23,0	20,5					
theta_deg2	[°]	26,3	24,2	22,0	20,4					
sz_FRC	[mm]	90	80	70	60					
nr_cracks	[1/m]	11,1	12,5	14,3	16,7					
w_tot	[mm/m]	5,5	7,8	11,6	19,8					

INPUT DATA:			fct	4	[Mpa]
E_C25/30	[MPa]	31000			
fck	[MPa]	49,8			
a	[mm]	16			
bw	[mm]	220			
d	[mm]	314			
ffFtu	[Mpa]	0,4	0,8	1,2	1,6

Reinf.	Low. Long	Skin reinf.	Stirrups
ϕ [mm]	20	10	10
nr [-]	12	7	
s [mm]		100	100
d [mm]	314		
rho [-]	0,0625		0,0071

RESULTS													
fFtu/fct	[-]	0,1	0,2	0,3	0,4	0,5	0,6	0,7	0,8	0,9			
fFtu	[MPa]	0,4	0,8	1,2	1,6								
fct	[MPa]	4	4	4	4								
f1	[MPa]	1,82	1,96	2,06	2,20								
w	[mm]	0,31	0,36	0,52	0,82								
eps_1	[-]	0,00475	0,00619	0,01001	0,01790								
eps_11	[-]	0,00476	0,00620	0,01002	0,01791								
v_crack	[MPa]	9,07	10,06	11,59	13,55								
v_avg	[MPa]	9,15	9,98	11,55	13,60								
fsxcr	[MPa]	305	338	419	538								
fsy	[MPa]	500	500	500	500								
V_at_crack	[kN]	626,9	695,1	800,4	936,3								
V_btw_cracks	[kN]	631,7	689,1	798,1	939,2								
eps_x	[-]	0,00110	0,00130	0,00170	0,00240								
eps_x2	[-]	0,00110	0,00128	0,00173	0,00239								
theta_deg	[°]	30,5	29,0	26,0	23,0								
theta_deg2	[°]	31,3	28,0	25,6	23,6								
sz_FRC	[mm]	90	80	70	60								
nr_cracks	[1/m]	11,1	12,5	14,3	16,7								
w_tot	[mm/m]	3,5	4,6	7,5	13,6								

INPUT DATA:		fct	5	[Mpa]
E_C25/30	[MPa]	31000		
fck	[MPa]	49,8		
a	[mm]	16		
bw	[mm]	220		
d	[mm]	314		
fftu	[Mpa]	0,5	1	1,5

Reinf.	Low. Long	Skin reinf.	Stirrups
ϕ [mm]	20	10	10
nr [-]	12	7	
s [mm]		100	100
d [mm]	314		
rho [-]	0,0625		0,0071

RESULTS													
fftu/fct	[-]	0,1	0,2	0,3	0,4	0,5	0,6	0,7	0,8	0,9			
fftu	[MPa]	0,5	1	1,5	2	2,5							
fct	[MPa]	5	5	5	5	5							
f1	[MPa]	2,57	2,60	2,73	2,88	3,09							
w	[mm]	0,18	0,26	0,35	0,52	0,79							
eps_1	[-]	0,00277	0,00446	0,00688	0,01152	0,02075							
eps_11	[-]	0,00278	0,00447	0,00689	0,01153	0,02076							
v_crack	[MPa]	8,67	9,83	11,35	13,24	15,71							
v_avg	[MPa]	8,77	9,88	11,36	13,23	15,70							
fsxcr	[MPa]	258	301	367	461	604							
fsy	[MPa]	500	500	500	500	500							
V_at_crack	[kN]	599,1	679,3	784,3	914,7	1085,0							
V_btw_cracks	[kN]	605,5	682,6	784,6	913,9	1084,2							
eps_x	[-]	0,00080	0,00110	0,00140	0,00190	0,00270							
eps_x2	[-]	0,00080	0,00106	0,00142	0,00194	0,00271							
theta_deg	[°]	35,0	32,0	29,0	26,0	23,0							
theta_deg2	[°]	35,9	32,5	29,1	25,9	22,8							
sz_FRC	[mm]	90	80	70	60	50							
nr_cracks	[1/m]	11,1	12,5	14,3	16,7	20,0							
w_tot	[mm/m]	2,0	3,2	5,1	8,6	15,8							

INPUT DATA:		fct	6	[Mpa]
E_C25/30	[MPa]	31000		
fck	[MPa]	49,8		
a	[mm]	16		
bw	[mm]	220		
d	[mm]	314		
ffftu	[Mpa]	0,6	1,2	1,8	2,4	3	3,6	4,2	4,8	5,4

Reinf.	Low. Long	Skin reinf.	Stirrups
ϕ [mm]	20	10	10
nr [-]	12	7	
s [mm]		100	100
d [mm]	314		
rho [-]	0,0625		0,0071

RESULTS											
ffftu/fct	[-]	0,1	0,2	0,3	0,4	0,5	0,6	0,7	0,8	0,9	
ffftu	[MPa]	0,6	1,2	1,8	2,4	3					
fct	[MPa]	6	6	6	6	6					
f1	[MPa]	3,56	3,52	3,43	3,60	3,78					
w	[mm]	0,09	0,13	0,25	0,35	0,60					
eps_1	[-]	0,00135	0,00228	0,00499	0,00803	0,01601					
eps_11	[-]	0,00136	0,00229	0,00500	0,00804	0,01602					
v_crack	[MPa]	8,19	9,45	11,13	12,98	15,76					
v_avg	[MPa]	8,21	9,41	11,20	12,93	15,77					
fsxcr	[MPa]	204	247	323	398	550					
fsy	[MPa]	500	500	500	500	500					
V_at_crack	[kN]	565,5	652,6	769,1	896,4	1088,5					
V_btw_cracks	[kN]	566,8	650,2	773,7	893,4	1089,4					
eps_x	[-]	0,00050	0,00070	0,00120	0,00160	0,00240					
eps_x2	[-]	0,00047	0,00072	0,00116	0,00158	0,00240					
theta_deg	[°]	41,0	37,0	32,0	29,0	25,0					
theta_deg2	[°]	41,2	36,7	32,7	28,5	25,2					
sz_FRC	[mm]	90	80	70	60	50					
nr_cracks	[1/m]	11,1	12,5	14,3	16,7	20,0					
w_tot	[mm/m]	1,0	1,6	3,6	5,9	12,0					

INPUT DATA:		fct	7	[Mpa]		Reinf.	Low. Long	Skin reinf.	Stirrups
						ϕ [mm]	20	10	10
E C25/30	[MPa]	31000				nr [-]	12	7	
fck	[MPa]	49,8				s [mm]		100	100
a	[mm]	16				d [mm]	314		
bw	[mm]	220				rho [-]	0,0625	0,0071	
d	[mm]	314							
fFtu	[Mpa]	0,7	1,4	2,1	2,8	3,5	4,2	4,9	5,6	6,3

RESULTS											
fFtu/fct	[-]	0,1	0,2	0,3	0,4	0,5	0,6	0,7	0,8	0,9	
fFtu	[MPa]	0,7	1,4	2,1	2,8	3,5					
fct	[MPa]	7	7	7	7	7					
f1	[MPa]	5,11	4,67	4,31	4,38	4,50					
w	[mm]	0,02	0,06	0,15	0,24	0,46					
eps_1	[-]	0,00037	0,00102	0,00296	0,00555	0,01233					
eps_11	[-]	0,00038	0,00103	0,00297	0,00556	0,01234					
v_crack	[MPa]	7,72	8,93	10,82	12,78	15,82					
v_avg	[MPa]	7,81	8,83	10,85	12,72	15,85					
fsxcr	[MPa]	157	191	271	347	502					
fsy	[MPa]	500	500	500	500	500					
V_at_crack	[kN]	533,4	616,5	747,3	882,9	1092,7					
V_btw_cracks	[kN]	539,6	610,2	749,2	878,4	1094,8					
eps_x	[-]	0,00015	0,00039	0,00086	0,00130	0,00210					
eps_x2	[-]	0,00015	0,00038	0,00085	0,00128	0,00213					
theta_deg	[°]	48,0	43,0	36,0	32,0	27,0					
theta_deg2	[°]	48,7	42,3	36,2	31,4	27,3					
sz_FRC	[mm]	90	80	70	60	50					
nr_cracks	[1/m]	11,1	12,5	14,3	16,7	20,0					
w_tot	[mm/m]	0,3	0,7	2,1	4,0	9,2					

INPUT DATA:		fct	8	[Mpa]
E C25/30	[MPa]	31000		
fck	[MPa]	49,8		
a	[mm]	16		
bw	[mm]	220		
d	[mm]	314		
fFtu	[Mpa]	0,8	1,6	2,4

Reinf.	Low. Long	Skin reinf.	Stirrups
ϕ [mm]	20	10	10
nr [-]	12	7	
s [mm]		100	100
d [mm]	314		
rho [-]	0,0625		0,0071

RESULTS											
fFtu/fct	[-]	0,1	0,2	0,3	0,4	0,5	0,6	0,7	0,8	0,9	
fFtu	[MPa]		1,6	2,4	3,2	4	4,8				
fct	[MPa]		8	8	8	8	8				
f1	[MPa]		6,07	5,40	5,14	5,32	5,57				
w	[mm]		0,02	0,07	0,19	0,31	0,60				
eps_1	[-]		0,00037	0,00150	0,00431	0,00833	0,02003				
eps_11	[-]		0,00038	0,00151	0,00432	0,00834	0,02004				
v_crack	[MPa]		8,55	10,34	12,86	15,47	19,62				
v_avg	[MPa]		8,68	10,32	12,92	15,39	19,60				
fsxcr	[MPa]		155	215	322	428	652				
fsy	[MPa]		500	500	500	500	500				
V_at_crack	[kN]		590,8	714,2	888,5	1068,6	1355,1				
V_btw_cracks	[kN]		599,5	712,8	892,5	1063,1	1353,8				
eps_x	[-]		0,00014	0,00052	0,00110	0,00170	0,00290				
eps_x2	[-]		0,00014	0,00052	0,00112	0,00171	0,00292				
theta_deg	[°]		48,0	41,0	34,0	30,0	25,0				
theta_deg2	[°]		48,9	40,8	34,5	29,2	24,8				
sz_FRC	[mm]		80	70	60	50	40				
nr_cracks	[1/m]		12,5	14,3	16,7	20,0	25,0				
w_tot	[mm/m]		0,3	1,1	3,1	6,1	15,1				

INPUT DATA:		fct	9	[Mpa]
E_C25/30	[MPa]	31000		
fck	[MPa]	49,8		
a	[mm]	16		
bw	[mm]	220		
d	[mm]	314		
fFtu	[Mpa]	0,9	1,8	2,7

Reinf.	Low. Long	Skin reinf.	Stirrups
ϕ [mm]	20	10	10
nr [-]	12	7	
s [mm]		100	100
d [mm]	314		
rho [-]	0,0625		0,0071

RESULTS											
fFtu/fct	[-]	0,1	0,2	0,3	0,4	0,5	0,6	0,7	0,8	0,9	
fFtu	[MPa]			2,7	3,6	4,5	5,4				
fct	[MPa]			9	9	9	9				
f1	[MPa]			6,74	6,13	6,10	6,36				
w	[mm]			0,03	0,11	0,24	0,45				
eps_1	[-]			0,00062	0,00258	0,00662	0,01516				
eps_11	[-]			0,00063	0,00259	0,00663	0,01517				
v_crack	[MPa]			9,87	12,41	15,51	19,56				
v_avg	[MPa]			9,96	12,41	15,47	19,49				
fsxcr	[MPa]			169	263	390	587				
fsy	[MPa]			500	500	500	500				
V_at_crack	[kN]			681,6	857,4	1071,1	1351,5				
V_btw_cracks	[kN]			687,9	857,5	1068,6	1346,2				
eps_x	[-]			0,00023	0,00078	0,00150	0,00250				
eps_x2	[-]			0,00023	0,00078	0,00149	0,00255				
theta_deg	[°]			46,0	38,0	32,0	27,0				
theta_deg2	[°]			46,7	38,0	31,6	26,1				
sz_FRC	[mm]			70	60	50	40				
nr_cracks	[1/m]			14,3	16,7	20,0	25,0				
w_tot	[mm/m]			0,4	1,8	4,8	11,3				